[American Journal of Science, Vol. 309, February, 2009, P. 132–187, DOI 10.2475/02.2009.03]

THE GEOCHRONOLOGICAL FRAMEWORK OF THE IRUMIDE BELT: A PROLONGED CRUSTAL HISTORY ALONG THE MARGIN OF THE BANGWEULU CRATON

B. De WAELE*, I.C.W. FITZSIMONS*, M.T.D. WINGATE**, F. TEMBO***, B. MAPANI[§], and E. A. BELOUSOVA[§§]

ABSTRACT. Ion microprobe U-Th-Pb analyses of zircon from 40 granitoid rocks collected from the late Mesoproterozoic Irumide Belt in Central Southern Africa, along the southern margin of the Archean to Paleoproterozoic Bangweulu Block, provide a comprehensive set of age data for this complex orogen. The data indicate that the Irumide Belt is constructed on a basement of principally Paleoproterozoic (ca. 2.05–1.93 Ga) age with a subordinate Neoarchean (ca. 2.73 Ga) component, which is overlain by a platformal quartzite-pelite succession known as the Muva Supergroup. Previously published U-Pb detrital zircon data for the Paleoproterozoic Muva Supergroup, which show age populations that match all of the pre-1.9 Ga basement components identified within the Irumide Belt, suggest that the pre-Muva basement was assembled as a coherent block by ~1.8 Ga, which we refer to as the Bangweulu Craton. The southern margin of the Bangweulu Craton was then intruded by a previously unrecognized suite of biotite-bearing granitoid rocks between 1.66 and 1.55 Ga, not recorded elsewhere in the region, and was later the site of emplacement of voluminous granitoid magmatism during the Irumide Orogeny at between 1.05 and 1.00 Ga. Hf isotopic data from zircon in these suites indicate variable influence from cryptic Archean rocks in the lower crustal melting zone of the Bangweulu Block. U-Pb analyses of inherited zircon cores in magmatic zircon in these granitoid rocks, directly confirm the presence of this reworked cryptic Archean basement of the Bangweulu Craton. The age data confirm previously proposed tectonic models for the Mesoproterozoic evolution of central Africa, refuting the presence of a continent-spanning Grenvillian-aged Orogen, including the Kibaran Belt, Irumide Belt and Choma-Kalomo Block of central Africa and connecting with Mesoproterozoic terranes further south along the margins of the Kalahari Craton. The data clearly show that the Proterozoic tectonic evolution of the Bangweulu Craton, which became attached to the southern margin of the larger Congo Craton during the Mesoproterozoic, involved a series of distinct convergent orogenic episodes affecting and reworking its southern (passive) margin. The mismatch in timing of Mesoproterozoic orogenic activity along the Bangweulu Craton, compared to that on the margins of the Kalahari, is compatible with the notion that these continental fragments were not juxtaposed along these Mesoproterozoic belts and in their present-day relative positions at the time. Whether either of these central and southern African cratons did form part of Rodinia, however, remains a matter for debate.

INTRODUCTION

The Irumide Belt is an east-northeast-trending orogenic belt situated on the southern margin of the Bangweulu Block, part of the Congo Craton. It is composed of Paleoproterozoic basement and supracrustal units intruded by various granitoid suites. To the southwest, lithologies of the Irumide Belt are structurally overlain by Neopro-

* Tectonics Special Research Centre, Department of Applied Geology, Curtin University of Technology, GPO Box U1987, Perth, Western Australia 6845, Australia; (Present address: BDW, SRK Consulting, 10 Richardson Street, West Perth, Western Australia 6005, Australia, bdewaele@srk.com.au)
** The Geological Survey of Western Australia, 100 Plain Street, East Perth, Western Australia 6004, Australia
*** Geology Department, School of Mines, University of Zambia, P.O. BOX 32379, Lusaka, Zambia
§ Geology Department, University of Namibia, Windhoek, Namibia
§§ GEMOC Key Centre, Department of Earth and Planetary Sciences, Macquarie University, New South Wales 2109, Australia

terozoic nappes of the Lufilian Belt (in the literature also referred to as Lufilian Arc, Katangan Belt or central African Copperbelt) and the Zambezi Belt (fig. 1A), making precise delineation of the southwestern margin of the Irumide Belt tenuous. Local tectonic windows through the Neoproterozoic cover occur south of the Mwembeshi Shear Zone (figs. 1A and B) and indicate the presence of Mesoproterozoic units below the Zambezi Belt (Mpande Gneiss, 1.10 Ga, Hanson and others, 1988; Munali Granite, 1.09 Ga, Katongo and others, 2004), but their relation to the Irumide Belt proper remains unclear. Farther southwest, the Choma-Kalomo Block comprises Mesoproterozoic granitoids dated at 1.38 and 1.18 Ga (Bulambo and others, 2004, 2006). To the northeast, Irumide structures are truncated by Neoproterozoic shear zones within the reactivated Paleoproterozoic Ubendian Belt (fig. 1B). Possible correlations between units in the Irumide Belt and lithologies farther southeast are hampered by the intervening Phanerozoic Karoo graben (fig. 1B) and, until recently, a lack of reliable geochronological data, especially to the southeast of the graben.

The Irumide Belt was first described by Ackermann (1950, 1960) as a fold and thrust belt, which showed a marked divergence from northwest-directed thrusting towards a foreland in the Bangweulu Block to southeast-directed back-thrusting towards the terranes of the Zambezi and Southern Irumide belts that were overprinted during subsequent Neoproterozoic tectonism. Ackermann (1950, 1960) recognized a crystalline basement, termed the Mkushi Gneiss, unconformably, and in places structurally, overlain by a metasedimentary succession of quartzite and metapelite called "die Muva". Later mapping revealed that the Mkushi Gneiss and the Muva were intruded by various granitoid plutons (Stillman, 1965), while the Muva itself comprised amphibolite- and greenschist-facies components. Daly and Unrug (1982) proposed the name Muva Supergroup to include all pre-Neoproterozoic sedimentary successions of northern Zambia. The terms Kanona Group and Manshya River Group were formalized by De Waele and Mapani (2002) to denote the deformed metasedimentary sequences of the Muva Supergroup within the southwestern and northeastern Irumide Belt respectively (see fig. 1B). The Irumide Belt was interpreted by Daly (ms, 1986) as a thin-skinned fold- and thrust belt, with northwest-directed tectonic transport, in which extensive crustal shortening was accommodated through tight folding and thrusting within the Irumide Belt and along lateral shear zones within the Ubendian Belt. Back-thrusting described by Ackermann (1950) in the southwestern Irumide Belt was interpreted by Daly (ms, 1986) as a pop-up structure within an overall northwest-directed tectonic regime. The absence of reliable geochronological constraints has for a long time hampered a detailed understanding of the geological evolution of the Irumide Belt. Neither the age of basement units, the depositional age and detrital provenance of the Kanona and Manshya River groups, the age of granitoid rocks intruding both basement and supracrustals, and the timing of tectonism were constrained until recent years (see Ph. D. dissertation of De Waele, 2005).

This contribution presents zircon U-Pb SHRIMP and Laser Ablation Lu-Hf data on granitoid magmatism in the Irumide Belt, and ages of zircon xenocrysts within these intrusions, which constrain the age of cryptic basement components within the Irumide Belt. The geochronological database reported here refines and supersedes preliminary ages reported in De Waele and others (2003, 2006a, 2006b) and Johnson and others (2005b). Detailed descriptions of the samples and treatment of the data are also reported in the Ph. D. dissertation of De Waele (2005).

Geology and previous geochronology of the Irumide Belt

The following major lithotectonic components have been recognized within the Irumide Belt: (a) a gneissic granitoid basement complex that has yielded Paleoproterozoic (2.05–1.96 Ga) and subordinate Archean (2.7 Ga) crystallization ages; (b) the 1.94 to 1.66 Ga Kanona and Manshya River Group metasedimentary succession of quartzite

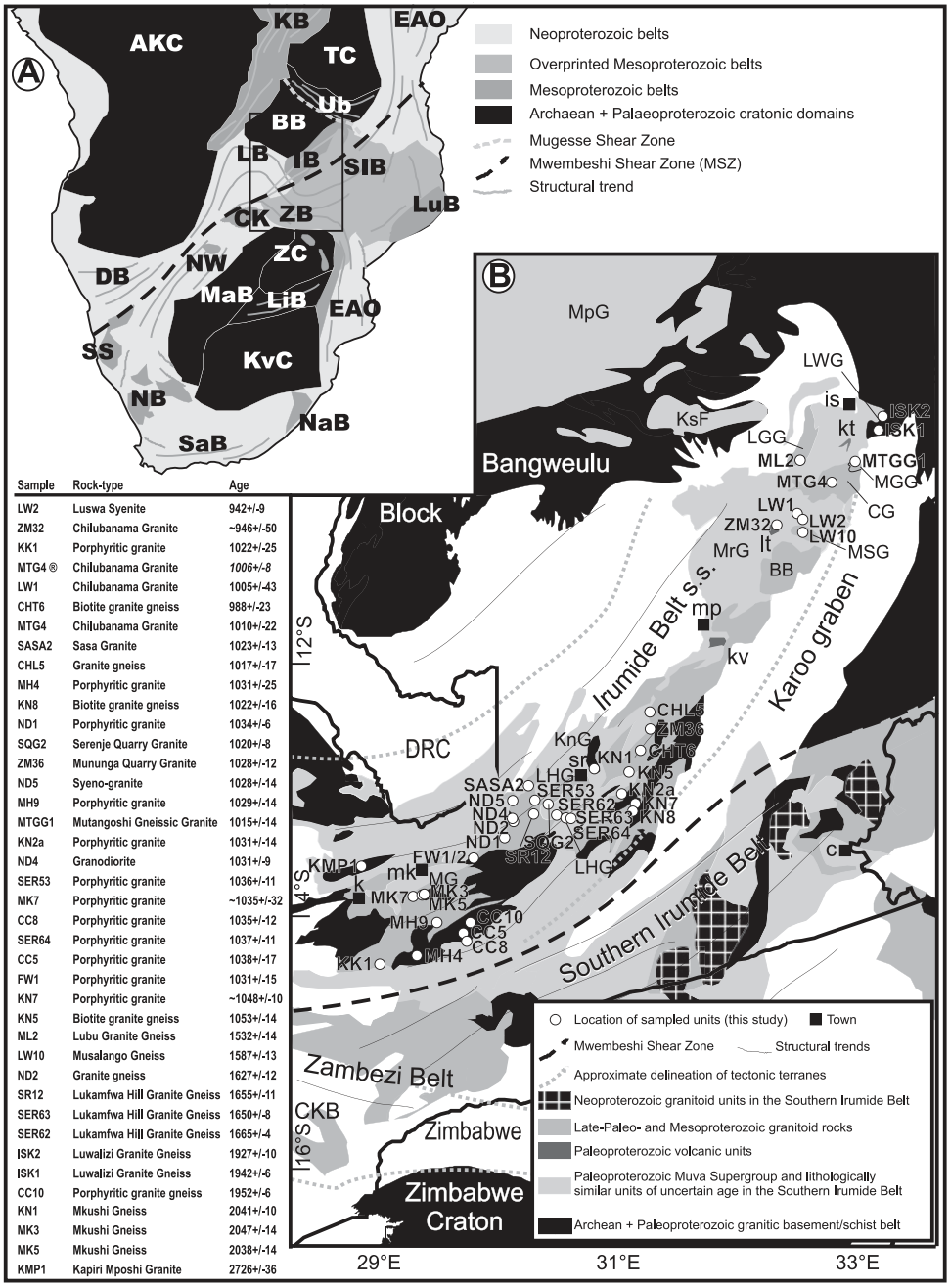

Sample	Rock-type	Age
LW2	Luswa Syenite	942+/-9
ZM32	Chilubanama Granite	~946+/-50
KK1	Porphyritic granite	1022+/-25
MTG4 ®	Chilubanama Granite	*1006+/-8*
LW1	Chilubanama Granite	1005+/-43
CHT6	Biotite granite gneiss	988+/-23
MTG4	Chilubanama Granite	1010+/-22
SASA2	Sasa Granite	1023+/-13
CHL5	Granite gneiss	1017+/-17
MH4	Porphyritic granite	1031+/-25
KN8	Biotite granite gneiss	1022+/-16
ND1	Porphyritic granite	1034+/-6
SQG2	Serenje Quarry Granite	1020+/-8
ZM36	Mununga Quarry Granite	1028+/-12
ND5	Syeno-granite	1028+/-14
MH9	Porphyritic granite	1029+/-14
MTGG1	Mutangoshi Gneissic Granite	1015+/-14
KN2a	Porphyritic granite	1031+/-14
ND4	Granodiorite	1031+/-9
SER53	Porphyritic granite	1036+/-11
MK7	Porphyritic granite	~1035+/-32
CC8	Porphyritic granite	1035+/-12
SER64	Porphyritic granite	1037+/-11
CC5	Porphyritic granite	1038+/-17
FW1	Porphyritic granite	1031+/-15
KN7	Porphyritic granite	~1048+/-10
KN5	Biotite granite gneiss	1053+/-14
ML2	Lubu Granite Gneiss	1532+/-14
LW10	Musalango Gneiss	1587+/-13
ND2	Granite gneiss	1627+/-12
SR12	Lukamfwa Hill Granite Gneiss	1655+/-11
SER63	Lukamfwa Hill Granite Gneiss	1650+/-8
SER62	Lukamfwa Hill Granite Gneiss	1665+/-4
ISK2	Luwalizi Granite Gneiss	1927+/-10
ISK1	Luwalizi Granite Gneiss	1942+/-6
CC10	Porphyritic granite gneiss	1952+/-6
KN1	Mkushi Gneiss	2041+/-10
MK3	Mkushi Gneiss	2047+/-14
MK5	Mkushi Gneiss	2038+/-14
KMP1	Kapiri Mposhi Granite	2726+/-36

Fig. 1. (A) Simplified regional tectonic map of central and southern Africa (modified after Hanson, 2003) showing the approximate location of figure 1(B); AKC=Angola-Kasai Craton; BB=Bangweulu Block; CK=Choma-Kalomo Block; DB=Damara Belt; EAO=East African Orogen; IB=Irumide Belt; KB=Kibaran Belt; KvC=Kaapvaal Craton; LB=Lufilian Belt; LiB=Limpopo Belt; LuB=foreland to the Lurio Belt; MaB=Magondi Belt; NaB=Natal Belt; NB=Namaqua Belt; NW=northwest Botswana Rift; SIB=Southern Irumide Belt; SS=Sinclair Sequence; SaB=Saldania Belt; TC=Tanzania Craton; Ub=Ubendian-Usagaran Belt; ZB=Zambezi Belt; ZC=Zimbabwe Craton. (B) Regional geological map of central Zambia showing location and age of samples in this study; abbreviations used: BB=Bemba Batholith (also known as Lufila Granite); CG=Chilubanama Granite; KnG=Kanona Group; KsF=Kasama Formation; LGG=Lubu Granite Gneiss; LHG=Lukamfwa Hill Granite Gneiss; LWG=Luwalizi Granite Gneiss; MG=Mkushi Gneiss; MpG=Mporokoso Group; MrG=Manshya River Group; kv=Katibunga Volcanic rocks; lt=Luswa Tuff; kt=Kachinga Tuff. Location names: c=Chipata; is=Isoka; k=Kapiri Mposhi; mk=Mkushi; mp=Mpika; sr=Serenje. The sample denoted with ® reflects the age of low Th/U metamorphic zircon rims.

and metapelite, which forms part of the regionally defined Muva Supergroup of Daly and Unrug (1982), and in which volcanic units have been dated at between 1.88 and 1.85 Ga; (c) 1.66 and 1.52 Ga granitoid plutons that intrude the Kanona and Manshya River groups; and (d) 1.05 and 0.95 granitoid bodies emplaced during, and immediately following the Irumide Orogeny. These are described in more detail in the following sections.

Basement Units to the Muva Supergroup

Granitic basement identified in the Irumide Belt is referred to as the Mkushi Gneiss in the southwest (De Waele and Mapani, 2002), and the Mwambwa River, Lubu and Luwalizi Granite Gneiss in the northeast (MSG and LGG on fig. 1B, Daly, 1995a, 1995b). Similar basement units described further northeast, and referred to as the Mulungwizi Gneiss (Van Tuijl and Verhoog, 1995; Verhoog and Van Tuijl, 1995a, 1995b) and the Nyika Granite (Dodson and others, 1975; Vrána and others, 2004) form part of the Paleoproterozoic Ubendian Belt and are not further described here. The Mkushi Gneiss comprises a complex of deformed granitoid gneisses occurring throughout much of the southwestern part of the Irumide Belt (Rainaud and others, 2002, 2003, 2005). Previously reported zircon U-Pb dating has shown that similar basement extends westwards underneath the Lufilian Belt within the Domes region of the Copperbelt. This basement comprises granitic rocks dated between 2.05 and 1.97 Ga and a volcano-plutonic suite with crystallization ages between 1.88 and 1.87 Ga (Ngoyi and others, 1991; John and others, 1999; John, ms, 2001; Key and others, 2001; Rainaud and others, 2002, 2003, 2005). The Mkushi Gneiss itself is best exposed in a large quarry south of Mkushi (location labelled MG on fig. 1B), where it is biotite-bearing, and intruded by pink biotite granite and numerous large cupriferous aplites. Even though the entire complex is strongly deformed, the expression of foliation ranges from weak to extremely strong. Heterogeneous strain distribution led to the occurrence of gradational zones from mylonitic gneiss to coarse phenocrystic granite within the same gneiss body, which prompted many previous authors to include all granitoids into the Mkushi Gneiss (for example Stillman, 1965; Smith, 1966; Cvetcovic, 1973). Locally, however, sharp intrusive contacts can be observed between largely undeformed porphyritic granitoids and the Mkushi Gneiss, and intrusive contacts between phenocrystic granite and the metasedimentary successions, showing that at least some of the granitoid units post-date the Mkushi Gneiss Complex and the deposition of the regionally defined Muva Supergroup.

The basement underneath the northeastern Irumide Belt comprises deformed granitic gneiss units, which were called the Lubu and Luwalizi Granite Gneiss (LGG and LWG respectively on fig. 1B, Daly, ms, 1986). The Luwalizi Granite Gneiss yielded zircon U-Pb SHRIMP crystallization ages between 1.94 and 1.93 Ga, but the Lubu Granite Gneiss yielded a much younger age of 1.55 Ga (De Waele and others, 2003, 2006a, 2006b) indicating it post-dates deposition of at least part of the Muva Supergroup and does not form part of the basement.

Metasedimentary Successions of the Irumide Belt

The Muva Supergroup extends from the northwest foreland of the Irumide Belt (Bangweulu Block) into the Irumide Belt itself. Within the Irumide Belt, the Muva Supergroup is polydeformed and metamorphosed, whereas in the foreland it is little deformed and virtually unmetamorphosed. Within the Irumide Belt, the stratigraphy has been simplified into two groups, the Kanona Group in the southwest and the Manshya River Group in the northwest (KnG and MrG respectively on fig. 1B, De Waele and Mapani, 2002; De Waele and Fitzsimons, 2007). In unmetamorphosed foreland and lower-grade parts within the northeastern Irumide Belt, the succession has been described as a sequence of alternating quartzites and pelites, the purity,

sorting and primary fabrics of which indicate shallow marine to coastal deposition (Daly and Unrug, 1982). Various conglomeratic units occur, but never over a wide enough area to allow them to be used as marker beds. The thickness of the sedimentary pile in the foreland has been estimated to be up to 6 kilometers. In the Irumide Belt itself this increases to 12 kilometers (Mapani, 1999) due to tectonic duplication during Irumide tectonics. High metamorphic grades, especially towards the internal portions of the Irumide Belt to the southeast, are locally expressed by anatexis of the metasedimentary pile, giving rise to formation of migmatite and paragneiss. Some isolated small occurrences of conformable rhyolitic units have been reported within the Manshya River Group in the northeast (Mosley and Marten, 1979; Daly, 1995b; Sykes, 1995). The most extensive occurrence, the Kachinga tuff, is located south of Isoka (kt on fig. 1B) and comprises a thinly layered sequence of recrystallized rhyolitic tuff of an estimated thickness of 300 meters. Smaller occurrences include the Luswa River Tuff southwest of Chinsali and the Katibunga volcanics southeast of Mpika (lt and kv on fig. 1B). Samples collected from these three locations yielded zircon U-Pb SHRIMP ages between 1.88 and 1.85 Ga, dating the age of deposition at these stratigraphic levels (De Waele, ms, 2005; De Waele and Fitzsimons, 2007).

Post-Muva Supergroup Granitoid Intrusions

Various granitoid bodies, now recognized to post-date deposition of the Muva Supergroup, have been described from the northern Irumide Belt. In the past, these were erroneously attributed to the Paleoproterozoic basement complex. These granitoid bodies can be distinguished into pre-tectonic and late-tectonic suites with respect to the Irumide Orogeny, based on internal fabrics, intrusive relationships, and the occurrence and character of xenoliths they contain. Pre-Irumide bodies are strongly deformed into granite gneiss, with or without feldspar augen, whereas late-Irumide bodies are only weakly foliated. A large proportion of granite bodies, both pre- and late-Irumide, are megacrystic with microcline phenocrysts of several tens of centimeters.

Pre-Irumide Granitoid Bodies Intruding the Basement and Muva Supergroup

Pre-Irumide granitoid bodies that post-dated deposition of the Muva Supergroup are known as the Mutangoshi Gneissic Granite and Musalango Gneiss in the northeast (MSG on fig. 1B), and the Lukamfwa Hill Granite Gneiss in the southwest (LHG on fig. 1B). These consist of strongly foliated, in places migmatitic, biotite granite gneiss, which often contain xenoliths of mafic composition and are cut by various mafic dikes and pegmatites. Coarser varieties contain K-feldspar phenocrysts, and are imparted with a strong biotite foliation, which predominantly affects the matrix, but in places gives rise to a distinct augen texture. Four samples from the Lukamfwa Hill Granite suite yielded preliminary zircon U-Pb SHRIMP crystallization ages between 1.66 and 1.63 Ga (De Waele and others, 2003, 2006a, 2006b; De Waele, ms, 2005), but two strongly tectonized samples of the Mutangoshi Gneissic Granite yielded crystallization ages of between 1.98 and 1.95 Ga, with growth of metamorphic zircon between 1.06 and 1.03 Ga (De Waele, ms, 2005; De Waele and others, 2006a). A previously reported whole-rock Rb-Sr date for the Mutangoshi Gneissic Granite of 1407 ± 33 Ma reported by Daly (ms, 1986) is therefore reinterpreted to reflect a partially reset and mixed age to which no geological interpretation can be ascribed. The Musalango Gneiss yielded a preliminary zircon U-Pb crystallization age of 1.61 Ga (recalculated here as 1587 ± 13 Ma) and is therefore slightly younger than the Lukamfwa Hill Granite Gneiss of the southwestern Irumide Belt (De Waele and others, 2006a). The Lubu Granite Gneiss, previously considered a part of the Paleoproterozoic basement (Daly, ms, 1986), yielded a preliminary crystallization age of 1.55 Ga (De Waele and others, 2003, 2006a, 2006b), recalculated here to 1532 ± 14 Ma.

Irumide Granitoid Bodies

The 1.05 to 0.95 Ga Irumide granitoid rocks form batholiths and smaller plutonic bodies, composed of coarse biotite granite, leucogranite and syeno-granite. They show evidence of extensive crustal assimilation, and contain numerous mafic and felsic inclusions, xenoliths and large rafts of country rock, including metasedimentary rocks which could have been derived from the Muva Supergroup. In the northeast, the young granites are known as the Bemba Batholith [or Lufila granite, (Daly, ms, 1986), marked BB on fig. 1B], the Kaunga Granite, and the Chilubanama Granite [or Grey Granite, (Daly, ms, 1986), marked CG on fig. 1B]. In the southwest, the granites have often been ascribed to the Mkushi Gneiss Complex, and are represented by voluminous intrusions of porphyritic granite with clear intrusive relationship with the Mkushi Gneiss, the Muva Supergroup and the Lukamfwa Hill Granite Gneiss. Preliminary age data were reported by De Waele and others (2003, 2006a, 2006b) and bracket magmatism between 1.05 and 0.95 Ga.

U-Pb SHRIMP METHODOLOGY

Granitoid lithologies that range from undeformed to foliated were sampled from across the belt (refer for zircon characteristics to table 1, and for sample localities to fig. 1B and table 2). Zircon was extracted using conventional crushing and sieving over a 300μm mesh, followed by density and magnetic separation. Individual zircon grains were hand picked under binocular microscope, and mounted together with CZ3 zircon standard in epoxy resin mount, polished and gold coated. The mount was imaged using transmitted, reflected and cathodo-luminescence (CL) imaging, and analysis spots selected (Representative CL and optical images are presented in fig. 2). The mount was loaded into the SHRIMP [an acronym of "Sensitive High (mass) Resolution Ion MicroProbe"] sample lock 24 hours before actual analysis, and pumped to high vacuum to minimize hydrogen interferences. Each analyzed spot was rastered with the primary ion beam for 90 to 120 seconds prior to analysis, to reduce surface-related contamination. Analyses were conducted during several sessions, with standards interspersed at a one to four ratio, approximately one every 90 minutes. Count/delay times (seconds) on each mass were Zr_2O (2/4), ^{204}Pb (10/1), background (10/1), ^{206}Pb (10/1), ^{207}Pb (30/1), ^{208}Pb (10/1), ^{238}U (5/3), ThO_2 (5/2) and UO_2 (2/2). Data were reduced using SQUID and ISOPLOT (Ludwig, 2001a, 2001b). Corrections for common lead were based on measured ^{204}Pb, and assuming an isotopic composition appropriate for the age of the sample (Stacey and Kramers, 1975). Common Pb (or Pb_c) is reported as the proportion of non-radiogenic ^{206}Pb in total ^{206}Pb (f_{206}). The standard used was a gem zircon called CZ3, for which a uranium content of 551 ppm and age of 564 Ma were assumed, corresponding to a $^{206}Pb/^{238}U$ ratio of 0.09143 (Pidgeon and others, 1994). The error on the decay constant has been propagated in the age calculations, but the error on the standard was not included where analyses were conducted in a single session. Where analyses obtained during several sessions were combined, however, the standard error was added in quadrature to the data. Standard errors are quoted in the data tables for each session. All ages are reported at the 2σ (or 95%) confidence level, but spot ages in the tables are reported at 1σ level. The data are shown in figure 3 and figures 5 through 12 as Tera-Wasserburg plots, with error crosses at 2σ confidence level. Analyses indicated in gray were not included in the calculation of a pooled age.

Lu-Hf METHODOLOGY

Hf-isotope analyses were conducted on separate zircon grain mounts, that is on zircons from the same separates as those used for SHRIMP analysis. The setup comprised a 213 nm Nd:YAG laser microprobe attached to a Nu Plasma multi-collector

Table 1

Sample location and characteristics of zircon from the Irumide Belt, Zambia

Sample	Size (μm)	Aspect-ratio	Shape	Clarity	Color	CL-response and zoning	Interpretation
KMP1	100-250	2:1 - 4:1	euhedral	clear, minor inclusions	pale yellow	Low- to high CL; oscillatory zoning, narrow high CL rims	Magmatic zircon
MK3	200-350	2:1 - 4:1	euhedral	clear	pale yellow	Low- to high CL; oscillatory zoning, some low CL rims with "ghost" concentric zoning	Magmatic zircon, some secondary rim overgrowths
MK5	50-300	1:1 - 3:1	euhedral	clear, minor inclusions	pale yellow	Low- to high CL; oscillatory zoning, some high CL zoned core domains	Magmatic zircon
CC10	100-300	2:1 - 3:1	euhedral	clear, minor inclusions	pale yellow	Low- to high CL; oscillatory zoning	Magmatic zircon
KN1	100-400	1:1 - 3:1	euhedral	clear, some small inclusions	pale yellow-light brown	Low- to medium CL with some high CL zoned core domains	Magmatic zircon
ISK1	100-500	1:1 - 5:1	subhedral to euhedral	clear, minor inclusions	pale to dark brown	Low- to high CL; broad oscillatory zoning, some narrow high CL rims	Magmatic zircon
ISK2	100-300	1:1 - 2:1	subhedral to euhedral	clear, some small inclusions	colorless to pale brown	Low- to high CL; broad oscillatory zoning	Magmatic zircon
MTGG1	100-300	2:1 - 6:1	euhedral	clear, some small inclusions	colorless to pale yellow	Low- to high CL; oscillatory zoning, some broad low CL rims	Magmatic zircon, some secondary rim overgrowths
SR62	100-300	2:1 - 4:1	euhedral	clear, minor inclusions	colorless to pale yellow	Low- to high CL; oscillatory zoning	Magmatic zircon
SR63	50-300	1:1 - 4:1	euhedral	clear, minor inclusions	pale yellow to brownish	Low- to medium CL; oscillatory zoning	Magmatic zircon
SR12	100-350	2:1 - 5:1	euhedral	clear, minor inclusions	colorless to pale yellow	Medium- to high CL; vague oscillatory zoning	Magmatic zircon
ND2	100-300	3:1 - 5:1	euhedral	clear, minor inclusions	colorless to dark yellow	Low- to medium CL; oscillatory zoning	Magmatic zircon
ML2	100-300	1:1 - 3:1	euhedral	turbid, many inclusions	dark yellow to brownish	Low- to medium CL; faint to clear oscillatory zoning, some solid-state recrystallization	Magmatic zircon
LW10	100-200	1:1 - 3:1	euhedral	clear, minor inclusions	yellow to light-brown	Low- to high CL; oscillatory and sector zoning with homogenized zones	Magmatic zircon
KK1	200-400	2:1 - 4:1	euhedral	clear, minor inclusions	colorless to pale yellow	Medium- to high CL; oscillatory zoning	Magmatic zircon
MH4	150-250	3:1 - 5:1	euhedral	clear, minor inclusions	colorless to pale yellow	Low- to high CL; oscillatory zoning	Magmatic zircon
MH9	200-350	3:1 - 4:1	euhedral	clear, minor inclusions	colorless to pale yellow	Medium- to high CL; oscillatory zoning	Magmatic zircon
CC5	150-250	2:1 - 4:1	euhedral	clear, minor inclusions	colorless to pale yellow	Low- to high CL; oscillatory zoning	Magmatic zircon

Table 1
(continued)

Sample	Size (μm)	Aspect-ratio	Shape	Clarity	Color	CL-response and zoning	Interpretation
CC8	200-300	3:1 - 4:1	euhedral	clear, minor inclusions	colorless to pale yellow	Low- to high CL; oscillatory zoning	Magmatic zircon
MK7	100-250	2:1 - 3:1	euhedral	clear, minor inclusions	colorless to pale yellow	Low- to high CL; oscillatory zoning. Some low CL, unzoned rim overgrowths	Magmatic zircon, some metamorphic rim overgrowths
ND1	100-300	3:1 - 5:1	subhedral to euhedral	turbid, some inclusions	yellowish to brownish	Lo-CL and high-CL grains. Faint concentric zoning in low-CL sectors.	Magmatic zircon
ND4	200-400	1:1 - 2:1	euhedral	clear, minor inclusions	colorless to pale yellow	Low- to high CL; oscillatory zoning	Magmatic zircon
ND5	200-300	2:1 - 4:1	euhedral	clear, minor inclusions	colorless to pale yellow	Low- to high CL; oscillatory zoning	Magmatic zircon
FW1	200-350	3:1 - 4:1	euhedral	clear, minor inclusions	pale yellow	Low- to medium CL; oscillatory zoning	Magmatic zircon
FW2	100-300	1:1 - 4:1	subhedral to euhedral	clear to turbid, minor inclusions	colorless to brownish	Low- to high CL; oscillatory zoning. Complex grains with core-rim sectors ± small low CL overgrowths	Magmatic zircon, xenocrystic cores
SASA2	50-150	1:1 - 3:1	subhedral to euhedral	clear to turbid, minor inclusions	yellow to brownish	Low- to medium CL; oscillatory zoning. Some complex grains with oscillatory zoned core and rim	Magmatic zircon
SER53	150-400	2:1 - 4:1	euhedral	clear, minor inclusions	pale yellow	Low- to high CL; oscillatory zoning	Magmatic zircon
SER64	50-300	1:1 - 4:1	euhedral	clear, minor inclusions	pale yellow	Low- to high CL; oscillatory zoning. Some irregular cores overgrown by zoned rims	Magmatic zircon, some xenocrystic core
SQG2	100-300	2:1 - 5:1	euhedral	clear, minor inclusions	pale yellow	Low- to medium CL; oscillatory zoning	Magmatic zircon
KN2A	200-400	1:1 - 3:1	euhedral	clear, minor inclusions	colorless to pale yellow	Low- to medium CL; oscillatory zoning sometimes faint	Magmatic zircon
KN5	200-400	1:1 - 3:1	euhedral	clear, minor inclusions	pale yellow	Low- to high CL; oscillatory zoning. Some euhedral cores overgrown by zoned rims	Magmatic zircon
KN7	200-350	2:1 - 4:1	subhedral to euhedral	clear, minor inclusions	pale yellow	Low- to high CL; oscillatory zoning. Some complex core-rim relationships	Magmatic zircon, some xenocrystic cores
KN8	100-300	2:1 - 4:1	euhedral	clear, minor inclusions	colorless to pale yellow	Medium- to high CL; oscillatory zoning sometimes faint. Some core-rim pairs	Magmatic zircon, some xenocrystic cores
CHT6	200-500	3:1 - 6:1	euhedral	clear, minor inclusions	colorless to pale yellow	Medium- to high CL; oscillatory zoning sometimes faint.	Magmatic zircon
ZM36	150-300	2:1 - 3:1	euhedral	clear, minor inclusions	colorless to pale yellow	Medium- to high CL; clear oscillatory zoning	Magmatic zircon

Table 1
(continued)

Sample	Size (μm)	Aspect-ratio	Shape	Clarity	Color	CL-response and zoning	Interpretation
CHL5	150-400	3:1 - 6:1	euhedral	clear, minor inclusions	colorless to pale yellow	Low- to high CL; oscillatory zoning often faint	Magmatic zircon
LW1	100-300	2:1 - 3:1	euhedral	clear, minor inclusions	colorless to pale yellow	Low- to high CL; oscillatory zoning often faint	Magmatic zircon
LW2	150-250	1:1 - 2:1	anhedral	turbid, some inclusions	pale yellow to brown	Medium- to high CL; sector zoning and dark CL unzoned sectors	Magmatic zircon
MTG4	50-200	1:1 - 2:1	subhedral to euhedral	clear to turbid, minor inclusions	colorless to pale yellow	Low- to high CL; oscillatory zoning often faint. Some core-rim relationships. Rims low CL and unzoned	Magmatic zircon and xenocrystic core, some overgrown by metamorphic rims
ZM32	50-200	1:1 - 2:1	subhedral to euhedral	clear to turbid, minor inclusions	colorless to pale yellow	Low- to high CL; some oscillatory zoning and core-rim relationships.	Magmatic zircon and xenocrystic core, some overgrown by metamorphic rims

TABLE 2

Sample locations and zircon U-Pb SHRIMP data

Spot Name	f_{206} (%)	U (ppm)	Th (ppm)	Th/U	$^{207}Pb/^{206}Pb$ (±1σ)	$^{206}Pb/^{238}U$ (±1σ)	$^{207}Pb/^{206}Pb$ Age (±1σMa)	C(%)
Sample KMP1 : Kapiri Mposhi Granite Gneiss (13.7458 S - 28.6799 E)								
Analyses conducted during a single session. 10 CZ3 standard analyses yielded a 2σ error of the mean of 0.36%								
KMP1-1	0.160	361	109	0.31	0.18520±0.00058	0.49807±0.00196	2700.0±5.1	96.5
KMP1-2	5.328	300	192	0.66	0.23768±0.02128	0.60223±0.06121	3104.5±142.7	97.9
KMP1-1r	1.134	559	358	0.66	0.18360±0.00145	0.45528±0.00159	2685.7±13.0	90.1
KMP1-3	1.946	714	440	0.64	0.18677±0.00507	0.44983±0.00260	2713.9±44.7	88.2
KMP1-4	0.087	597	416	0.72	0.18951±0.00043	0.53337±0.00163	2737.9±3.7	100.6
KMP1-5	0.421	665	226	0.35	0.18727±0.00067	0.40214±0.00154	2718.3±5.9	80.2
Sample MK3 : Mkushi Gneiss (13.9367 S - 29.1490 E)								
Analyses conducted during a single session. 10 CZ3 standard analyses yielded a 2σ error of the mean of 0.36%								
MK3-1	0.038	228	194	0.88	0.12646±0.00066	0.36575±0.00188	2049.3±9.2	98.1
MK3-2r	0.024	770	56	0.08	0.12404±0.00047	0.35671±0.00101	2015.1±6.7	97.6
MK3-3r	0.002	891	88	0.10	0.12515±0.00034	0.36597±0.00100	2031.0±4.8	99.0
MK3-4r	0.000	137	122	0.91	0.12605±0.00082	0.36105±0.00244	2043.6±11.6	97.2
MK3-4c	0.089	466	411	0.91	0.12560±0.00054	0.32834±0.00133	2037.3±7.7	89.8
Sample MK5 : Mkushi Gneiss (13.9432 S - 29.1490 E)								
Analyses conducted during two sessions								
Session 1 : 10 CZ3 standard analyses yielded a 2σ error of the mean of 0.98%								
Session 2 : 10 CZ3 standard analyses yielded a 2σ error of the mean of 0.36%								
1MK5-1	0.167	569	351	0.64	0.12591±0.00064	0.35801±0.00496	2041.6±9.0	96.6
1MK5-2	0.013	681	369	0.56	0.12508±0.00027	0.36034±0.00460	2029.9±3.9	97.7
1MK5-3	0.712	687	408	0.61	0.12480±0.00065	0.31352±0.00400	2026.0±9.2	86.8
2MK5-4	0.090	804	367	0.47	0.12116±0.00048	0.32508±0.00095	1973.4±7.1	91.9
2MK5-5r	0.034	587	329	0.58	0.12669±0.00044	0.36302±0.00221	2052.5±6.2	97.3
2MK5-6	0.050	505	409	0.84	0.12639±0.00129	0.37341±0.00170	2048.3±18.0	99.9
2MK5-7	0.280	224	139	0.64	0.12665±0.00079	0.35236±0.00197	2051.9±11.0	94.8
Sample CC10 : Mkushi Gneiss (14.3932 S - 29.6785 E)								
Analyses conducted during a single session. 16 CZ3 standard analyses yielded a 2σ error of the mean of 2.10%								
CC10-1.1	0.000	693	612	0.91	0.12058±0.00034	0.37259±0.01464	1964.9±5.1	103.9
CC10-2.1	0.851	460	343	0.77	0.11507±0.00428	0.30681±0.01212	1881.0±67.0	91.7
CC10-3.1	0.163	514	296	0.60	0.11950±0.00046	0.35108±0.01380	1948.7±6.9	99.5
CC10-4.1	0.426	167	121	0.75	0.11864±0.00203	0.34657±0.01371	1935.9±30.6	99.1
CC10-5.1	0.051	403	283	0.72	0.11942±0.00050	0.33052±0.01300	1947.6±7.5	94.5
CC10-6.1	0.005	390	273	0.72	0.11898±0.00046	0.33719±0.01326	1940.9±6.9	96.5
Sample KN1 : Mkushi Gneiss (12.9652 S - 30.6258 E)								
Analyses conducted during a single session. 12 CZ3 standard analyses yielded a 2σ error of the mean of 1.56%								
KN1-1	0.002	335	198	0.61	0.12935±0.00067	0.30750±0.00816	2089.1±9.1	82.7
KN1-2	0.005	268	68	0.26	0.12518±0.00068	0.33974±0.00833	2031.3±9.6	92.8
KN1-3	0.041	307	112	0.38	0.12539±0.00056	0.36288±0.00896	2034.3±7.9	98.1
KN1-4	0.000	440	215	0.51	0.12547±0.00045	0.35235±0.00855	2035.5±6.4	95.6
KN1-5	0.000	414	200	0.50	0.12570±0.00044	0.37025±0.00899	2038.7±6.1	99.6
KN1-6	0.007	386	223	0.60	0.12647±0.00046	0.37061±0.00901	2049.4±6.4	99.2
Sample ISK1 : Luwalizi Granite Gneiss (10.2443 S - 32.8449 E)								
Analyses conducted during a single session. 15 CZ3 standard analyses yielded a 2σ error of the mean of 0.51%								
ISK1-1	0.029	253	179	0.73	0.11875±0.00068	0.33595±0.00342	1937.5±10.2	96.4
ISK1-2	0.028	2669	110	0.04	0.11800±0.00055	0.36163±0.00369	1926.1±8.3	103.3
ISK1-3	0.855	93	175	1.93	0.11577±0.00191	0.34508±0.00413	1892.0±29.8	101.0
ISK1-4	0.077	565	110	0.20	0.11893±0.00050	0.34189±0.00322	1940.1±7.6	97.7
ISK1-5	0.061	521	109	0.22	0.11895±0.00042	0.34748±0.00325	1940.6±6.4	99.1
ISK1-6	0.212	945	169	0.19	0.11838±0.00110	0.32209±0.00634	1931.9±16.7	93.2
ISK1-7	0.000	504	204	0.42	0.11916±0.00038	0.34803±0.00340	1943.6±5.7	99.1
ISK1-8	0.060	396	156	0.41	0.11917±0.00050	0.33942±0.00345	1943.8±7.5	96.9
ISK1-9	0.194	785	595	0.78	0.12008±0.00122	0.34865±0.00318	1957.4±18.2	98.5
Sample ISK2 : Luwalizi Granite Gneiss (10.2030 S - 32.8094 E)								
Analyses conducted during a single session. 15 CZ3 standard analyses yielded a 2σ error of the mean of 0.51%								
ISK2-1	0.688	103	29	0.29	0.11666±0.00146	0.35250±0.00409	1905.7±22.5	102.1
ISK2-2	0.181	300	391	1.34	0.11926±0.00065	0.30654±0.00299	1945.2±9.8	88.6
ISK2-3	0.071	502	308	0.63	0.11781±0.00041	0.33415±0.00310	1923.3±6.2	96.6
ISK2-4	0.000	949	29	0.03	0.11919±0.00135	0.35460±0.01018	1944.2±20.2	100.6
ISK2-5	0.059	277	26	0.10	0.11879±0.00081	0.34057±0.00336	1938.1±12.2	97.5

TABLE 2
(continued)

Spot Name	f_{206} (%)	U (ppm)	Th (ppm)	Th/U	$^{207}Pb/^{206}Pb$ (±1σ)	$^{206}Pb/^{238}U$ (±1σ)	$^{207}Pb/^{206}Pb$ Age (±1σMa)	C(%)
Sample MTGG1 : Mutangoshi Gneiss (10.6796 S - 32.5138 E)								
Analyses conducted during a single session. 16 CZ3 standard analyses yielded a 2σ error of the mean of 0.81%								
MTGG1-1	0.025	1519	364	0.25	0.07177±0.00021	0.15839±0.00260	979.4±6.1	96.8
MTGG1-2	0.068	540	197	0.38	0.07304±0.00042	0.16698±0.00277	1015.1±11.6	98.1
MTGG1-3r	0.063	1265	217	0.18	0.07279±0.00027	0.16835±0.00276	1008.0±7.5	99.5
MTGG1-3c	0.643	264	112	0.44	0.12030±0.00099	0.34978±0.00586	1960.7±14.7	98.6
MTGG1-4c	0.000	227	107	0.49	0.07443±0.00059	0.16034±0.00274	1053.1±16.0	91.0
MTGG1-5	0.445	673	248	0.38	0.07256±0.00053	0.15909±0.00270	1001.7±14.8	95.0
MTGG1-6c	1.178	109	78	0.74	0.07366±0.00206	0.16557±0.00294	1032.1±56.7	95.7
MTGG1-6r	0.000	636	246	0.40	0.07369±0.00030	0.17452±0.00289	1033.0±8.2	100.4
MTGG1-7c	0.034	860	336	0.40	0.07352±0.00029	0.17377±0.00286	1028.3±8.0	100.4
MTGG1-7r	0.042	670	245	0.38	0.07349±0.00035	0.17052±0.00282	1027.5±9.7	98.8
MTGG1-8	0.000	291	160	0.57	0.07318±0.00053	0.17448±0.00294	1019.0±14.7	101.7
MTGG1-9	0.000	221	123	0.57	0.07380±0.00054	0.17427±0.00296	1036.1±14.7	100.0
MTGG1-11	0.091	1130	590	0.54	0.07357±0.00026	0.17951±0.00285	1029.7±7.2	103.3
MTGG1-12c	0.041	364	686	1.95	0.11992±0.00042	0.34793±0.00557	1955.1±6.2	98.4
MTGG1-13	2.942	2507	14	0.01	0.07241±0.00375	0.17572±0.00281	997.6±105.2	104.4
MTGG1-14	0.091	1130	590	0.54	0.07357±0.00026	0.17951±0.00285	1029.7±7.2	103.3
MTGG1-16c	3.491	112	101	0.93	0.12224±0.00468	0.35767±0.00608	1989.2±68.1	99.1
MTGG1-17	0.917	1329	533	0.41	0.07009±0.00113	0.13773±0.00219	930.9±33.2	88.1
MTGG1-19	8.217	1708	40	0.02	0.07313±0.01482	0.15059±0.00285	1017.6±410.4	87.5
MTGG1-20	0.091	1130	590	0.54	0.07357±0.00026	0.17951±0.00285	1029.7±7.2	103.3
MTGG1-21	0.000	273	144	0.55	0.07477±0.00044	0.18049±0.00292	1062.4±11.8	100.7
MTGG1-22	0.030	163	32	0.21	0.07279±0.00073	0.17983±0.00301	1008.0±20.5	105.4
MTGG1-25c	0.396	79	106	1.38	0.12150±0.00129	0.35993±0.00624	1978.3±18.9	100.2
Sample SER62c : Lukamfwa Hill Granite Gneiss (13.3121 S - 30.3506 E)								
Analyses conducted during a single session. 16 CZ3 standard analyses yielded a 2σ error of the mean of 1.18%								
SER62-26c	0.989	65	53	0.84	0.10376±0.00389	0.30047±0.00779	1692.5±69.2	100.1
SER62-26r	0.047	770	452	0.61	0.10228±0.00028	0.28729±0.00622	1665.8±5.0	97.7
SER62-27	0.146	316	326	1.07	0.10317±0.00056	0.29634±0.00664	1681.8±10.0	99.5
SER62-29	0.246	100	81	0.84	0.10405±0.00191	0.26150±0.00583	1697.6±33.8	88.2
SER62-32	0.040	2804	2342	0.86	0.10179±0.00027	0.28702±0.00617	1657.1±4.9	98.2
SER62-36	0.368	588	214	0.38	0.10021±0.00041	0.26012±0.00566	1627.9±7.6	91.6
SER62-37	0.108	489	390	0.82	0.10257±0.00070	0.30040±0.00676	1671.1±12.6	101.3
SER62-40	0.433	112	125	1.16	0.10214±0.00179	0.29847±0.00660	1663.4±32.4	101.2
SER62-41c	14.976	3965	2136	0.56	0.10197±0.00801	0.10059±0.00293	1660.2±145.4	37.2
SER62-41r	0.542	148	98	0.69	0.10007±0.00198	0.29888±0.00661	1625.3±36.9	103.7
Sample SER63 : Lukamfwa Hill Granite Gneiss (13.3319 S - 30.3927 E)								
Analyses conducted during a single session. 16 CZ3 standard analyses yielded a 2σ error of the mean of 1.18%								
SER63-1	0.056	470	339	0.74	0.10201±0.00043	0.29684±0.00644	1661.0±7.8	100.9
SER63-2	0.183	320	259	0.84	0.10158±0.00092	0.29511±0.00721	1653.1±16.7	100.8
SER63-5	0.187	467	361	0.80	0.10014±0.00104	0.29069±0.00628	1626.6±19.3	101.1
SER63-6	0.062	378	309	0.84	0.10205±0.00074	0.29462±0.00654	1661.7±13.4	100.2
SER63-7	0.102	403	303	0.78	0.10176±0.00033	0.29662±0.00642	1656.6±6.0	101.1
SER63-8	0.359	331	356	1.11	0.10071±0.00214	0.28016±0.00610	1637.2±39.4	97.2
SER63-15	0.082	307	231	0.78	0.10193±0.00055	0.29725±0.00678	1659.6±10.0	101.1
SER63-19	0.178	280	211	0.78	0.09919±0.00125	0.27687±0.00631	1609.0±23.5	97.9
SER63-22	0.195	420	331	0.81	0.10099±0.00107	0.29160±0.00644	1642.3±19.7	100.4
SER63-29	0.057	501	288	0.59	0.10042±0.00070	0.27852±0.00635	1631.8±13.0	97.1
Sample SR12 : Lukamfwa Hill Granite Gneiss (13.2777 S - 30.1306 E)								
Analyses conducted during a single session. 5 CZ3 standard analyses yielded a 2σ error of the mean of 1.07%								
SR12-1	0.215	141	110	0.81	0.10132±0.00092	0.29495±0.00309	1648.4±16.8	101.1
SR12-2	0.000	198	204	1.07	0.10007±0.00155	0.28166±0.00288	1625.3±28.8	98.4
SR12-3	0.136	139	84	0.63	0.09898±0.00095	0.27508±0.00369	1604.9±17.9	97.6
SR12-4	0.067	179	138	0.79	0.10155±0.00076	0.29499±0.00294	1652.7±13.8	100.8
SR12-8	0.823	138	142	1.06	0.10024±0.00376	0.28273±0.00313	1628.6±69.7	98.6
SR12-9	0.093	103	117	1.17	0.10149±0.00121	0.29459±0.00361	1651.5±22.2	100.8
SR12-10	0.088	222	256	1.19	0.10082±0.00066	0.29085±0.00335	1639.3±12.2	100.4
Sample ND2 : Porphyrititic Granite Gneiss (13.4149 S - 29.8912 E)								
Analyses conducted during a single session. 14 CZ3 standard analyses yielded a 2σ error of the mean of 0.66%								
ND2-1	0.070	103	82	0.83	0.09989±0.00142	0.28323±0.00373	1622.0±26.5	99.1
ND2-2	0.000	185	144	0.80	0.10018±0.00061	0.29307±0.00349	1627.4±11.3	101.8
ND2-3	0.091	229	196	0.88	0.10031±0.00067	0.28161±0.00337	1629.7±12.5	98.1
ND2-4	0.025	181	154	0.88	0.10110±0.00097	0.28361±0.00661	1644.5±17.8	97.9

TABLE 2

(continued)

Spot Name	f_{206} (%)	U (ppm)	Th (ppm)	Th/U	$^{207}Pb/^{206}Pb$ (±1σ)	$^{206}Pb/^{238}U$ (±1σ)	$^{207}Pb/^{206}Pb$ Age (±1σMa)	C(%)
Sample ML2 : Lubu Granite Gneiss (10.4796 S - 32.4367 E)								
Analyses conducted during two sessions								
Session 1 : 5 CZ3 standard analyses yielded a 2σ error of the mean of 1.07%								
Session 2 : 9 CZ3 standard analyses yielded a 2σ error of the mean of 1.93%								
1ML2-1	0.070	171	279	1.69	0.09497±0.00075	0.25688±0.00261	1527.5±14.9	96.5
1ML2-8	0.232	262	517	2.04	0.09504±0.00078	0.25790±0.00252	1528.9±15.5	96.7
1ML2-5	3.913	326	572	1.81	0.09224±0.00632	0.25073±0.00259	1473.5±129.9	97.9
1ML2-10	4.250	256	445	1.80	0.09288±0.00432	0.23290±0.00240	1486.6±88.0	90.8
1ML2-11	3.107	284	472	1.72	0.09402±0.00362	0.21551±0.00211	1509.3±72.7	83.4
1ML2-12	0.777	415	687	1.71	0.09322±0.00157	0.24262±0.00223	1492.5±31.8	93.8
1ML2-13	1.260	195	322	1.70	0.09205±0.00175	0.23712±0.00240	1468.9±36.0	93.4
2ML2-21	0.037	265	498	1.94	0.09616±0.00069	0.26961±0.00638	1550.8±13.4	99.2
2ML2-22	4.673	283	461	1.68	0.10711±0.00822	0.21757±0.00524	1749.9±140.6	72.5
2ML2-23	0.725	319	407	1.32	0.09641±0.00160	0.24507±0.00579	1555.9±31.2	90.8
2ML2-24	0.392	348	568	1.69	0.09517±0.00095	0.25925±0.00610	1531.5±18.8	97.0
Sample LW10 : Musalango Gneiss (11.1352 S - 32.3463 E)								
Analyses conducted during two sessions								
Session 1 : 12 CZ3 standard analyses yielded a 2σ error of the mean of 0.65%								
Session 2 : 9 CZ3 standard analyses yielded a 2σ error of the mean of 1.93%								
1LW10-1	0.000	55	47	0.88	0.10202±0.00121	0.27148±0.00388	1661.2±22.0	93.2
1LW10-2	0.090	69	57	0.85	0.09954±0.00117	0.27964±0.00374	1615.4±22.0	98.4
1LW10-3	0.150	75	63	0.87	0.09906±0.00134	0.27641±0.00360	1606.4±25.2	97.9
1LW10-4	0.426	50	36	0.75	0.09350±0.00189	0.27859±0.00412	1498.0±38.3	105.8
1LW10-5	0.280	64	42	0.67	0.09479±0.00177	0.25952±0.00354	1523.9±35.1	97.6
1LW10-6	0.212	115	85	0.76	0.09707±0.00115	0.27708±0.00327	1568.6±22.2	100.5
1LW10-7	1.840	84	55	0.67	0.08926±0.00295	0.23250±0.00303	1409.8±63.3	95.6
1LW10-9	0.034	64	55	0.89	0.09879±0.00115	0.27653±0.00465	1601.4±21.7	98.3
1LW10-10	1.601	59	45	0.79	0.09288±0.00312	0.27515±0.00397	1485.4±63.6	105.5
2LW10-11	0.132	164	96	0.60	0.09807±0.00129	0.27897±0.00670	1587.7±24.5	99.9
2LW10-12	0.205	48	35	0.76	0.10017±0.00194	0.27610±0.00719	1627.3±36.0	96.6
2LW10-13	0.335	82	83	1.05	0.09742±0.00192	0.26469±0.00658	1575.3±36.9	96.1
2LW10-14	0.176	93	83	0.93	0.10079±0.00283	0.27730±0.00687	1638.7±52.0	96.3
Sample KK1 : Porphyritic granite (14.2854 S - 28.5491 E)								
Analyses conducted during a single session. 10 CZ3 standard analyses yielded a 2σ error of the mean of 0.36%								
KK1-1	0.271	182	208	1.18	0.07202±0.00125	0.16528±0.00111	986.5±35.3	99.9
KK1-2	0.268	117	130	1.15	0.07107±0.00163	0.16747±0.00138	959.3±46.9	104.0
KK1-3	0.426	262	126	0.50	0.07244±0.00233	0.16346±0.00098	998.3±65.3	97.8
KK1-4	0.920	56	74	1.35	0.07090±0.00391	0.16310±0.00207	954.6±112.6	102.0
KK1-5	0.000	183	166	0.94	0.07316±0.00073	0.17005±0.00112	1018.3±20.3	99.4
KK1-6	0.000	171	189	1.15	0.07442±0.00076	0.16554±0.00112	1052.8±20.7	93.8
Sample MH4 : Porphyritic granite (14.4302 S - 29.1847 E)								
Analyses conducted during two sessions								
Session 1 : 10 CZ3 standard analyses yielded a 2σ error of the mean of 0.98%								
Session 2 : 10 CZ3 standard analyses yielded a 2σ error of the mean of 0.36%								
1MH4-1	0.089	88	77	0.90	0.07264±0.00091	1.71845±0.03341	1003.9±25.4	101.7
1MH4-2	2.762	167	124	0.76	0.07159±0.00290	1.00004±0.04290	974.4±82.5	63.8
1MH4-3	0.142	394	636	1.67	0.07331±0.00091	1.72059±0.04192	1022.6±25.1	99.1
2MH4-4	0.743	1418	444	0.32	0.07233±0.00160	1.42415±0.03171	995.4±44.9	86.4
2MH4-5	1.938	425	206	0.50	0.07493±0.00734	1.54638±0.15199	1066.7±197.0	84.3
2MH4-6	0.127	301	168	0.58	0.07465±0.00073	1.61686±0.01781	1059.0±19.7	88.8
Sample MH9 : Porphyritic granite (14.1685 S - 28.3297 E)								
Analyses conducted during two sessions								
Session 1 : 10 CZ3 standard analyses yielded a 2σ error of the mean of 0.98%								
Session 2 : 10 CZ3 standard analyses yielded a 2σ error of the mean of 0.36%								
1MH9-1	0.133	363	294	0.84	0.07346±0.00065	1.67234±0.02688	986.2±31.0	99.9
1MH9-2	0.253	120	79	0.68	0.07302±0.00183	1.69526±0.04895	1050.4±30.6	95.5
1MH9-3	0.019	615	452	0.76	0.07418±0.00032	1.79513±0.02427	1077.0±14.6	96.8
2MH9-4	1.354	696	504	0.75	0.07486±0.00656	1.75921±0.15444	1064.7±176.1	95.3
2MH9-5	0.041	491	343	0.72	0.07386±0.00048	1.71359±0.01305	1037.8±13.1	96.6
2MH9-6	0.037	808	632	0.81	0.07342±0.00037	1.76861±0.01042	1025.6±10.1	101.2
2MH9-7	0.125	628	442	0.73	0.07333±0.00059	1.77452±0.01590	1023.1±16.2	101.9
2MH9-1	0.133	363	294	0.84	0.07346±0.00065	1.67234±0.02688	986.2±31.0	99.9

TABLE 2
(continued)

Spot Name	f_{206} (%)	U (ppm)	Th (ppm)	Th/U	$^{207}Pb/^{206}Pb$ (±1σ)	$^{206}Pb/^{238}U$ (±1σ)	$^{207}Pb/^{206}Pb$ Age (±1σMa)	C(%)
Sample CC5 : Porphyritic granite (14.2762 S - 28.5858 E)								
Analyses conducted during a single session. 16 CZ3 standard analyses yielded a 2σ error of the mean of 2.10%								
CC5-1	0.098	327	151	0.48	0.07301±0.00078	0.17914±0.00706	1014.2±21.7	104.7
CC5-2	0.000	145	57	0.40	0.07454±0.00109	0.17549±0.00697	1056.0±29.4	98.7
CC5-3.1	0.000	195	102	0.54	0.07671±0.00110	0.17598±0.00699	1113.6±28.5	93.8
CC5-3.2	0.684	338	204	0.62	0.07234±0.00186	0.16622±0.00660	995.5±52.3	99.6
CC5-4	0.000	311	133	0.44	0.07398±0.00071	0.17326±0.00685	1040.9±19.3	99.0
CC5-5	0.000	198	110	0.57	0.07375±0.00071	0.17047±0.00674	1034.7±19.5	98.1
Sample CC8 : Porphyritic granite (14.3956 S - 28.5872 E)								
Analyses conducted during a single session. 16 CZ3 standard analyses yielded a 2σ error of the mean of 2.10%								
CC8-1	0.000	476	214	0.46	0.07414±0.00053	0.17374±0.00683	1045.3±14.4	98.8
CC8-2	0.000	257	139	0.56	0.07360±0.00062	0.16806±0.00664	1030.4±17.0	97.2
CC8-3	0.000	393	178	0.47	0.07376±0.00050	0.17462±0.00687	1034.8±13.8	100.3
CC8-4	0.000	406	260	0.66	0.07421±0.00049	0.17340±0.00682	1047.2±13.2	98.4
CC8-5	0.652	361	164	0.47	0.07191±0.00146	0.15855±0.00625	983.3±41.3	96.5
CC8-6	0.063	570	230	0.42	0.07341±0.00048	0.17011±0.00668	1025.4±13.3	98.8
Sample MK7 : Porphyritic granite (13.9592 S - 29.1176 E)								
Analyses conducted during two sessions								
Session 1 : 10 CZ3 standard analyses yielded a 2σ error of the mean of 0.98%								
Session 2 : 10 CZ3 standard analyses yielded a 2σ error of the mean of 0.36%								
1MK7-1	0.660	199	415	2.16	0.07376±0.00118	1.65756±0.03473	1034.9±32.2	94.1
1MK7-2c	1.670	333	284	0.88	0.12323±0.00248	4.45448±0.10767	2003.4±35.8	74.9
1MK7-2r	0.530	1815	64	0.04	0.06881±0.00056	1.39160±0.02089	892.9±16.7	98.8
2MK7-3	1.569	261	422	1.67	0.07879±0.00201	1.59315±0.04186	1166.9±50.6	75.6
2MK7-4	1.296	192	228	1.23	0.07985±0.00253	1.28480±0.04190	1193.2±62.6	59.6
2MK7-5	2.088	1199	175	0.15	0.06873±0.00366	1.13515±0.06128	890.7±110.0	81.9
Sample ND1 : Porphyritic granite (13.4914 S - 29.8885 E)								
Analyses conducted during a single session. 14 CZ3 standard analyses yielded a 2σ error of the mean of 0.66%								
ND1-1	1.348	1300	486	0.39	0.07944±0.00934	0.16120±0.00216	1183.1±232.3	81.4
ND1-2	0.000	288	419	1.50	0.07371±0.00052	0.17831±0.00219	1033.5±14.3	102.3
ND1-3	0.777	238	266	1.16	0.08212±0.00285	0.16971±0.00211	1248.3±67.9	81.0
ND1-4	0.291	1057	481	0.47	0.07402±0.00165	0.17261±0.00190	1042.0±44.9	98.5
ND1-5r	0.512	999	532	0.55	0.07818±0.00160	0.16041±0.00176	1151.5±40.6	83.3
ND1-5c	0.003	1864	493	0.27	0.07314±0.00025	0.17789±0.00201	1017.7±6.9	103.7
ND1-7	4.316	1926	917	0.49	0.10095±0.02577	0.15316±0.00437	1641.7±473.8	56.0
ND1-8	6.367	1718	490	0.29	0.12801±0.08145	0.14736±0.00752	2070.8±1121.2	42.8
ND1-9	0.000	1977	55	0.03	0.07348±0.00021	0.17610±0.00203	1027.2±5.8	101.8
ND1-10	0.014	2459	1017	0.43	0.07322±0.00024	0.17671±0.00191	1020.2±6.6	102.8
Sample ND4 : Granodiorite (13.3736 S - 29.9484 E)								
Analyses conducted during a single session. 14 CZ3 standard analyses yielded a 2σ error of the mean of 0.66%								
ND4-1	0.000	324	370	1.18	0.07357±0.00053	0.17253±0.00205	1029.7±14.7	99.6
ND4-2	0.071	271	288	1.10	0.07353±0.00078	0.17504±0.00206	1028.7±21.6	101.1
ND4-3	0.071	398	650	1.69	0.07364±0.00053	0.17264±0.00200	1031.7±14.5	99.5
ND4-4	0.011	306	328	1.11	0.07444±0.00054	0.17156±0.00210	1053.5±14.5	96.9
Sample ND5 : Syeno-granite (13.2011 S - 29.9472 E)								
Analyses conducted during a single session. 14 CZ3 standard analyses yielded a 2σ error of the mean of 0.66%								
ND5-1	0.721	263	332	1.31	0.07687±0.00134	0.16182±0.00190	1117.9±34.8	86.5
ND5-2	0.097	230	311	1.39	0.07293±0.00090	0.17429±0.00208	1012.1±24.9	102.3
ND5-3	0.036	241	253	1.09	0.07347±0.00083	0.17202±0.00204	1027.0±23.0	99.6
ND5-4	0.623	242	401	1.72	0.07501±0.00128	0.16700±0.00204	1068.7±34.4	93.2
Sample FW1 : Porphyritic granite (13.6684 S - 29.6242 E)								
Analyses conducted during a single session. 7 CZ3 standard analyses yielded a 2σ error of the mean of 1.65%								
FW1-1	0.452	2020	422	0.22	0.07069±0.00064	1.69632±0.03287	948.5±18.5	109.1
FW1-2	0.108	1069	382	0.37	0.07417±0.00057	1.78742±0.03402	1046.0±15.6	99.3
FW1-3	0.484	203	359	1.82	0.07207±0.00183	1.77925±0.05690	988.0±51.6	107.5
FW1-4	1.112	389	499	1.32	0.07156±0.00266	1.64344±0.06824	973.4±75.9	102.0
FW1-5	0.000	1327	148	0.12	0.07464±0.00043	1.88767±0.03439	1058.9±11.6	102.5
FW1-6	1.112	712	776	1.13	0.07299±0.00166	1.70267±0.04924	1013.7±46.2	99.4
FW1-7	0.517	982	617	0.65	0.07217±0.00097	1.79415±0.03954	990.7±27.3	107.9

TABLE 2

(continued)

Spot Name	f_{206} (%)	U (ppm)	Th (ppm)	Th/U	$^{207}Pb/^{206}Pb$ (±1σ)	$^{206}Pb/^{238}U$ (±1σ)	$^{207}Pb/^{206}Pb$ Age (±1σMa)	C(%)
Sample FW2 : Aplite in porphyritic granite (13.6684 S - 29.6242 E)								
Analyses conducted during a single session. 7 CZ3 standard analyses yielded a 2σ error of the mean of 1.65%								
FW2-1	0.391	120	70	0.60	0.12523±0.00195	6.35520±0.16284	2032.1±27.5	99.4
FW2-2	1.017	345	94	0.28	0.08254±0.00436	1.99952±0.11282	1258.3±103.2	82.9
FW2-3	0.089	968	96	0.10	0.12607±0.00055	6.44670±0.11521	2043.9±7.8	99.5
FW2-4	0.210	191	87	0.47	0.19366±0.00273	14.32643±0.33874	2773.5±23.2	99.8
FW2-5	0.325	209	72	0.36	0.11233±0.00173	4.56871±0.11198	1837.4±27.9	90.7
FW2-6	0.056	1375	122	0.09	0.12414±0.00067	6.47916±0.11706	2016.5±9.5	102.6
FW2-7	0.134	307	22	0.07	0.12370±0.00145	6.33304±0.13892	2010.3±20.8	101.3
FW2-8	0.597	77	40	0.54	0.12984±0.00281	7.04491±0.22442	2095.8±38.1	102.1
FW2-9	0.465	114	237	2.16	0.13000±0.00483	6.53413±0.31931	2097.9±65.2	95.5
FW2-10	0.884	185	87	0.49	0.12534±0.00216	6.23497±0.16391	2033.6±30.5	97.7
FW2-11	0.086	343	221	0.67	0.11927±0.00262	6.15944±0.17685	1945.3±39.3	105.4
FW2-12	0.549	157	115	0.76	0.10069±0.00251	4.11285±0.13133	1636.9±46.4	102.2
FW2-13	0.066	648	83	0.13	0.16268±0.00073	8.84789±0.16048	2483.7±7.6	86.3
Sample SASA2 : Sasa granite (13.0040 S - 30.0832 E)								
Analyses conducted during a single session. 16 CZ3 standard analyses yielded a 2σ error of the mean of 1.18%								
SASA2-1	2.481	48	110	2.38	0.06921±0.01622	0.17652±0.00516	905.1±482.9	115.8
SASA2-2	0.707	912	780	0.88	0.07271±0.00054	0.17402±0.00413	1005.8±15.1	102.8
SASA2-3c	0.268	465	281	0.62	0.07472±0.00128	0.16978±0.00398	1060.9±34.5	95.3
SASA2-3r	0.823	1932	467	0.25	0.07254±0.00113	0.15492±0.00333	1001.0±31.6	92.8
SASA2-5	0.301	417	404	1.00	0.07653±0.00149	0.14188±0.00340	1109.0±39.0	77.1
SASA2-10	1.723	228	279	1.26	0.07278±0.00333	0.16983±0.00427	1008.0±92.7	100.3
SASA2-11	0.294	1974	66	0.03	0.07403±0.00064	0.16416±0.00387	1042.3±17.3	94.0
SASA2-12c	0.858	1059	371	0.36	0.07295±0.00087	0.17077±0.00367	1012.7±24.1	100.4
SASA2-12r	0.311	1133	326	0.30	0.07414±0.00265	0.17338±0.00375	1045.3±72.1	98.6
SASA2-15	0.890	186	266	1.48	0.07038±0.00357	0.17803±0.00399	939.5±104.0	112.4
SASA2-17	0.945	252	329	1.35	0.07226±0.00112	0.16976±0.00407	993.3±31.5	101.8
SASA2-18	1.335	193	279	1.49	0.07682±0.00499	0.14176±0.00329	1116.6±129.6	76.5
Sample SER53 : Porphyritic granite (13.1270 S - 30.1349 E)								
Analyses conducted during a single session. 14 CZ3 standard analyses yielded a 2σ error of the mean of 1.11%								
SER53-1	0.041	257	248	1.00	0.07388±0.00076	0.17373±0.00329	1038.2±20.8	99.5
SER53-2	0.001	252	123	0.50	0.07371±0.00075	0.17480±0.00336	1033.7±20.4	100.5
SER53-3	0.416	117	198	1.74	0.07069±0.00229	0.16569±0.00341	948.5±66.4	104.2
SER53-4	0.000	813	761	0.97	0.07387±0.00042	0.17557±0.00321	1037.9±11.5	100.5
SER53-5	0.000	317	292	0.95	0.07488±0.00069	0.17544±0.00332	1065.4±18.5	97.8
SER53-6	0.054	244	261	1.10	0.07259±0.00080	0.17680±0.00341	1002.5±22.5	104.7
SER53-7	0.101	513	455	0.92	0.07327±0.00073	0.16920±0.00344	1021.4±20.1	98.7
SER53-8	0.170	457	409	0.92	0.07259±0.00068	0.17488±0.00331	1002.6±19.0	103.6
SER53-9	0.420	189	197	1.08	0.07034±0.00173	0.16331±0.00334	938.2±50.6	103.9
SER53-10	4.930	346	392	1.17	0.07239±0.00472	0.16601±0.00330	997.1±132.5	99.3
Sample SER64 : Porphyritic granite (13.3873 S - 30.3958 E)								
Analyses conducted during a single session. 14 CZ3 standard analyses yielded a 2σ error of the mean of 1.11%								
SER64-1	0.632	171	382	2.31	0.07237±0.00174	0.14368±0.00283	996.3±48.8	86.9
SER64-2	0.000	260	71	0.28	0.07517±0.00078	0.17481±0.00332	1073.1±20.9	96.8
SER64-3	0.000	1252	248	0.20	0.07398±0.00036	0.18155±0.00328	1040.8±9.9	103.3
SER64-4	0.000	237	712	3.11	0.07339±0.00078	0.17228±0.00333	1024.7±21.6	100.0
SER64-5	0.000	449	670	1.54	0.07283±0.00066	0.17375±0.00328	1009.1±18.3	102.3
SER64-6	0.701	50	99	2.04	0.06717±0.00406	0.16809±0.00428	842.9±125.7	118.8
SER64-7	0.000	1038	140	0.14	0.07344±0.00042	0.17694±0.00349	1026.0±11.6	102.4
SER64-8	0.603	898	292	0.34	0.07516±0.00099	0.15197±0.00281	1072.8±26.5	85.0
SER64-9	0.000	889	979	1.14	0.12301±0.00044	0.37536±0.00694	2000.4±6.4	102.7
SER64-10	0.292	213	562	2.73	0.07507±0.00403	0.17522±0.00373	1070.4±107.8	97.2
Sample SQG2 : Serenje Quarry Granite (13.2148 S - 30.2486 E)								
Analyses conducted during a single session. 16 CZ3 standard analyses yielded a 2σ error of the mean of 0.81%								
SQG2-72	0.000	460	463	1.04	0.07474±0.00051	0.17773±0.00270	1061.6±13.7	99.3
SQG2-70	0.000	187	88	0.49	0.07616±0.00114	0.18443±0.00825	1099.4±29.9	99.3
SQG2-26	0.004	402	187	0.48	0.07480±0.00040	0.16799±0.00253	1063.0±10.8	94.2
SQG2-60	0.012	689	348	0.52	0.07370±0.00031	0.16831±0.00249	1033.3±8.5	97.1
SQG2-7	0.027	699	259	0.38	0.07329±0.00034	0.17155±0.00253	1021.9±9.5	99.9
SQG2-17	0.040	136	90	0.68	0.07244±0.00083	0.17304±0.00273	998.4±23.3	103.0
SQG2-77	0.042	133	97	0.76	0.07241±0.00069	0.18131±0.00288	997.6±19.3	107.7
SQG2-48	0.043	702	346	0.51	0.07362±0.00034	0.16623±0.00245	1031.2±9.4	96.1
SQG2-20	0.074	411	249	0.62	0.07357±0.00061	0.17071±0.00257	1029.8±16.9	98.7
SQG2-1	0.088	233	144	0.64	0.07264±0.00060	0.17245±0.00263	1003.8±16.8	102.2
SQG2-14	1.201	575	284	0.51	0.07218±0.00129	0.16418±0.00251	990.9±36.3	98.9

TABLE 2
(continued)

Spot Name	f_{206} (%)	U (ppm)	Th (ppm)	Th/U	$^{207}Pb/^{206}Pb$ (±1σ)	$^{206}Pb/^{238}U$ (±1σ)	$^{207}Pb/^{206}Pb$ Age (±1σMa)	C(%)
Sample KN2a : Porphyritic granite (13.0991 S - 30.8204 E)								
Analyses conducted during a single session. 12 CZ3 standard analyses yielded a 2σ error of the mean of 1.56%								
KN2a-1	0.000	204	282	1.43	0.07378±0.00071	0.17375±0.00411	1035.6±19.4	99.7
KN2a-2	0.018	225	117	0.54	0.08606±0.00084	0.16993±0.00347	1339.6±18.8	75.5
KN2a-3	0.000	116	177	1.58	0.07873±0.00095	0.17796±0.00374	1165.3±24.0	90.6
KN2a-4	0.000	165	146	0.91	0.08220±0.00130	0.17712±0.00365	1250.3±30.8	84.1
KN2a-5	0.000	1421	882	0.64	0.07915±0.00119	0.17420±0.00352	1176.0±29.7	88.0
KN2a-6	0.056	131	147	1.16	0.07527±0.00096	0.17795±0.00370	1075.7±25.7	98.1
KN2a-7	0.000	236	176	0.77	0.07668±0.00075	0.17284±0.00352	1113.0±19.6	92.3
KN2a-8	0.066	247	144	0.60	0.07634±0.00082	0.17257±0.00351	1103.9±21.4	93.0
Sample KN5 : Porphyritic granite (12.9634 S - 30.8840 E)								
Analyses conducted during a single session. 12 CZ3 standard analyses yielded a 2σ error of the mean of 1.56%								
KN5-1	0.000	456	212	0.48	0.07463±0.00046	0.17865±0.00358	1058.6±12.5	100.1
KN5-2	0.098	181	356	2.03	0.08078±0.00128	0.17909±0.00369	1216.0±31.1	87.3
KN5-3r	0.050	2299	231	0.10	0.07580±0.00109	0.13595±0.00294	1089.8±28.9	75.4
KN5-3c	0.025	332	177	0.55	0.07797±0.00081	0.17663±0.00356	1146.1±20.7	91.5
KN5-4	0.000	273	138	0.52	0.07652±0.00075	0.17761±0.00360	1108.6±19.6	95.1
KN5-5	0.021	247	120	0.50	0.07979±0.00066	0.17543±0.00356	1191.8±16.3	87.4
KN5-6	0.000	338	180	0.55	0.07487±0.00054	0.17867±0.00360	1065.1±14.4	99.5
KN5-7	0.000	281	132	0.49	0.07650±0.00060	0.17752±0.00359	1108.1±15.6	95.1
KN5-8	0.000	298	153	0.53	0.07624±0.00059	0.18036±0.00365	1101.3±15.4	97.1
Sample KN7 : Porphyritic granite (13.1872 S - 30.9113 E)								
Analyses conducted during a single session. 12 CZ3 standard analyses yielded a 2σ error of the mean of 1.56%								
KN7-1	0.003	973	825	0.88	0.12417±0.00028	0.36971±0.00738	2017.0±4.1	100.5
KN7-2	0.000	506	155	0.32	0.12212±0.00108	0.33971±0.00680	1987.4±15.8	94.9
KN7-3r	0.399	2878	39994	14.36	0.19049±0.01292	0.07975±0.00159	2746.4±111.5	18.0
KN7-3c	0.000	184	258	1.45	0.19596±0.00156	0.41147±0.00899	2792.8±13.1	79.5
KN7-4	0.000	209	30	0.15	0.12215±0.00064	0.37122±0.00753	1987.8±9.3	102.4
KN7-5	0.049	230	87	0.39	0.11920±0.00307	0.34343±0.00939	1944.3±46.0	97.9
KN7-6	0.010	259	818	3.26	0.08331±0.00069	0.15308±0.00310	1276.5±16.2	71.9
KN7-7	0.032	740	235	0.33	0.07422±0.00038	0.17678±0.00352	1047.6±10.2	100.2
Sample KN8 : Porphyritic granite (13.2260 S - 30.8976 E)								
Analyses conducted during a single session. 12 CZ3 standard analyses yielded a 2σ error of the mean of 1.56%								
KN8-1r	0.018	245	191	0.81	0.08522±0.00068	0.19321±0.00399	1320.4±15.6	86.2
KN8-1c	0.007	117	58	0.51	0.12664±0.00092	0.37348±0.00773	2051.8±12.8	99.7
KN8-2	0.000	496	1171	2.44	0.08071±0.00091	0.16912±0.00338	1214.4±22.2	82.9
KN8-3	0.000	107	124	1.19	0.08184±0.00128	0.17658±0.00371	1241.6±30.7	84.4
KN8-4c	0.031	406	88	0.23	0.12828±0.00255	0.32698±0.00657	2074.5±35.0	87.9
KN8-4r	0.000	315	176	0.58	0.07506±0.00059	0.16945±0.00343	1070.0±15.8	94.3
KN8-5	0.000	382	256	0.69	0.07682±0.00057	0.16490±0.00331	1116.4±14.9	88.1
KN8-6	0.033	310	228	0.76	0.07609±0.00140	0.17208±0.00356	1097.4±36.7	93.3
KN8-7	0.000	321	134	0.43	0.10008±0.00164	0.24025±0.00483	1625.6±30.4	85.4
KN8-8	0.002	378	348	0.95	0.07472±0.00063	0.17771±0.00357	1060.9±17.0	99.4
KN8-9	0.000	113	164	1.50	0.08671±0.00137	0.17318±0.00364	1354.1±30.4	76.0
KN8-10	0.002	725	586	0.83	0.07918±0.00047	0.17180±0.00342	1176.7±11.9	86.9
KN8-11	0.091	215	267	1.29	0.07687±0.00091	0.17315±0.00353	1117.9±23.6	92.1
Sample CHT6 : Porphyritic granite (12.7766 S - 30.9725 E)								
Analyses conducted during a single session. 7 CZ3 standard analyses yielded a 2σ error of the mean of 1.65%								
CHT6-1	0.869	144	117	0.84	0.07304±0.00306	1.74172±0.08690	1015.1±84.8	101.3
CHT6-2	1.150	147	178	1.25	0.06558±0.00336	1.53049±0.08469	792.9±107.5	127.1
CHT6-3	0.460	415	282	0.70	0.07373±0.00161	1.71450±0.04876	1034.2±44.1	97.1
CHT6-4	0.225	300	214	0.74	0.07371±0.00113	1.74871±0.04221	1033.5±30.9	99.0
CHT6-5	2.414	148	111	0.77	0.06606±0.00561	1.43724±0.12602	808.3±177.7	116.9
CHT6-6	0.680	164	175	1.11	0.07541±0.00311	1.73153±0.07990	1079.3±82.9	92.0
CHT6-7	0.778	113	99	0.91	0.07232±0.00356	1.66512±0.09000	994.9±100.2	100.1
CHT6-8	1.591	93	124	1.38	0.06590±0.00529	1.50833±0.12608	803.3±168.0	123.2
CHT6-9	1.253	140	143	1.06	0.07048±0.00587	1.62685±0.13995	942.3±170.7	105.9
Sample ZM36 : Mununga Quarry Granite (12.6259 S - 31.0434 E)								
Analyses conducted during a single session. 14 CZ3 standard analyses yielded a 2σ error of the mean of 1.11%								
ZM36-1	0.000	91	94	1.07	0.07842±0.00227	0.17709±0.00381	1157.5±57.4	90.8
ZM36-2	0.193	145	138	0.98	0.07180±0.00144	0.17875±0.00354	980.3±40.7	108.1
ZM36-3	0.000	32	30	0.95	0.08094±0.00861	0.17282±0.00519	1220.0±209.1	84.2
ZM36-4	0.026	491	269	0.57	0.07344±0.00055	0.17008±0.00315	1026.2±15.1	98.7
ZM36-5	0.014	487	298	0.63	0.07348±0.00063	0.17624±0.00326	1027.3±17.5	101.9
ZM36-6	0.358	64	65	1.05	0.06967±0.00246	0.16523±0.00395	918.6±72.8	107.3

TABLE 2
(continued)

Spot Name	f_{206} (%)	U (ppm)	Th (ppm)	Th/U	$^{207}Pb/^{206}Pb$ (±1σ)	$^{206}Pb/^{238}U$ (±1σ)	$^{207}Pb/^{206}Pb$ Age (±1σMa)	C(%)
Sample ZM36 : Mununga Quarry Granite (12.6259 S - 31.0434 E								
Analyses conducted during a single session. 14 CZ3 standard analyses yielded a 2σ error of the mean of 1.11%								
ZM36-7	0.015	568	340	0.62	0.07328±0.00067	0.16720±0.00314	1021.7±18.5	97.6
ZM36-8	0.174	206	164	0.82	0.07253±0.00189	0.16960±0.00379	1000.9±52.9	100.9
ZM36-9	0.081	567	359	0.65	0.07358±0.00069	0.17231±0.00322	1030.0±19.0	99.5
ZM36-10	0.054	615	292	0.49	0.07418±0.00060	0.17079±0.00318	1046.4±16.3	97.1
Sample CHL5 : Porphyritic granite (12.4491 S - 31.0459 E)								
Analyses conducted during a single session. 7 CZ3 standard analyses yielded a 2σ error of the mean of 1.65%								
CHL5-1	0.506	227	368	1.68	0.07432±0.00129	1.79657±0.05688	1050.3±34.9	99.1
CHL5-2	0.723	269	488	1.87	0.07373±0.00221	1.69087±0.07479	1034.0±60.6	95.9
CHL5-3	0.610	244	44	0.18	0.07236±0.00213	1.71635±0.06805	996.1±59.9	102.7
CHL5-4	0.069	130	351	2.78	0.07794±0.00232	1.94345±0.07815	1145.3±59.1	93.6
CHL5-5	0.066	328	586	1.85	0.07694±0.00086	1.91776±0.05474	1119.6±22.4	95.7
CHL5-6	0.547	268	185	0.71	0.07340±0.00218	1.74131±0.06934	1024.9±60.2	99.9
CHL5-7	0.635	421	418	1.03	0.07197±0.00121	1.65353±0.05147	985.1±34.3	100.9
CHL5-8	0.582	332	454	1.41	0.07228±0.00165	1.70937±0.05026	993.7±46.4	102.7
Sample LW1 : Chilubanama Granite (10.9920 S - 32.3037 E)								
Analyses conducted during a single session. 12 CZ3 standard analyses yielded a 2σ error of the mean of 0.65%								
LW1-7	0.617	44	54	1.27	0.09440±0.00279	0.26390±0.00411	1516.2±55.8	99.6
LW1-4	0.970	57	83	1.50	0.08642±0.00296	0.25221±0.00372	1347.5±66.2	107.6
LW1-2	0.392	498	1001	2.08	0.09277±0.00059	0.23907±0.00232	1483.2±12.1	93.2
LW1-1	0.762	87	82	0.97	0.09554±0.00242	0.27213±0.00503	1538.8±47.7	100.8
LW1-5	0.282	402	670	1.72	0.07268±0.00077	0.16794±0.00169	1005.0±21.4	99.6
LW1-6	0.697	34	51	1.56	0.09377±0.00229	0.26772±0.00450	1503.4±46.2	101.7
Sample LW2 : Chilubanama Granite (11.0550 S - 32.3299 E)								
Analyses conducted during a single session. 12 CZ3 standard analyses yielded a 2σ error of the mean of 0.65%								
LW2-1	0.334	163	87	0.55	0.07036±0.00135	0.16688±0.00192	939.0±39.3	105.9
LW2-2	0.844	68	221	3.36	0.06581±0.00287	0.16812±0.00244	800.5±91.4	125.1
LW2-9	0.307	196	34	0.18	0.06984±0.00124	0.16932±0.00188	923.6±36.4	109.2
LW2-3	0.036	196	63	0.33	0.07220±0.00090	0.16983±0.00187	991.7±25.4	102.0
LW2-4	0.120	261	255	1.01	0.07078±0.00077	0.15796±0.00168	951.2±22.2	99.4
LW2-10	1.293	559	695	1.28	0.07170±0.00202	0.16308±0.00161	977.5±57.5	99.6
LW2-5	0.138	354	239	0.70	0.07042±0.00065	0.15807±0.00161	940.7±18.9	100.6
LW2-6	0.099	255	216	0.88	0.07085±0.00063	0.15605±0.00166	953.1±18.2	98.1
Sample MTG4 : Chilubanama Granite (10.6636 S - 32.4918 E)								
Analyses conducted during a single session. 16 CZ3 standard analyses yielded a 2σ error of the mean of 0.81%								
MTG4-9r	0.000	435	9	0.02	0.07315±0.00038	0.17075±0.00255	1018.1±10.4	99.8
MTG4-10r	0.000	587	10	0.02	0.07289±0.00042	0.16688±0.00247	1010.8±11.7	98.4
MTG4-8r	0.000	577	9	0.02	0.07296±0.00032	0.17056±0.00259	1012.9±9.0	100.2
MTG4-7c	0.033	216	131	0.63	0.12369±0.00053	0.35853±0.00550	2010.1±7.6	98.3
MTG4-10c	0.082	1201	26	0.02	0.07368±0.00029	0.17054±0.00250	1032.9±7.8	98.3
MTG4-9c	0.235	124	146	1.22	0.07099±0.00103	0.17281±0.00275	957.1±29.6	107.4
MTG4-6c	0.253	521	63	0.12	0.07348±0.00053	0.16841±0.00250	1027.1±14.6	97.7
MTG4-4r	0.265	564	39	0.07	0.07130±0.00053	0.16329±0.00242	966.0±15.1	100.9
MTG4-1c	0.236	268	29	0.11	0.12620±0.00076	0.40044±0.00685	2045.7±10.7	106.1
MTG4-4c	0.656	132	81	0.63	0.12419±0.00118	0.35275±0.00549	2017.2±16.8	96.6
MTG4-1r	1.041	522	139	0.27	0.07170±0.00091	0.16941±0.00252	977.3±25.9	103.2
MTG4-8c	2.478	218	282	1.34	0.08996±0.00222	0.24300±0.00374	1424.8±47.0	98.4
MTG4-5c	4.327	624	820	1.36	0.07249±0.00260	0.14984±0.00225	999.7±72.9	90.0
Sample ZM32 : Chilubanama Granite (11.0171 S - 32.0762 E)								
Analyses conducted during a single session. 14 CZ3 standard analyses yielded a 2σ error of the mean of 1.11%								
ZM32-1	0.315	268	286	1.10	0.11369±0.00123	0.31815±0.00871	1859.3±19.5	95.8
ZM32-2	0.119	464	404	0.90	0.10135±0.00123	0.29651±0.00809	1649.0±22.6	101.5
ZM32-3	1.024	414	434	1.08	0.07062±0.00173	0.16744±0.00478	946.4±50.1	105.5
ZM32-4	23.894	471	393	0.86	0.08282±0.00822	0.14496±0.00408	1265.0±193.8	69.0
ZM32-5	0.042	78	63	0.84	0.12553±0.00216	0.35921±0.01072	2036.3±30.5	97.2
ZM32-6	0.750	90	45	0.52	0.06751±0.00277	0.16150±0.00488	853.4±85.4	113.1

f_{206} = the proportion of common ^{206}Pb in the total ^{206}Pb; Th/U = $^{232}Th/^{238}U$; %C = % concordance

All ratios and ages corrected for common Pb using measured ^{204}Pb and composition appropriate to the age of the zircon (Stacey and Kramers, 1975)

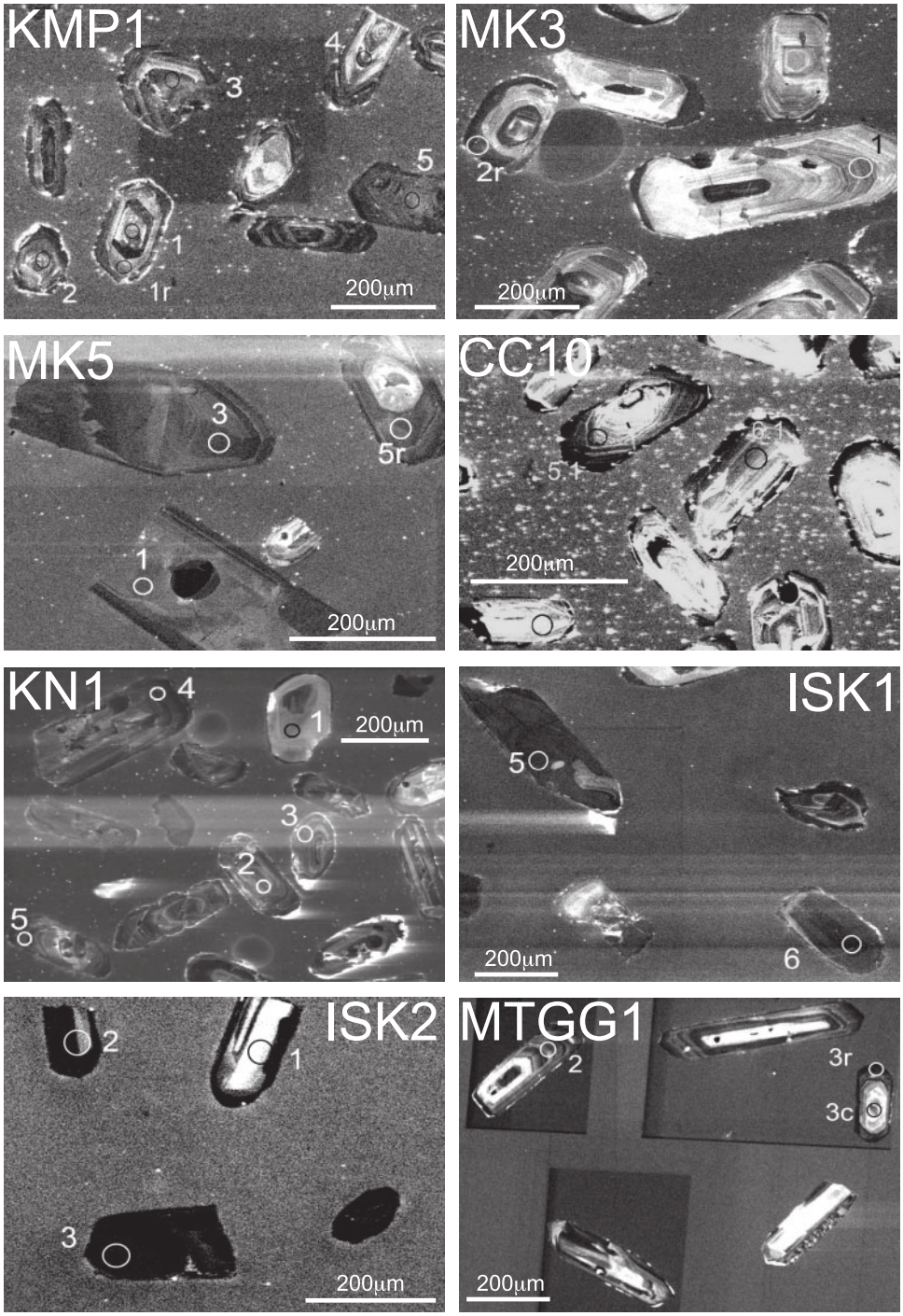

Fig. 2A-E. Cathodo-luminescence images (except sample ZM32 on fig. 2E, which is an optical image) of polished zircons, indicating analyzed spots within the field of view (refer to table 2 for age data).

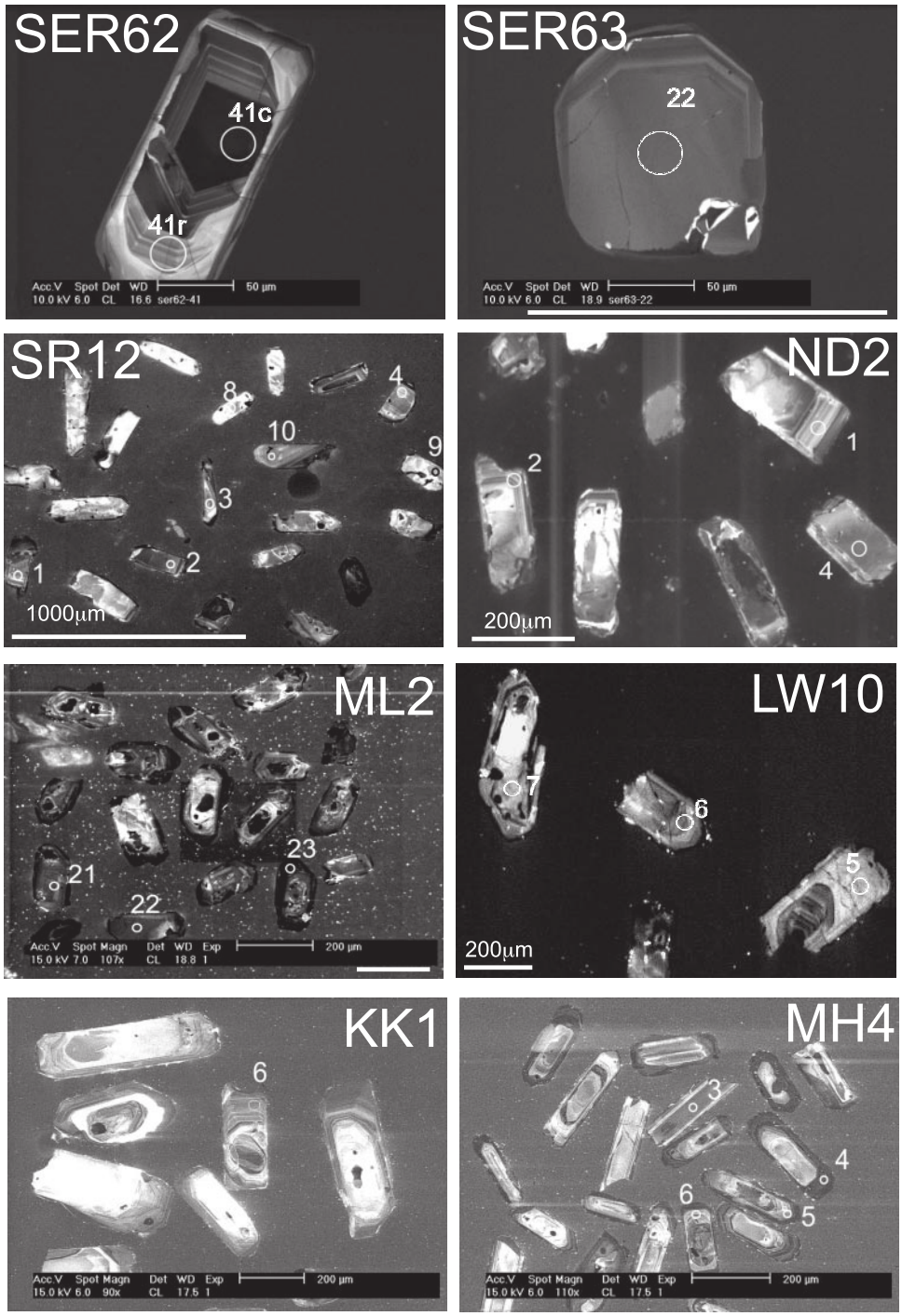
SER62
41c
41r
Acc.V Spot Det WD 50 µm
10.0 kV 6.0 CL 16.6 ser62-41
SER63
22
Acc.V Spot Det WD 50 µm
10.0 kV 6.0 CL 18.9 ser63-22
SR12
8
4
10
9
3
1
2
1000µm
ND2
1
2
4
200µm
ML2
23
21
22
Acc.V Spot Magn Det WD Exp 200 µm
15.0 kV 7.0 107x CL 18.8 1
LW10
7
6
5
200µm
KK1
6
Acc.V Spot Magn Det WD Exp 200 µm
15.0 kV 6.0 90x CL 17.5 1
MH4
3
4
6
5
Acc.V Spot Magn Det WD Exp 200 µm
15.0 kV 6.0 110x CL 17.5 1

Fig. 2B.

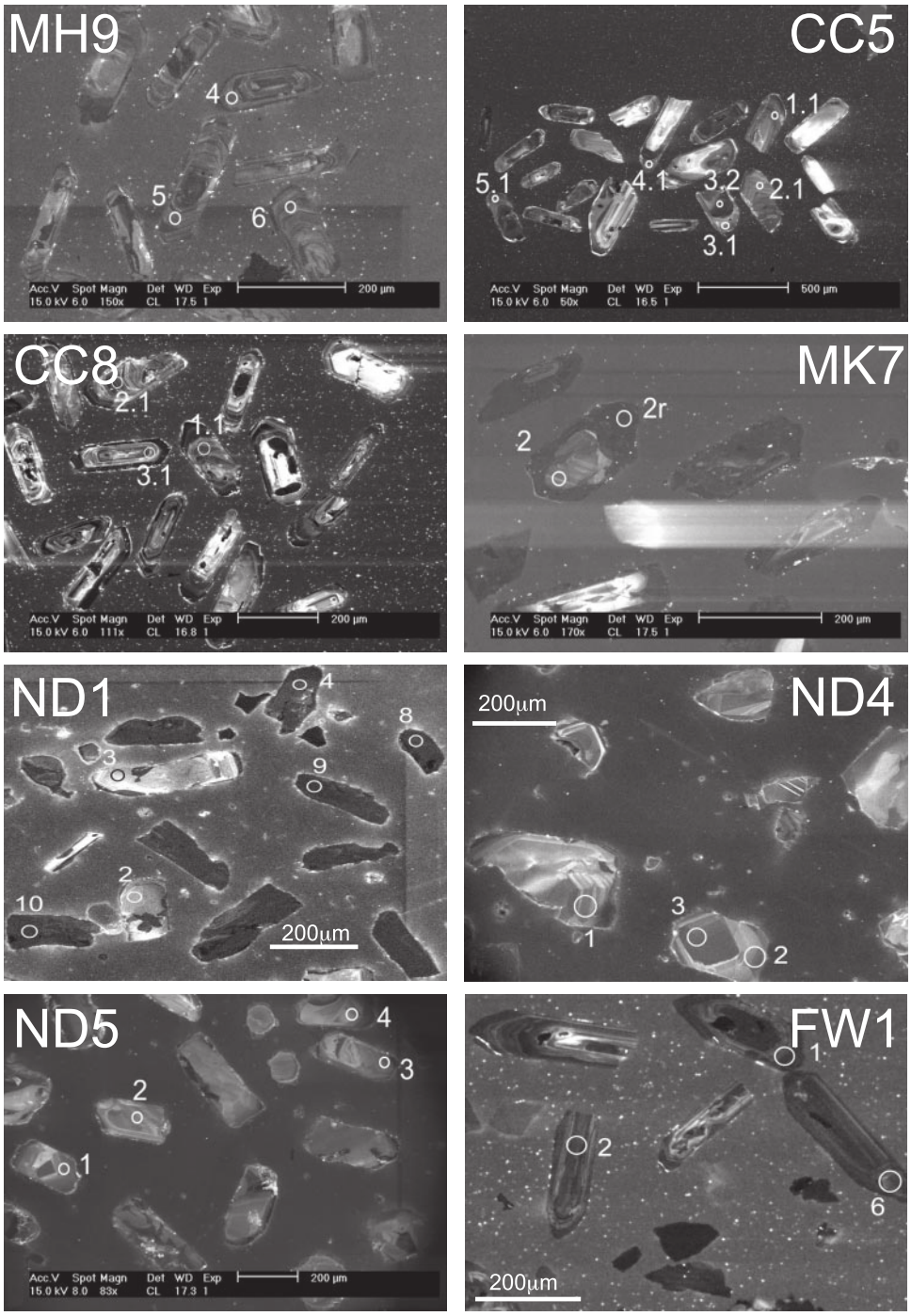
MH9
4
5
6
Acc.V Spot Magn Det WD Exp
15.0 kV 6.0 150x CL 17.5 1
200 µm
CC5
1.1
5.1
4.1
3.2
2.1
3.1
Acc.V Spot Magn Det WD Exp
15.0 kV 6.0 50x CL 16.5 1
500 µm
CC8
2.1
1.1
3.1
Acc.V Spot Magn Det WD Exp
15.0 kV 6.0 111x CL 16.8 1
200 µm
MK7
2r
2
Acc.V Spot Magn Det WD Exp
15.0 kV 6.0 170x CL 17.5 1
200 µm
ND1
4
8
3
9
2
10
200µm
200µm
ND4
1
3
2
ND5
4
3
2
1
Acc.V Spot Magn Det WD Exp
15.0 kV 8.0 83x CL 17.3 1
200 µm
FW1
1
2
6
200µm

Fig. 2C.

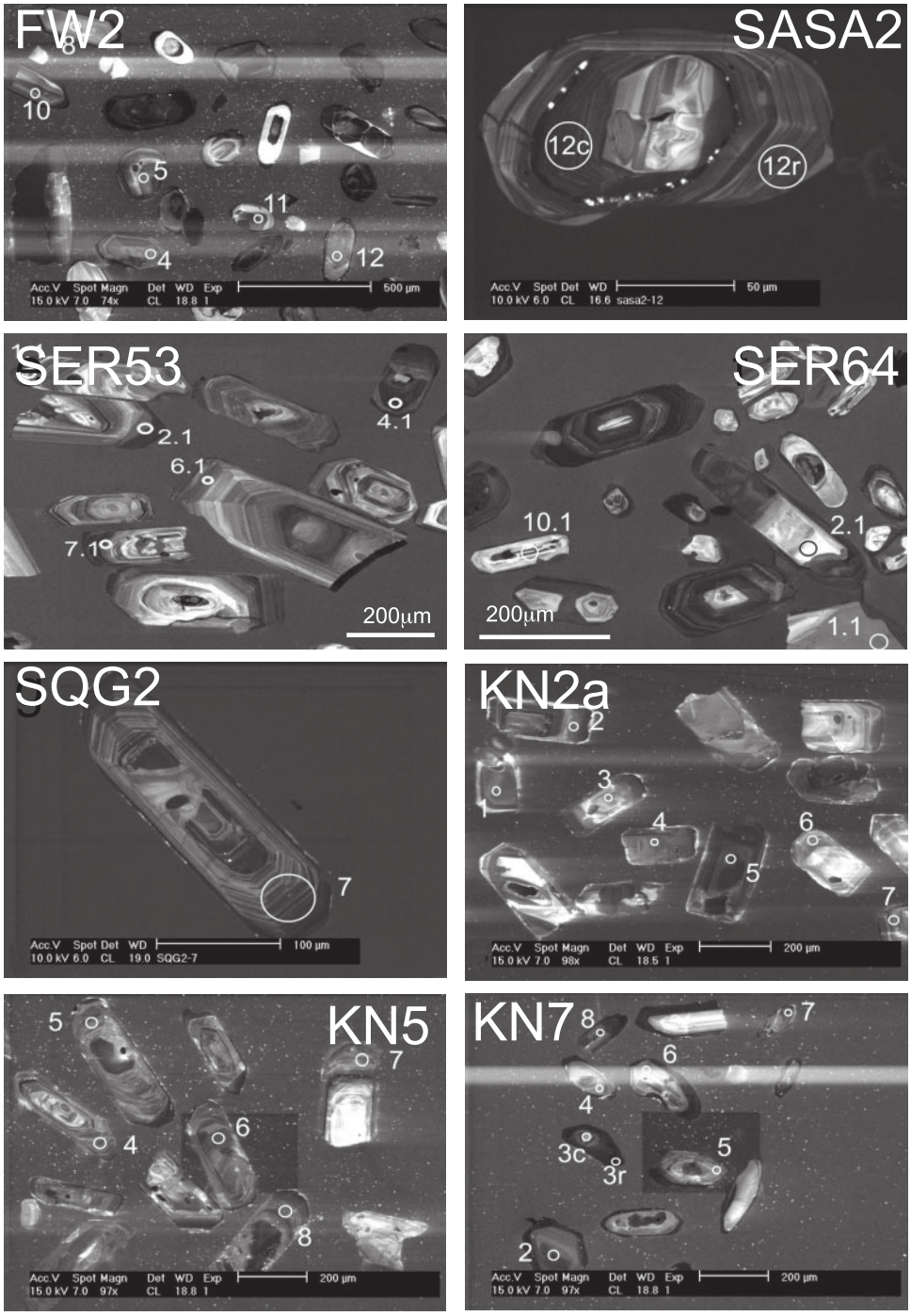
FW2
10
5
11
4
12
Acc.V Spot Magn Det WD Exp
15.0 kV 7.0 74x CL 18.8 1
500 µm
SASA2
12c
12r
Acc.V Spot Det WD
10.0 kV 6.0 CL 16.6 sasa2-12
50 µm
SER53
4.1
2.1
6.1
7.1
200µm
SER64
10.1
2.1
200µm
1.1
SQG2
7
Acc.V Spot Det WD
10.0 kV 6.0 CL 19.0 SQG2-7
100 µm
KN2a
2
3
1
4
6
5
7
Acc.V Spot Magn Det WD Exp
15.0 kV 7.0 98x CL 18.5 1
200 µm
5
KN5
7
4
6
8
Acc.V Spot Magn Det WD Exp
15.0 kV 7.0 97x CL 18.8 1
200 µm
KN7
8
7
6
4
3c
3r
5
2
Acc.V Spot Magn Det WD Exp
15.0 kV 7.0 97x CL 18.8 1
200 µm

Fig. 2D.

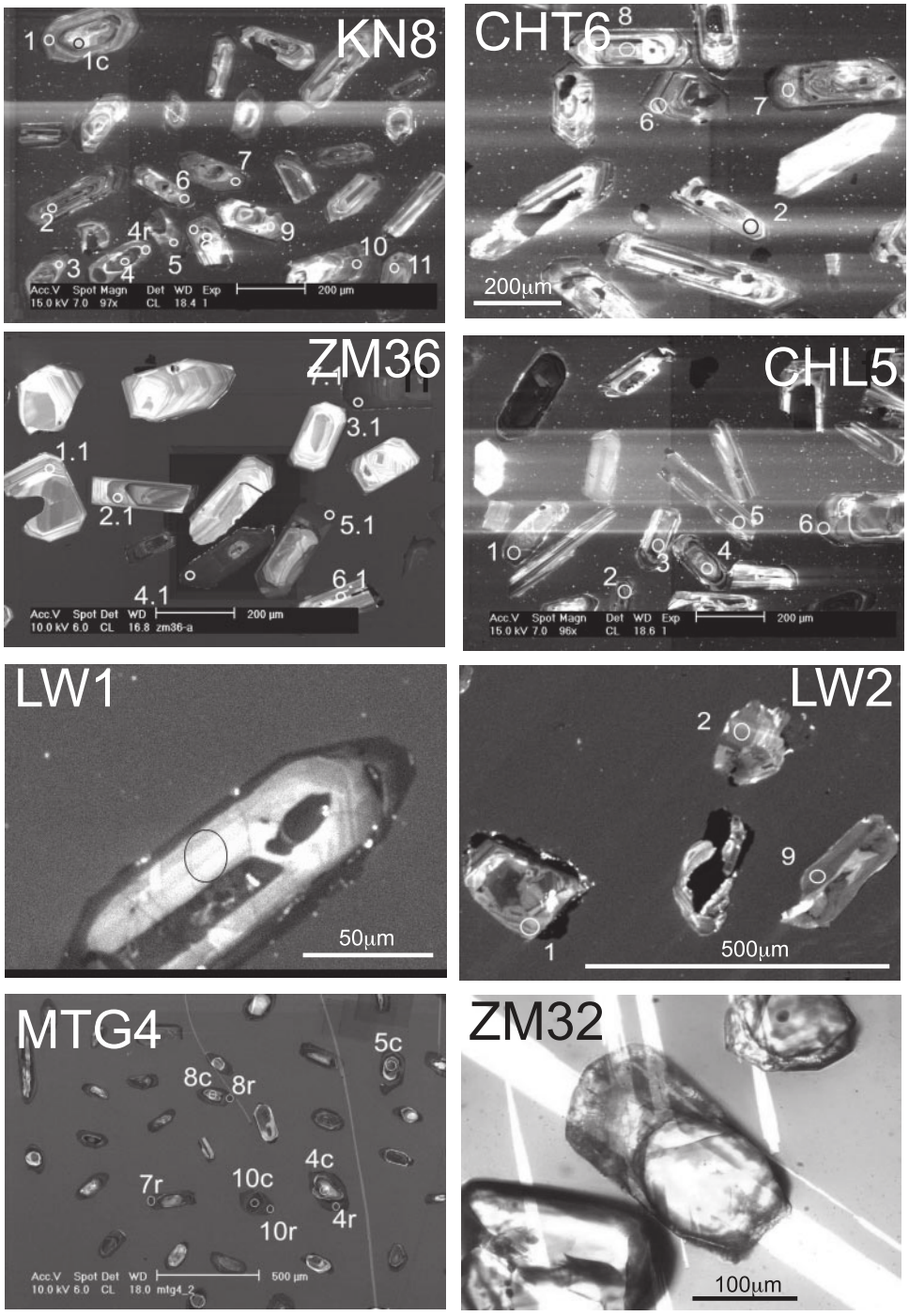
KN8
1
1c
2
3
4
4r
5
6
7
8
9
10
11
Acc.V Spot Magn Det WD Exp
15.0 kV 7.0 97x CL 18.4 1
200 µm
CHT6
8
6
7
2
200µm
ZM36
7.1
3.1
1.1
2.1
5.1
6.1
4.1
Acc.V Spot Det WD
10.0 kV 6.0 CL 16.8 zm36-a
200 µm
CHL5
1
2
3
4
5
6
Acc.V Spot Magn Det WD Exp
15.0 kV 7.0 96x CL 18.6 1
200 µm
LW1
50µm
LW2
2
9
1
500µm
MTG4
5c
8c
8r
4c
7r
10c
4r
10r
Acc.V Spot Det WD
10.0 kV 6.0 CL 18.0 mtg4_2
500 µm
ZM32
100µm

Fig. 2E.

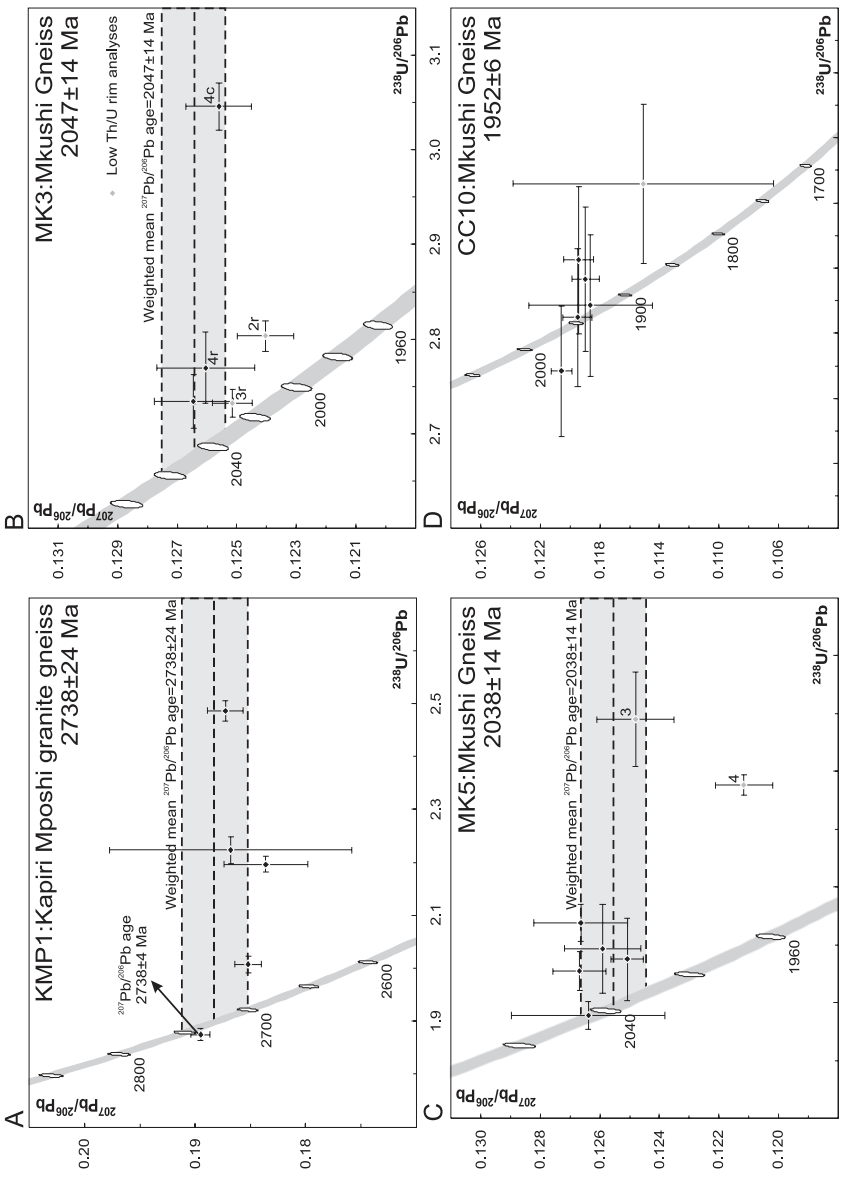

Fig. 3. U-Pb evolution diagram showing data for (A) KMP1; (B) MK3; (C) MK5 and (D) CC10.

ICP-MS system. The methodology is described in detail by Griffin and others (2000, 2004). Analyses were carried out with a beam diameter of ~40μm, a 5 Hz repetition rate, 60 percent power output and a laser energy of ~0.13 mJ. The ablation times were 100 to 200 seconds. We used the chondritic values of Blichert-Toft and others (1997) for the calculation of $\varepsilon_{Hf}(t)$ values. Hf model ages (T_{DM}) were calculated based on a depleted-mantle source with $(^{176}Hf/^{177}Hf)_I = 0.279718$ and $^{176}Hf/^{177}Hf = 0.0384$. This results in a value of $^{176}Hf/^{177}Hf$ of 0.28325 for a mid-ocean ridge basalt at 4.56 Ga. 2σ errors on the determination of $^{176}Lu/^{177}Hf$ isotopic composition were between 1 and 2 percent, which at the ratios obtained here result in an error on $\varepsilon_{Hf}(t)$ of less than 1 unit.

ZIRCON U-Pb GEOCHRONOLOGY AND Lu-Hf DETERMINATIONS

Zircon Characteristics

Zircons from the granitoid bodies are generally large, between 200 and 400 μm, and euhedral in shape. Length to width ratios vary from equant to 4:1 and most analyzed crystals are colorless to pale yellow in transmitted light, and largely free of large inclusions or cracks. CL imaging brings out distinct oscillatory zoning in all but a few cases, indicative of magmatic crystallization. Only a limited number of granitoid bodies appeared to contain complex zircons, with core and rim domains, which are discussed in detail for those samples. Characteristics of zircon are tabulated in table 1 while CL or optical imagery of representative grains for each sample are shown in figures 2A-E. All U-Pb data are reported in table 2 and Lu-Hf data in table 3.

U-Pb and Lu-Hf Results

The Mkushi Gneiss (samples KMP1, MK3, MK5, CC10 and KN1).—The Mkushi Gneiss was sampled from five different localities (samples KMP1, MK3, MK5, CC10 and KN1, see fig. 1 and table 2). Sample KMP1 was collected from a strongly foliated granite gneiss in a quarry along the sealed road north of Kapiri-Mposhi. Samples MK3 and MK5 were taken from biotite granite gneiss, and pinkish biotite granite gneiss in Munshiwemba Quarry south of Mkushi (MG, fig. 1B). Samples CC10 and KN1 were collected from biotite granite gneiss further east. Munshiwemba Quarry is the type locality, and offers excellent exposure of the Mkushi Gneiss, which is cross-cut by numerous large aplite dikes and pegmatites, most of which contain abundant chalcopyrite. At least two varieties of the Mkushi Gneiss occur in the quarry. The dominant variant is a foliated pink biotite granite gneiss (sample MK5) which locally gives way to a subordinant, highly sheared, strongly foliated dark gray biotite gneiss (sample MK3). Zircon from a sample of the biotite granite gneiss as well as the aplites in the quarry was previously dated by Rainaud and others (2002, 2005) using the U-Pb SHRIMP technique and yielded crystallization ages of 2049 ± 6 Ma (gneiss) and 2036 ± 22 Ma (aplite) respectively. A later magmatic event is recognized in magmatic rim overgrowths on zircon from the aplite, which give a poorly constrained age of 1088 ± 159 Ma.

Sample KMP1—Six analyses were conducted on five zircon grains (fig. 3A, table 2). Th/U ratios range between 0.3 and 0.7, with U+Th content between 430 and 1050 ppm. One data point recorded high non-radiogenic lead (common Pb or Pb_c) and defines an imprecise $^{207}Pb/^{206}Pb$ age of 3105 ± 143 Ma, possibly indicating a Mesoarchean xenocrystic component. The remaining data record variable Pb_c and Pb-loss, positively correlated with U and Th content. A broad trend parallel to the $^{238}U/^{206}Pb$ axis indicates that the majority of Pb was lost in recent times. A weighted mean $^{207}Pb/^{206}Pb$ age of 2723 ± 24 Ma [MSWD (Mean Square of Weighted Deviates) = 9.3] can be calculated from the data. The most concordant data point, which also records the lowest amount of Pb_c, has a $^{207}Pb/^{206}Pb$ age of 2738 ± 8 Ma, within error of the weighted mean age. Although the data are inadequate to unequivocally

TABLE 3

Laser Ablation ICP-MS Lu-Hf data for zircon from granitoid rocks in the Irumide Belt

Analysis No.	$^{176}Hf/^{177}Hf$ 1σ abs		$^{176}Lu/^{177}Hf$	$^{176}Yb/^{177}Hf$	$^{176}Hf/^{177}Hf$ initial	$\varepsilon_{Hf}(t)$ 1σ	T(DM) Hf (Ga)	Chur (t)	Hf DM (t)
SQG-01	0.281817	0.000010	0.001464	0.057735	0.281788	-11.4 ± 0.3	1.97	0.282109	0.282485
SQG-02	0.281752	0.000011	0.000896	0.037813	0.281734	-13.3 ± 0.4	2.03	0.282109	0.282485
SQG-03	0.281876	0.000013	0.001985	0.088863	0.281836	-9.7 ± 0.5	1.92	0.282109	0.282485
SQG-04	0.281776	0.000010	0.001293	0.059384	0.281750	-12.7 ± 0.3	2.02	0.282109	0.282485
SQG-05	0.281770	0.000007	0.000906	0.039462	0.281752	-12.7 ± 0.3	2.01	0.282109	0.282485
SQG-06	0.281964	0.000010	0.002702	0.124003	0.281910	-7.1 ± 0.4	1.83	0.282109	0.282485
SQG-07	0.281825	0.000012	0.001061	0.047872	0.281804	-10.8 ± 0.4	1.94	0.282109	0.282485
SQG-08	0.282020	0.000013	0.003313	0.156771	0.281954	-5.5 ± 0.5	1.79	0.282109	0.282485
SQG-09	0.281880	0.000013	0.002382	0.107775	0.281832	-9.8 ± 0.5	1.93	0.282109	0.282485
SQG-10	0.281807	0.000008	0.000749	0.031837	0.281792	-11.2 ± 0.3	1.95	0.282109	0.282485
SQG-11	0.281771	0.000011	0.001187	0.049366	0.281747	-12.8 ± 0.4	2.02	0.282109	0.282485
SQG-12	0.281774	0.000011	0.001252	0.054246	0.281749	-12.8 ± 0.4	2.02	0.282109	0.282485
Median value						**-11.3 ± 0.4**	**1.96**		
ZM36-01	0.281682	0.000008	0.000616	0.028817	0.281670	-15.6 ± 0.3	2.11	0.282109	0.282484
ZM36-02	0.281659	0.000010	0.000630	0.028771	0.281646	-16.4 ± 0.4	2.14	0.282109	0.282484
ZM36-03	0.281728	0.000013	0.000807	0.038463	0.281712	-14.1 ± 0.5	2.06	0.282109	0.282484
ZM36-04	0.281740	0.000012	0.001054	0.043792	0.281719	-13.8 ± 0.4	2.05	0.282109	0.282484
ZM36-05	0.281671	0.000011	0.000747	0.034156	0.281656	-16.0 ± 0.4	2.13	0.282109	0.282484
ZM36-06	0.281705	0.000017	0.000757	0.035435	0.281690	-14.8 ± 0.6	2.08	0.282109	0.282484
ZM36-07	0.281486	0.000011	0.001495	0.067239	0.281456	-23.1 ± 0.4	2.42	0.282109	0.282484
ZM36-08	0.281796	0.000011	0.000559	0.023304	0.281785	-11.5 ± 0.4	1.95	0.282109	0.282484
ZM36-09	0.281748	0.000008	0.002079	0.097359	0.281706	-14.3 ± 0.3	2.10	0.282109	0.282484
ZM36-10	0.281705	0.000006	0.000674	0.030041	0.281692	-14.8 ± 0.2	2.08	0.282109	0.282484
ZM36-11	0.281727	0.000010	0.000800	0.037578	0.281711	-14.1 ± 0.3	2.06	0.282109	0.282484
ZM36-12	0.281719	0.000008	0.000746	0.034606	0.281704	-14.3 ± 0.3	2.07	0.282109	0.282484
Median value						**-14.6 ± 0.4**	**2.08**		
MH9C-01	0.281754	0.000006	0.000250	0.008254	0.281749	-12.7 ± 0.2	1.99	0.282106	0.282481
MH9C-02	0.281738	0.000010	0.000639	0.024921	0.281725	-13.5 ± 0.3	2.03	0.282106	0.282481
MH9C-03	0.281830	0.000012	0.001687	0.075506	0.281796	-11.0 ± 0.4	1.97	0.282106	0.282481
MH9C-04	0.281727	0.000008	0.000492	0.022538	0.281717	-13.8 ± 0.3	2.04	0.282106	0.282481
MH9C-05	0.281764	0.000009	0.000700	0.031753	0.281750	-12.6 ± 0.3	2.00	0.282106	0.282481
MH9C-06	0.281766	0.000008	0.000860	0.040138	0.281749	-12.7 ± 0.3	2.01	0.282106	0.282481
MH9C-07	0.281703	0.000012	0.000525	0.024316	0.281692	-14.7 ± 0.4	2.07	0.282106	0.282481
MH9C-08	0.281801	0.000012	0.000986	0.039468	0.281781	-11.5 ± 0.4	1.97	0.282106	0.282481
Median value						**-12.7 ± 0.3**	**2.01**		
KN2A-01	0.281755	0.000009	0.001216	0.057286	0.281731	-13.3 ± 0.3	2.04	0.282105	0.282479
KN2A-02	0.281738	0.000009	0.000696	0.031617	0.281724	-13.5 ± 0.3	2.04	0.282105	0.282479
KN2A-03	0.281725	0.000010	0.000450	0.020186	0.281716	-13.8 ± 0.3	2.04	0.282105	0.282479
KN2A-04	0.281726	0.000008	0.000539	0.024229	0.281715	-13.8 ± 0.3	2.04	0.282105	0.282479
KN2A-05	0.281708	0.000013	0.000888	0.042241	0.281690	-14.7 ± 0.5	2.09	0.282105	0.282479
KN2A-06	0.281708	0.000008	0.000739	0.032807	0.281693	-14.6 0.3	2.08	0.282105	0.282479
KN2A-07	0.281748	0.000009	0.001241	0.056824	0.281723	-13.5 ± 0.3	2.05	0.282105	0.282479
KN2A-08	0.281701	0.000012	0.000588	0.027078	0.281689	-14.7 ± 0.4	2.08	0.282105	0.282479
Median value						**-13.8 ± 0.3**	**2.05**		
ND4-01	0.281796	0.000009	0.000706	0.027257	0.281782	-11.4 ± 0.3		0.282105	0.282479
ND4-02	0.281746	0.000013	0.000529	0.020183	0.281735	-13.1 ± 0.5	2.02	0.282105	0.282479
ND4-03	0.281826	0.000009	0.003856	0.173260	0.281749	-12.6 ± 0.3	2.09	0.282105	0.282479
ND4-04	0.281819	0.000014	0.002492	0.110076	0.281769	-11.9 ± 0.5	2.02	0.282105	0.282479
ND4-05	0.281810	0.000010	0.001114	0.044241	0.281788	-11.2 ± 0.4	1.96	0.282105	0.282479
ND4-06	0.281763	0.000010	0.000858	0.034262	0.281746	-12.7 ± 0.4	2.01	0.282105	0.282479
ND4-07	0.281802	0.000011	0.000929	0.035891	0.281783	-11.4 ± 0.4	1.96	0.282105	0.282479
ND4-08	0.281807	0.000009	0.000793	0.029889	0.281791	-11.1 ± 0.3	1.95	0.282105	0.282479
ND4-09	0.281812	0.000011	0.000598	0.022854	0.281800	-10.8 ± 0.4	1.93	0.282105	0.282479
ND4-10	0.281780	0.000009	0.000699	0.027245	0.281766	-12.0 ± 0.3	1.98	0.282105	0.282479
Median value						**-11.7 ± 0.4**	**1.98**		

Table 3

(continued)

Analysis No.	$^{176}Hf/^{177}Hf$	1σ abs	$^{176}Lu/^{177}Hf$	$^{176}Yb/^{177}Hf$	$^{176}Hf/^{177}Hf$ initial	$\varepsilon_{Hf}(t)$ 1σ	T(DM) Hf (Ga)	Chur (t)	Hf DM (t)
ML2-01	0.281796	0.000015	0.000900	0.036899	0.281769	0.2 ± 0.5	1.97	0.281763	0.282084
ML2-02	0.281814	0.000012	0.001152	0.056596	0.281779	0.6 ± 0.4	1.96	0.281763	0.282084
ML2-03	0.281831	0.000011	0.001381	0.057970	0.281789	0.9 ± 0.4	1.95	0.281763	0.282084
ML2-04	0.281848	0.000007	0.001211	0.057235	0.281811	1.7 ± 0.3	1.92	0.281763	0.282084
ML2-05	0.281830	0.000011	0.001165	0.058746	0.281795	1.1 ± 0.4	1.94	0.281763	0.282084
ML2-06	0.281794	0.000010	0.000979	0.046523	0.281764	0.0 ± 0.4	1.98	0.281763	0.282084
ML2-07	0.281856	0.000009	0.001295	0.064138	0.281817	1.9 ± 0.3	1.91	0.281763	0.282084
ML2-08	0.281833	0.000015	0.001312	0.061822	0.281793	1.1 ± 0.5	1.94	0.281763	0.282084
ML2-09	0.281926	0.000013	0.000841	0.037107	0.281900	4.9 ± 0.5	1.80	0.281763	0.282084
ML2-10	0.282034	0.000011	0.003592	0.168602	0.281925	5.7 ± 0.4	1.78	0.281763	0.282084
Median value						**1.1 ± 0.4**	**1.94**		
LW10-01	0.281592	0.000009	0.000628	0.029195	0.281572	-5.4 ± 0.3	2.23	0.281724	0.282039
LW10-02	0.281650	0.000019	0.000628	0.028650	0.281630	-3.3 ± 0.7	2.15	0.281724	0.282039
LW10-03	0.281518	0.000009	0.000702	0.032742	0.281496	-8.1 ± 0.3	2.33	0.281724	0.282039
LW10-04	0.281611	0.000009	0.000687	0.031814	0.281589	-4.8 ± 0.3	2.20	0.281724	0.282039
LW10-05	0.281618	0.000010	0.000928	0.036091	0.281589	-4.8 ± 0.3	2.21	0.281724	0.282039
LW10-06	0.281598	0.000009	0.000732	0.034011	0.281575	-5.3 ± 0.3	2.22	0.281724	0.282039
LW10-07	0.281663	0.000011	0.000845	0.037824	0.281636	-3.1 ± 0.4	2.14	0.281724	0.282039
LW10-08	0.281634	0.000014	0.001734	0.067302	0.281579	-5.1 ± 0.5	2.23	0.281724	0.282039
LW10-09	0.281318	0.000016	0.001185	0.057261	0.281281	-15.7 ± 0.6	2.62	0.281724	0.282039
LW10-10	0.281650	0.000013	0.000975	0.042360	0.281619	-3.7 ± 0.5	2.17	0.281724	0.282039
LW10-11	0.281567	0.000011	0.000592	0.027823	0.281548	-6.2 ± 0.4	2.26	0.281724	0.282039
LW10-12	0.281620	0.000012	0.000753	0.035998	0.281596	-4.5 ± 0.4	2.20	0.281724	0.282039
LW10-13	0.281596	0.000010	0.000875	0.041062	0.281568	-5.5 ± 0.4	2.23	0.281724	0.282039
LW10-14	0.281576	0.000008	0.000792	0.038365	0.281551	-6.1 ± 0.3	2.26	0.281724	0.282039
Median value						**-5.2 ± 0.4**	**2.22**		
ND2-01	0.281879	0.000047	0.002740	0.105585	0.281792	2.8 ± 1.6	1.95	0.281713	0.282026
ND2-02	0.281726	0.000013	0.001175	0.051600	0.281689	-0.9 ± 0.5	2.08	0.281713	0.282026
ND2-03	0.281866	0.000014	0.000621	0.020406	0.281846	4.7 ± 0.5	1.86	0.281713	0.282026
ND2-04	0.281775	0.000022	0.003093	0.118518	0.281676	-1.3 ± 0.8	2.12	0.281713	0.282026
ND2-05	0.281780	0.000015	0.000871	0.042136	0.281752	1.4 ± 0.5	1.99	0.281713	0.282026
ND2-06	0.281729	0.000012	0.000898	0.043506	0.281700	-0.4 ± 0.4	2.06	0.281713	0.282026
ND2-07	0.281722	0.000024	0.001640	0.070276	0.281670	-1.5 0.8	2.11	0.281713	0.282026
ND2-08	0.281780	0.000014	0.001014	0.047495	0.281748	1.2 ± 0.5	2.00	0.281713	0.282026
Median value						**0.4 ± 0.7**	**2.03**		
SER63-01	0.282077	0.000012	0.004451	0.211394	0.281933	8.4 ± 0.4	1.76	0.281696	0.282007
SER63-02	0.281932	0.000009	0.003912	0.181492	0.281805	3.9 ± 0.3	1.94	0.281696	0.282007
SER63-03	0.281829	0.000008	0.001761	0.081006	0.281772	2.7 ± 0.3	1.97	0.281696	0.282007
SER63-04	0.281846	0.000008	0.001447	0.066983	0.281799	3.6 ± 0.3	1.93	0.281696	0.282007
SER63-05	0.281718	0.000007	0.001002	0.047427	0.281686	-0.4 ± 0.3	2.08	0.281696	0.282007
SER63-06	0.281807	0.000028	0.001582	0.080215	0.281756	2.1 ± 1.0	1.99	0.281696	0.282007
SER63-07	0.281778	0.000009	0.001594	0.075933	0.281726	1.1 ± 0.3	2.03	0.281696	0.282007
SER63-08	0.281767	0.000014	0.001209	0.058797	0.281728	1.1 ± 0.5	2.03	0.281696	0.282007
SER63-09	0.281835	0.000013	0.001816	0.090178	0.281776	2.8 ± 0.5	1.97	0.281696	0.282007
SER63-10	0.282030	0.000012	0.001780	0.089395	0.281972	9.8 ± 0.4	1.70	0.281696	0.282007
SER63-11	0.281825	0.000011	0.001765	0.084841	0.281768	2.5 ± 0.4	1.98	0.281696	0.282007
SER63-12	0.282027	0.000013	0.001159	0.047383	0.281989	10.4 ± 0.5	1.67	0.281696	0.282007
Median value						**2.8 ± 0.4**	**1.97**		
SER6-2C-01	0.281705	0.000010	0.001163	0.055492	0.281667	-0.8 ± 0.3	2.11	0.281688	0.281998
SER6-2C-02	0.281691	0.000013	0.000662	0.031210	0.281669	-0.7 ± 0.5	2.10	0.281688	0.281998
SER6-2C-03	0.281751	0.000011	0.002750	0.115877	0.281661	-1.0 ± 0.4	2.13	0.281688	0.281998
SER6-2C-04	0.281727	0.000014	0.001009	0.048149	0.281694	0.2 ± 0.5	2.07	0.281688	0.281998
SER6-2C-05	0.281665	0.000009	0.000533	0.023983	0.281648	-1.5 ± 0.3	2.12	0.281688	0.281998
SER6-2C-06	0.281696	0.000010	0.000667	0.030818	0.281674	-0.5 ± 0.4	2.09	0.281688	0.281998
SER6-2C-07	0.281652	0.000008	0.000596	0.026716	0.281633	-2.0 ± 0.3	2.15	0.281688	0.281998
SER6-2C-08	0.281709	0.000011	0.001083	0.051674	0.281674	-0.5 ± 0.4	2.10	0.281688	0.281998
Median value						**-0.7 ± 0.4**	**2.10**		

TABLE 3
(continued)

Analysis No.	$^{176}Hf/^{177}Hf$ 1σ abs		$^{176}Lu/^{177}Hf$	$^{176}Yb/^{177}Hf$	$^{176}Hf/^{177}Hf$ initial	$\varepsilon_{Hf}(t)$ 1σ	T(DM) Hf (Ga)	Chur (t)	Hf DM (t)
ISK1-01	0.281569	0.000007	0.001009	0.045046	0.281530	0.9 ± 0.2	2.28	0.281504	0.281784
ISK1-02	0.281605	0.000009	0.000599	0.025713	0.281582	2.8 ± 0.3	2.21	0.281504	0.281784
ISK1-03	0.281555	0.000007	0.001003	0.044119	0.281517	0.5 ± 0.2	2.30	0.281504	0.281784
ISK1-04	0.281583	0.000015	0.001780	0.074750	0.281515	0.4 ± 0.5	2.31	0.281504	0.281784
ISK1-05	0.281593	0.000010	0.001353	0.058850	0.281541	1.3 ± 0.3	2.27	0.281504	0.281784
ISK1-06	0.281835	0.000038	0.003580	0.173185	0.281698	6.9 ± 1.3	2.06	0.281504	0.281784
ISK1-07	0.281662	0.000012	0.001584	0.074269	0.281602	3.5 ± 0.4	2.19	0.281504	0.281784
ISK1-08	0.281634	0.000012	0.001083	0.039637	0.281593	3.1 ± 0.4	2.20	0.281504	0.281784
Median value						**2.0 ± 0.5**	**2.24**		
KN1-01	0.280800	0.000020	0.000689	0.035820	0.280772	**-23.8 ± 0.7**	**3.26**	0.281441	0.281712
MK3-01	0.281439	0.000010	0.000640	0.028258	0.281413	-0.9 ± 0.4	2.43	0.281437	0.281707
MK3-02	0.281476	0.000011	0.001031	0.047157	0.281435	-0.1 ± 0.4	2.40	0.281437	0.281707
MK3-03	0.281566	0.000015	0.001436	0.060529	0.281508	2.5 ± 0.5	2.31	0.281437	0.281707
MK3-04	0.281525	0.000013	0.001304	0.057755	0.281473	1.2 ± 0.5	2.36	0.281437	0.281707
MK3-05	0.281456	0.000008	0.000818	0.037361	0.281423	-0.5 ± 0.3	2.42	0.281437	0.281707
MK3-06	0.281420	0.000010	0.000826	0.037954	0.281387	-1.8 ± 0.3	2.46	0.281437	0.281707
MK3-07	0.281527	0.000011	0.001244	0.056279	0.281477	1.4 ± 0.4	2.35	0.281437	0.281707
MK3-08	0.281468	0.000014	0.000769	0.034297	0.281437	-0.0 ± 0.5	2.40	0.281437	0.281707
Median value						**-0.1 ± 0.4**	**2.40**		

assign a crystallization age for sample KMP1, we conclude that the protolith to the Kapiri Mposhi granite gneiss component of the Mkushi Gneiss crystallized at ca. 2723 ± 24 Ma.

Sample MK3—Five analyses were conducted on four grains (fig. 3B, table 2). Three analyses were located on rims (2r, 3r and 4r), one analysis was conducted on a single-domain zircon (1) and one analysis sampled a zircon core (4c). Rim analyses 2r and 3r recorded low Th/U ratios (0.08 and 0.10 respectively), suggestive of a metamorphic origin (Hoskin and Black, 2000) and have the youngest $^{207}Pb/^{206}Pb$ ages of 2015 ± 13 and 2031 ± 10 Ma. Analysis pair 4r-4c yielded $^{207}Pb/^{206}Pb$ crystallization ages of 2044 ± 23 and 2037 ± 15 Ma respectively. All five data points yield a weighted mean $^{207}Pb/^{206}Pb$ age of 2032 ± 15 Ma (MSWD = 2.8). The relatively high MSWD indicates that these data indeed comprise multiple populations. Excluding the two low Th/U rim analyses, on the basis that they represent slightly younger zircon growth, and the most discordant data point, a weighted mean $^{207}Pb/^{206}Pb$ age of 2047 ± 14 Ma (MSWD = 0.15) can be calculated, which provides the best estimate for the crystallization of the precursor of this component of the Mkushi Gneiss, and is within error of the age of 2049 ± 6 Ma reported by Rainaud and others (2005). The slightly younger low Th/U rims indicate that this emplacement was directly followed by additional zircon growth between 2031 ± 10 and 2015 ± 13 Ma, perhaps linked to the intrusion of aplites, one of which dated by Rainaud and others (2005) at 2036 ± 22 Ma. Eight zircon grains were analyzed for Lu/Hf isotopic composition, and gave $\varepsilon_{Hf}(t)$ values between −1.8 and 2.5 and T_{DM} model ages between 2.46 and 2.31 Ga indicating a crustal residence age of 300 to 400 Million years (table 3, fig. 4). This is in contrast with the whole rock Sm-Nd data reported for the same sample, which gave a $\varepsilon_{Nd}(t)$ value of −9.2 and a T_{DM} model age of 3.25 Ga, indicating a much longer crustal residence (De Waele and others, 2006b).

Sample MK5—Seven analyses were conducted on oscillatory zoned domains of seven zircon grains (fig. 3C, table 2). The data show relatively high U+Th content and typical magmatic Th/U ratios between 0.5 and 0.9. Five data points loosely define an

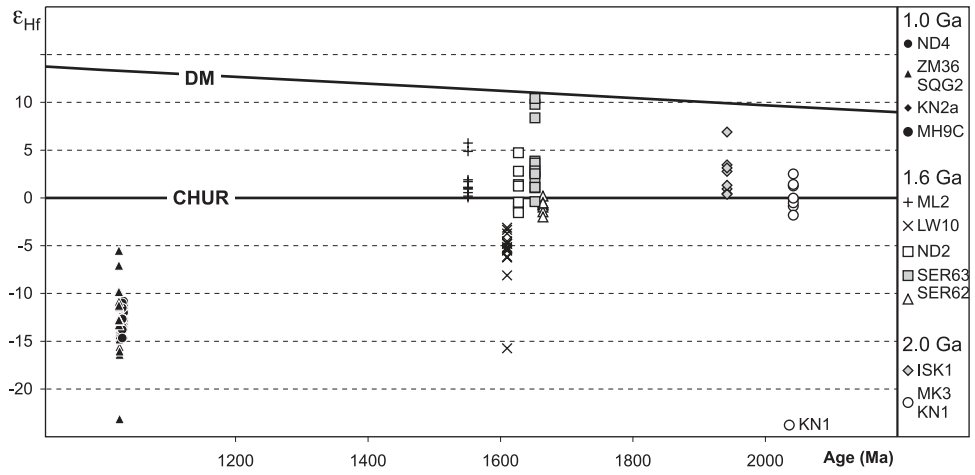

Fig. 4. $\varepsilon_{Hf}(t)$ versus age plot of data obtained on granitoid rocks in the Irumide Belt.

age group with a weighted mean $^{207}Pb/^{206}Pb$ age of 2038 ± 14 Ma (MSWD = 3.0), while the remaining data points (3 and 4) yield significantly younger discordant $^{207}Pb/^{206}Pb$ ages of 2026 ± 18 and 1973 ± 14 Ma. The age of 2038 ± 14 Ma can be adopted for the crystallization age of the granite protolith of this part of the Mkushi Gneiss, again within error of the ages reported by Rainaud and others (2005).

Sample CC10—Six zircon grains were analyzed and record relatively high U+Th content (300–1300 ppm) and Th/U ratios between 0.6 and 0.9 (table 2). The data yielded a weighted mean $^{207}Pb/^{206}Pb$ age of 1953 ± 6 Ma (MSWD = 2.19, fig. 3D). A Concordia age of 1952 ± 6 Ma (MSWD = 1.8) can be calculated from the five most concordant points, and is considered the best estimate for the crystallization age of the granite precursor to this sample.

Sample KN1—Six analyses were conducted on six zircon and gave U+Th contents between 330 and 650 ppm, with Th/U ratios in the range 0.3 to 0.6 (fig. 5A, table 2). The five most concordant analyses yield a weighted mean $^{207}Pb/^{206}Pb$ age of 2036 ± 6 Ma (MSWD = 1.0). The discordant analysis number 1 which yielded an age of 2089 Ma and may be a xenocryst, is excluded from the calculation. Using only the three most concordant data, a Concordia age of 2041 ± 10 Ma (MSWD = 0.83) can be calculated, which provides the best estimate for the crystallization age of the granite protolith. One zircon was analyzed for Lu-Hf isotopic composition (table 3, fig. 4), and recorded an $\varepsilon_{Hf}(t)$ value of −23.8 and T_{DM} of 3.26 Ga, possibly indicating that the granite represents a crustal melt. Additional work is needed to confirm the strongly reworked nature of this granite gneiss.

Luwalizi Granite (samples ISK1 and ISK2).—The Luwalizi Granite is a large body of weakly foliated coarse-grained biotite granite that extends from Chinsali (c on fig. 1B) northwards into the Bangweulu Block. It forms the basement to the Manshya River Group, and is correlated with the widespread granitoids of the Bangweulu Block of northern Zambia. Two samples were collected (ISK1 and ISK2 on fig. 1B), and both consist of coarse-grained foliated biotite granite.

Sample ISK1—Nine analyses were conducted on nine different zircon grains (fig. 5B, table 2). The data show very variable U and Th content, in the ranges 93 to 2669 ppm and 109 to 595 ppm respectively, giving variable Th/U ratios between 0.04 and 1.93 (table 2). Three analyses, 2, 3 and 6, are excluded from calculations. Analysis 2

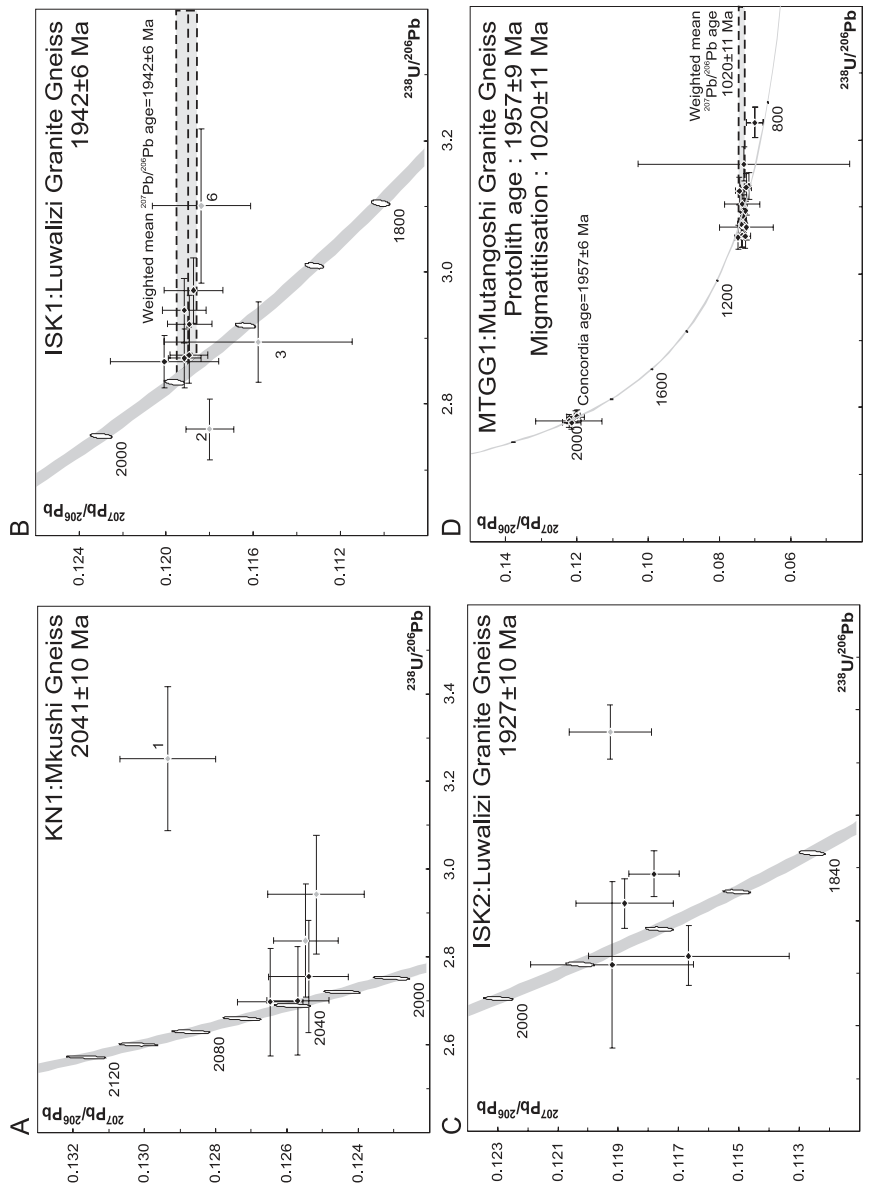

Fig. 5. U-Pb evolution diagram showing data for (A) KN1; (B) ISK1; (C) ISK2 and (D) MTGG1.

displays an unusually high concentration of U (2,669 ppm), whereas analysis 3 yielded high f_{206} (0.855%), low U (93 ppm) and high $^{232}Th/^{238}U$ (1.93). Analysis 6 is discordant and records high U content (860 ppm) and some Pb_c. The remaining analyses plot close to Concordia and define a weighted mean $^{207}Pb/^{206}Pb$ age of 1942 ± 6 Ma (MSWD = 0.23), taken to be the best estimate for the crystallization age of the granite in sample ISK1. Eight zircon were analyzed for Lu-Hf isotopic composition, and recorded $\varepsilon_{Hf}(t)$ values between 0.4 and 6.9 and T_{DM} in the range 2.31 to 2.06 Ga indicating some crustal residence (table 3, fig. 4).

Sample ISK2—Five analyses were conducted on five zircon grains (table 2, fig. 5C). The data show the same variable U and Th ratios, resulting in a wide range of Th/U between 0.03 and 1.34 (table 2). Four of the analyses group in a tight cluster close to Concordia and yield a Concordia age of 1927 ± 10 Ma (MSWD = 0.92), which we take as the best estimate for the crystallization age of the granite in sample ISK2. Note that the ages for samples ISK1 and ISK2 overlap within uncertainty.

Mutangoshi Granite Gneiss.—The Mutangoshi Granite Gneiss forms a body of strongly foliated to migmatitic biotite granite gneiss in the northeastern Irumide Belt. On the basis of Rb-Sr whole-rock analyses Daly (ms, 1986) determined an emplacement age of 1407 ± 33 Ma for this body. We collected one sample from a flat outcrop of migmatitic biotite granite gneiss mapped as Mutangoshi Gneissic Granite, near the contact with a younger, undeformed Irumide-age (~1.0 Ga) granitoid (Chilubanama Granite of Daly, ms, 1986). The migmatite is truncated by numerous quartz-rich melts related to the nearby Chilubanama Granite.

Sample MTGG 1—A total of 23 analyses were conducted on 17 different zircon grains (table 2, fig. 5D). Three sets of analyses were conducted on core-rim pairs (3, 6 and 7) one of which yielded significantly different ages. Two analyses were conducted on zircon core. Several analyses on rims and cores were aborted due to high ^{204}Pb counts and are not included in the data table. Analysis on core 3c yielded a $^{207}Pb/^{206}Pb$ age of 1961 ± 37 Ma (98.6% concordant), whereas the rim (3r) gave a $^{207}Pb/^{206}Pb$ age of 1008 ± 15 Ma (99.7% concordant). The age of the core compares well with analyses 12, 16c and 25c, which yielded concordant $^{207}Pb/^{206}Pb$ ages of 1955 ± 12, 1989 ± 136 and 1978 ± 38 Ma respectively. Taken together these four analyses yield a Concordia age of 1957 ± 6 Ma, which is considered the best estimate for the crystallization age of the precursor granite to the Mutangoshi Gneissic Granite. The remaining analyses, including two core-rim pairs (6 and 7) and one analysis on a core (4), define a cluster on the U-Pb evolution diagram (fig. 5D) defining a weighted mean $^{207}Pb/^{206}Pb$ age of 1020 ± 11 Ma (MSWD = 4.6). This age corresponds closely to the reported age of the Chilubanama Granite adjacent to the Mutangoshi Gneissic Granite (De Waele and others, 2003; De Waele, ms, 2005), and we interpret these zircons to have crystallized either from granitic melt of the Chilubanama Granite, or from *in situ* melts related to its intrusion.

POST-MUVA SUPERGROUP AND PRE-IRUMIDE GRANITOIDS AND GNEISSES IN THE IRUMIDE BELT

A suite of granitoid rocks has been recognized which postdates the Paleoproterozoic basement, but predates Irumide tectonism (1.02 Ga) and the voluminous syn- to late- and post-Irumide granitoids (1.05–0.95 Ga). These plutons are known as the Lukamfwa Hill Granite Gneiss in the southwest and as the Lubu Granite Gneiss and Musalango Gneiss in the northeast (LHG, LGG and MSG on fig. 1B). The Lubu Granite Gneiss, was previously believed to be Paleoproterozoic (Daly, ms, 1986), because of its similar character to the Luwalizi Granite Gneiss, which can be traced into granitoids of the Bangweulu Block. The Musalango Gneiss was considered equivalent to the Mutangoshi Gneissic Granite, which was dated using the whole-rock Rb-Sr isochron method at 1407 ± 33 Ma (Daly, ms, 1986). During this study four samples of

the Lukamfwa Hill Granite Gneiss (SER62, SER63, SR12 and ND2,), and one each of the Lubu Granite Gneiss (ML2,) and Musalango Gneiss (LW10, fig. 1B) were dated.

The Lukamfwa Hill Granite Gneiss

The Lukamfwa Granite Gneiss comprises leuco- to mesocratic biotite granite gneiss, with a strong foliation defined by aligned biotite and stretched feldspars. The unit exhibits proto-mylonitic fabrics in local shear zones and commonly contains two deformation fabrics. Samples SER62 and SER63 were collected from Lukamfwa Hill in the Serenje 1:100,000 scale map sheet, whereas SR12 and ND2 were collected from similar granitoid plutons west of Lukamfwa Hill.

Sample SER62—A total of 10 analyses were conducted on eight separate zircon grains (fig. 6A, table 2). U and Th contents were found to be variable, within the range 118 to 6101 ppm, with Th/U ratios between 0.38 and 1.16. A high U and Pb_c content for 41c led us to exclude this data point from age calculations. Using the seven most concordant points, a Concordia age of 1665 ± 4 Ma with MSWD of 0.14 is obtained, which we take as the best estimate for the crystallization age of this sample. Eight zircon grains were analyzed for Lu-Hf isotopic composition, and recorded $\varepsilon_{Hf}(t)$ values between −2.0 and 0.2 and a narrow range of T_{DM}, 2.15 to 2.07 Ga, slightly younger than the model age range for the Mkushi Gneiss (table 3, fig. 4). These data suggest that the Lukamfwa Granite Gneiss was largely derived from reworked crust, but received substantial juvenile input as well.

Sample SER63—Ten analyses were conducted on oscillatory zoned sectors of ten zircon grains (table 2, fig. 6B). U and Th contents were a lot more consistent, with ranges of 280 to 470 ppm and 211 to 356 ppm respectively, and a narrow range of Th/U ratios between 0.59 and 1.11. A Concordia age of 1650 ± 8 Ma can be calculated for the analyses (MSWD = 1.40), which we consider to be the best age estimate for the crystallization of the precursor granite in sample SER 6-3. Lu-Hf isotopic composition was obtained for twelve grains, and gave $\varepsilon_{Hf}(t)$ values between −0.4 and 10.4 and a range of T_{DM} 1.67 to 2.08 Ga indicating more juvenile input for this sample than for sample SR62 (table 3, fig. 4). Whole rock Sm-Nd data reported for a sample collected from the same locality (SR7, see De Waele and others, 2006b), yielded an $\varepsilon_{Nd}(t)$ value of −10.0 and a T_{DM} model age of 3.23 Ga, indicating significant crustal residence. It is unclear whether these data reflect a composite nature of the Lukamfwa Granite, with locally unmixed portions of juvenile magma within a dominantly reworked melt.

Sample SR12—Seven analyses were conducted on seven different zircon grains (table 2, fig. 6C). U+Th values range from 215 to 478 ppm, with Th/U ratios between 0.63 and 1.19. All data are near concordant and define a $^{207}Pb/^{206}Pb$ age of 1639 ± 14 Ma (MSWD = 0.91). However, a slight drift off Concordia could represent Pb-loss at 1020 Ma, the age of metamorphism in the Irumide Belt (De Waele and others, 2006a), and a regression towards that gives an upper intercept at 1638 ± 30 Ma (MSWD = 0.04). The four most concordant data points correspond to a Concordia age of 1655 ± 11 Ma (MSWD = 1.80), which we interpret as the best estimate for the crystallization age of this granite. Whole rock Sm-Nd data reported in De Waele and others (2006b), yielded an $\varepsilon_{Nd}(t)$ value of −8.8 and T_{DM} model age of 2.85 Ga, reflecting an origin by melting of Archean crust.

Sample ND2—Four analyses were conducted on four zircon grains (table 2, fig. 6D) and gave a narrow spread of U and Th values, 103 to 229 ppm and 82 to 196 ppm respectively, giving Th/U ratios between 0.83 and 0.90. The data are near concordant, and define an age group with Concordia age of 1627 ± 12 Ma (MSWD = 0.51), which is taken to represent the crystallization age of the granite protolith. Eight zircons were analyzed for Lu-Hf isotopic composition, and recorded $\varepsilon_{Hf}(t)$ values between −1.5 and

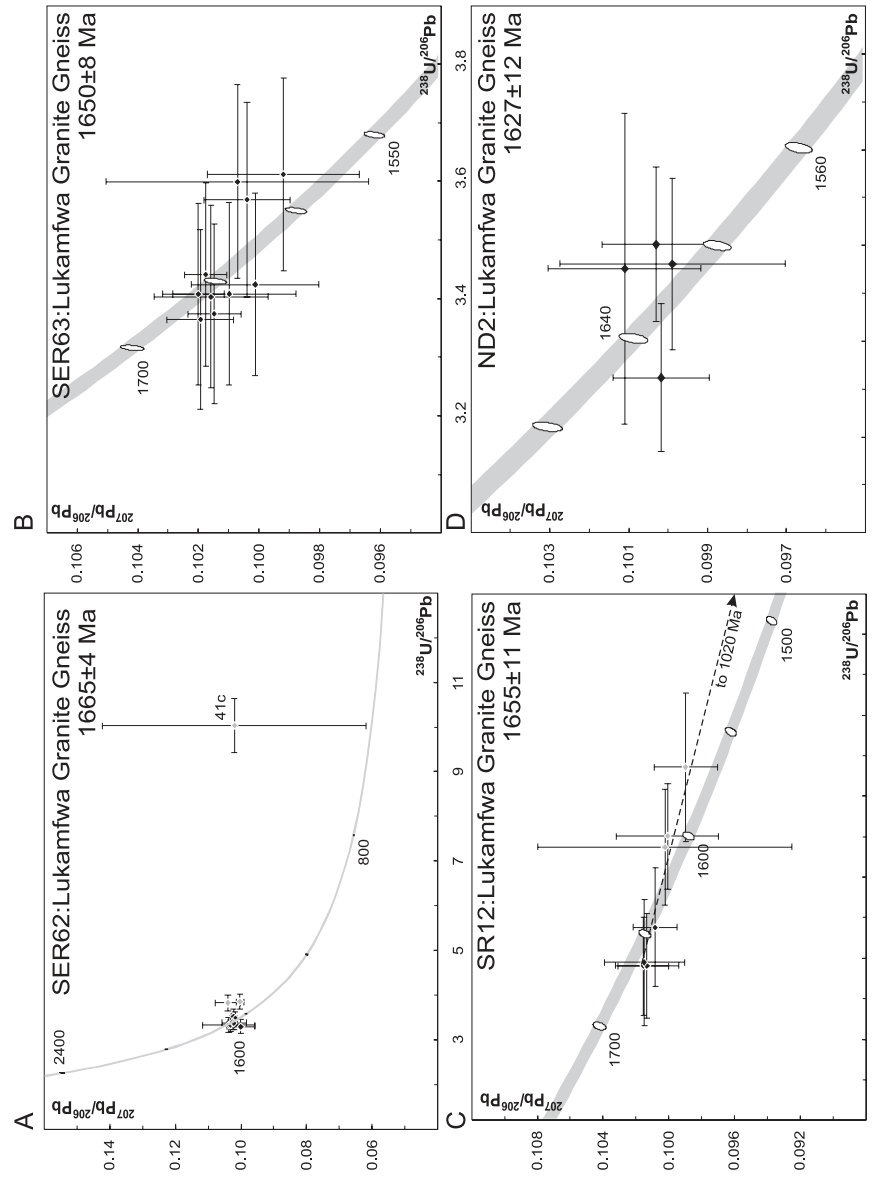

Fig. 6. U-Pb evolution diagram showing data for (A) SER62; (B) SER63; (C) SR12 and (D) ND2.

4.7 and a range of T_{DM} 2.12 to 1.86 Ga, indicating a mix of crustal and juvenile melt in the sample (table 3, fig. 4).

The Lubu Granite Gneiss

Sample ML2—Sample ML2 was collected from the Lubu Granite Gneiss (marked LGG, fig. 1B), which was interpreted by Daly (ms 1986, 1995a) to form the basement to the Muva Supergroup in the northeastern Irumide Belt. The Lubu Granite Gneiss is an equigranular, strongly foliated pink biotite granite gneiss, which in places is intruded by numerous small tightly folded pegmatites. Eleven clear, uncracked portions of eleven zircon crystals were analyzed during two separate sessions (table 2, fig. 7A). The data are characterized by high Pb_c and unusually high Th/U ratios (table 2). A regression line through all data points defines an upper intercept of 1547 ± 30 Ma and lower intercept 465 ± 440 Ma (MSWD = 0.76). A weighted mean $^{207}Pb/^{206}Pb$ age of all but the two most discordant points gives an age of 1532 ± 14 Ma (MSWD = 0.97). We take the latter to represent the best age estimate for crystallization of zircon in the protolith of the granite gneiss. Ten zircon grains were analyzed for Lu-Hf isotopic composition, and recorded $\varepsilon_{Hf}(t)$ values between 0.0 and 5.7 and a range of T_{DM} of 1.98 to 1.78 Ga, indicating a juvenile character with possibly some limited crustal residence time for the protolith of the Lubu Granite Gneiss (table 3, fig. 4).

The Musalango Gneiss

Sample LW10—The Musalango Gneiss forms a well-defined pluton in the northeastern Irumide Belt, comprising foliated gray biotite granite (MSG on fig. 1B). It was mapped by Daly (ms 1986, 1995a) as part of the Mutangoshi Gneissic Granite, which had yielded a whole-rock Rb-Sr date of ~1.4 Ga. Thirteen analyses were carried out on thirteen grains. The data are characterized by low U and Th content (see table 2), leading to relatively imprecise ratios. Excluding the five analyses with lowest U and highest Pb_c, a Concordia age of 1587 ± 13 Ma (MSWD = 2.4, see fig. 7B) can be calculated, which we take to represent the best estimate for the crystallization of zircon in sample LW10. 14 zircons yielded Lu-Hf isotopic compositions from which a range of $\varepsilon_{Hf}(t)$ values between −3.1 and −15.7 and T_{DM} between 2.62 and 2.14 Ga were calculated (table 3, fig. 4). These data clearly indicate a significant crustal component in this sample, with possible derivation from Mesoarchean source material.

LATE-MESOPROTEROZOIC INTRUSIONS: THE IRUMIDE GRANITOIDS

A total of 25 samples from Irumide granitoid bodies were collected across the Irumide Belt between Kapiri Mposhi and Isoka (k and is on fig. 1B, table 2) and include foliated and unfoliated granitoids. Sample KK1 was taken from a flat outcrop along the sealed road near Kapiri Mposhi, and consists of porphyritic biotite granite with elongate fine grained angular xenoliths of mafic material, possibly broken-up mafic dikes. A foliation along northerly direction, dipping steeply to the south, is defined by strongly aligned biotite, wrapping around essentially euhedral large microcline phenocrysts. Sample MH4 was collected from a flat outcrop of foliated porphyritic granite, cut by various aplite dikes, which are folded along axes plunging shallowly to the north. Microcline phenocrysts are euhedral and aligned along an east-west direction, defining a shallow northerly-dipping fabric interpreted as primary magmatic layering. Sample MH9 was taken from a large whaleback outcrop of megacrystic granite, with abundant megacrysts of microcline of up to 5 cm in length. The granite is cut by numerous shallow-dipping aplitic dikes, which appear to follow a flat-lying primary magmatic fabric defined by aligned megacrysts. A shallow north-dipping foliation along west-southwest direction is defined by alignment of biotite flakes. Sample CC5 was collected from a large flat outcrop of porphyritic granite, intruded by various aplite dikes. The granite also contains small late melt veins, in which abundant

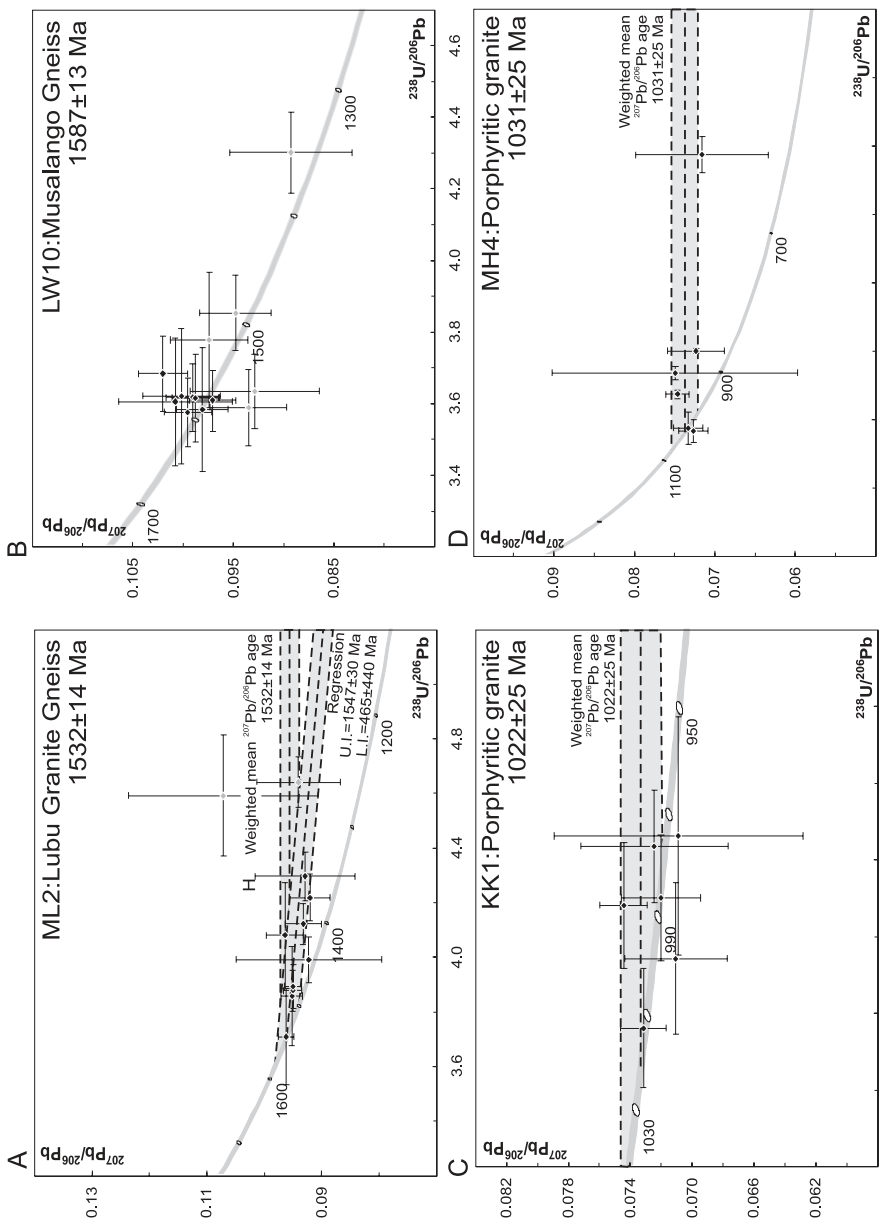

Fig. 7. U-Pb evolution diagram showing data for (A) ML2; (B) LW10; (C) KK1 and (D) MH4.

garnet was observed. Sample CC8 was collected from a flat outcrop of foliated porphyritic biotite granite similar to sample CC5. Sample MK7 was collected from foliated reddish biotite granite south of Mkushi (mk on fig. 1B). The granite is intruded by various cross-cutting small pegmatites. Both the granite and the pegmatites appear deformed and a series of mafic xenoliths occur along the foliation, which is trending east-northeast, dipping steeply to the east. Sample ND1 consists of coarse porphyritic biotite granite, with a very weak biotite foliation, and large microcline phenocrysts aligned along a north-south oriented magmatic layering. The phenocrysts are euhedral, and do not appear to be affected by the weak foliation. Sample ND4 was collected from a small circular body of granodiorite. The granodiorite is porphyritic, and contains minor quartz, large plagioclase and abundant hornblende in a subophitic texture, and subordinate biotite, defining a weak foliation. Sample ND5 was collected from a body of syeno-granite within the porphyritic granites. Although the contact between the porphyritic granites and the syeno-granite is not exposed, the weak deformation and similarities in fabric suggest the intrusion was emplaced at the same time as the granite. The rock consists of abundant phenocrysts of microcline set in a matrix of plagioclase and microcline, with subordinate quartz and biotite. The syeno-granite is cut by various aplitic dikes, which appear to display the same weak foliation as the host rock, and were emplaced perhaps during late stages of intrusion, and prior to the deformation that imparted the weak fabrics. Sample FW1 was collected from a flat outcrop of coarse porphyritic foliated granite, while sample FW2 came from an aplite dike cutting the granite. The foliation observed in the granite is defined by biotite, while microcline phenocrysts appear undeformed, and are aligned along a magmatic layering. The foliation does not seem to affect the aplite dikes, which consist of fine-grained microcline and quartz. Sample SASA2 was collected from a dome of leucocratic, mildly foliated granite north of Serenje (sr on fig. 1B), while sample SER53 came from a body of porphyritic biotite granite to the south of that. Samples SER64 and SQG2 come from similar K-feldspar porphyritic granitoid bodies south of Serenje. Sample KN2a was sampled from foliated biotite granite with large K-feldspar phenocrysts. Fine-grained aplitic dikes that contain garnet cut the granite gneiss. Sample KN5 was collected from a flat outcrop of foliated porphyritic biotite granite. The granite contains abundant xenoliths of mafic composition, as well as rafts of metasedimentary rocks, migmatitic material and fine-grained granite gneiss. The granite carries a prominent penetrative foliation along a north-south direction, dipping steeply to the west. Samples KN7 and KN8 were collected from two different inselbergs, consisting entirely of foliated two-mica granite. The granite is foliated along northeasterly trends, dipping shallowly to steeply to the northwest. Euhedral K-feldspar phenocrysts define a north-south trending primary magmatic fabric. Sample CHT6 comes from a flat lying outcrop of coarse, foliated biotite granite, which contains abundant small dark xenoliths of metasedimentary origin. The granite is cut by a biotite foliation oriented northeast and steeply dipping to the southeast. Sample ZM36 was collected from a leucocratic biotite granite in a quarry along the main road halfway between Serenje and Mpika (sr and mp respectively on fig. 1B). Sample CHL5 was taken from a flat outcrop to the southwest of Mpika, where strongly foliated micaceous granite gneiss is intruded by numerous small pegmatites. The gneiss shows a marked biotite-muscovite foliation along northeasterly trends, with steep north-directed dip. The Chilubanama Granite (or Grey Granite) described in detail by Daly (1995a), was sampled from four localities around Chinsali (samples LW1, LW2, MTG4 and ZM32). In all localities, the granite occurs as gray, biotite granite, with minor garnet in the case of sample MTG4. The Chilubanama Granite is commonly unfoliated and in places shows primary igneous fabrics.

Sample KK1—Six analyses were conducted on six single-domain zircon. U and Th show a narrow spread, with Th/U ratios between 0.50 and 1.35. The data show too much scatter to define a Concordia age, but define a narrow range of $^{207}Pb/^{206}Pb$ ratios, giving a weighted mean age of 1022 ± 25 Ma (MSWD = 1.08; fig. 7C). We consider this age a reasonable estimate for the timing of crystallization.

Sample MH4—Six zircons were analyzed during two sessions and yield variable U and Th contents, with U+Th in the range 165 to 1862 ppm, and Th/U ranging between 0.32 and 1.67. The data define a regression towards present-day Pb-loss, which gives an age of 1031 ± 25 Ma (MSWD = 0.55, fig. 7D). We take this to be the best estimate for the crystallization age of the granite.

Sample MH9—Seven analyses were conducted over two separate sessions (fig. 6A, table 2). U and Th contents are variable, in the ranges 120 to 808 ppm and 79 to 632 ppm respectively, but with a narrow range of Th/U ratios between 0.68 and 0.84. The data define a weighted mean $^{207}Pb/^{206}Pb$ age of 1035 ± 10 Ma (MSWD = 0.59, fig. 8A), which we take as the best estimate of the age of the granite. Eight Lu-Hf isotopic analyses were conducted, which record a narrow range of $\varepsilon_{Hf}(t)$ values between −11.0 and −14.7 and T_{DM} model ages between 2.07 and 1.97 Ga, indicating a substantial crustal component in the granite, with crustal residence times of up to a Billion years (table 3, fig. 4).

Sample CC5—Six analyses were conducted on five zircon crystals, including one core-rim pair (fig. 8B, table 2). The data define a narrow range of U and Th contents, and Th/U ratios between 0.40 and 0.62. The core-rim pair recorded overlapping ages and both are characterized by concentric zoning patterns indicative of magmatic crystallization. A Concordia age of 1038 ± 17 Ma (MSWD=0.32) can be calculated on all data points, and is taken as the best estimate for the crystallization age of the granite.

Sample CC8—Six analyses were conducted on six clear zircon grains (fig. 8C, table 2). U+Th content ranges from 396 to 800 ppm, with Th/U ratios between 0.42 and 0.66. One spot (5) shows an elevated Pb_c, and plots slightly away from a concordant cluster for which a Concordia age of 1035 ± 12 Ma (MSWD = 0.62) can be calculated, representing the best estimate for the age of crystallization of the granite.

Sample MK7—Six analyses were conducted on five zircons, including one core-rim pair (2c and 2r, see fig. 8D, table 2). A low Th/U ratio (0.04) was obtained from rim analysis 2r, which defines a concordant $^{206}Pb/^{238}U$ age of 883 ± 10 Ma and could reflect a metamorphic and/or metasomatic event. The analysis on the core (2c) yields a discordant data point which defines a $^{207}Pb/^{206}Pb$ age of 2003 ± 72 Ma and represents a xenocryst. The remaining four analyses display a range of $^{207}Pb/^{206}Pb$ isotopic ratios with a weighted mean of 1079 ± 150 Ma (MSWD = 2.5). The most concordant data point of this set gives a $^{207}Pb/^{206}Pb$ age of 1035 ± 32 Ma which could approximate the emplacement age of the granite. In summary, the data on this sample are insufficient to calculate an unequivocal age, neither for emplacement of the protolith or for the overprinting event(s).

Sample ND1—Ten analyses were conducted on nine zircon grains, including one core-rim pair (5c and 5r, fig. 9A, table 2). Analyses 1, 3, 5r, 7 and 8 yielded highly discordant results and are characterized by large f_{206} values and resulting poor precision (they are therefore now shown on the plot of fig. 9A). Five points do define a Concordia age of 1034 ± 6 Ma (fig. 9A), which we take as the best estimate for the crystallization age of the granite.

Sample ND4—Four analyses were conducted on four euhedral zircon grains (fig. 9B, table 2). The data are characterized by relatively high Th/U ratios, between 1.10 and 1.69. The data plot on Concordia and define a Concordia age of 1031 ± 9 Ma (MSWD = 0.74), which we consider the best estimate for crystallization of the granodiorite. Ten zircons were analyzed for Lu-Hf isotopic composition and record

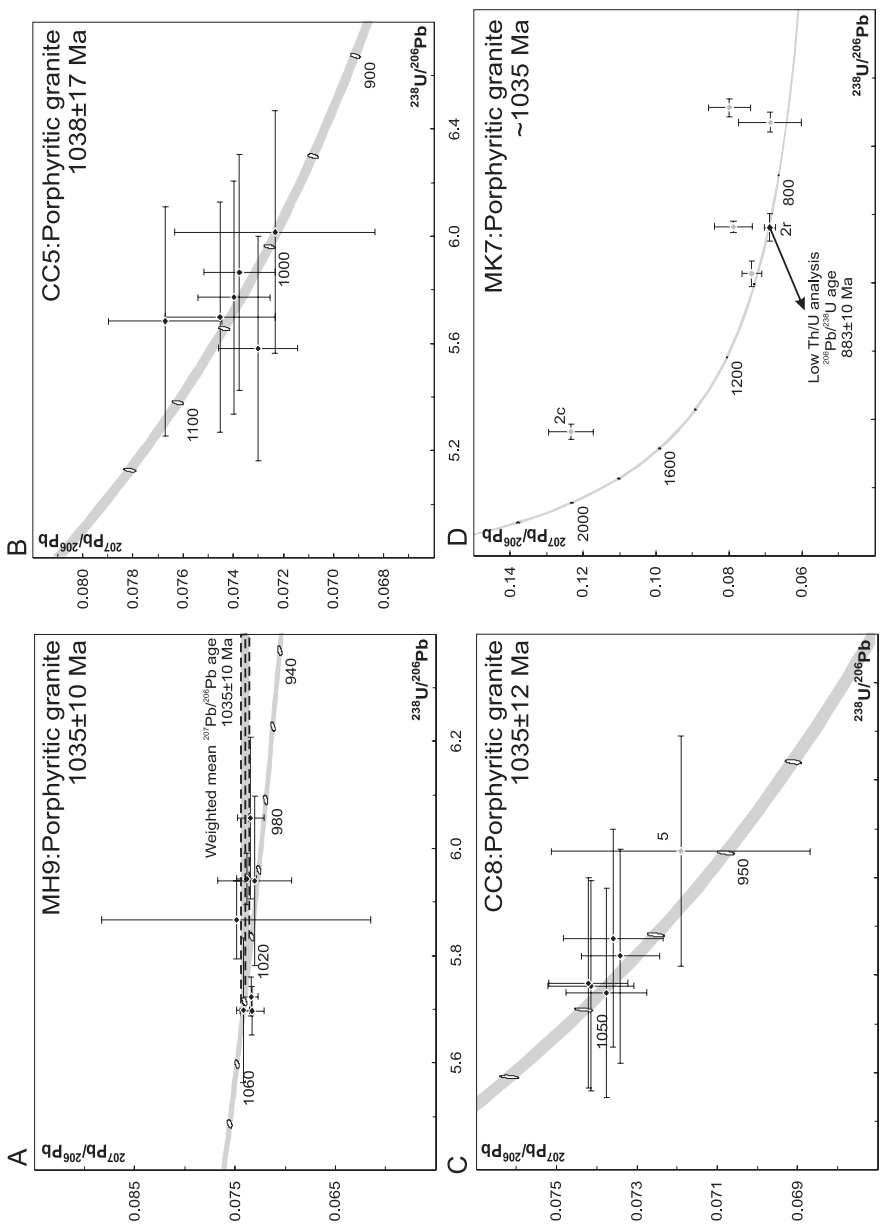

Fig. 8. U-Pb evolution diagram showing data for (A) MH9; (B) CC5; (C) CC8 and (D) MK7.

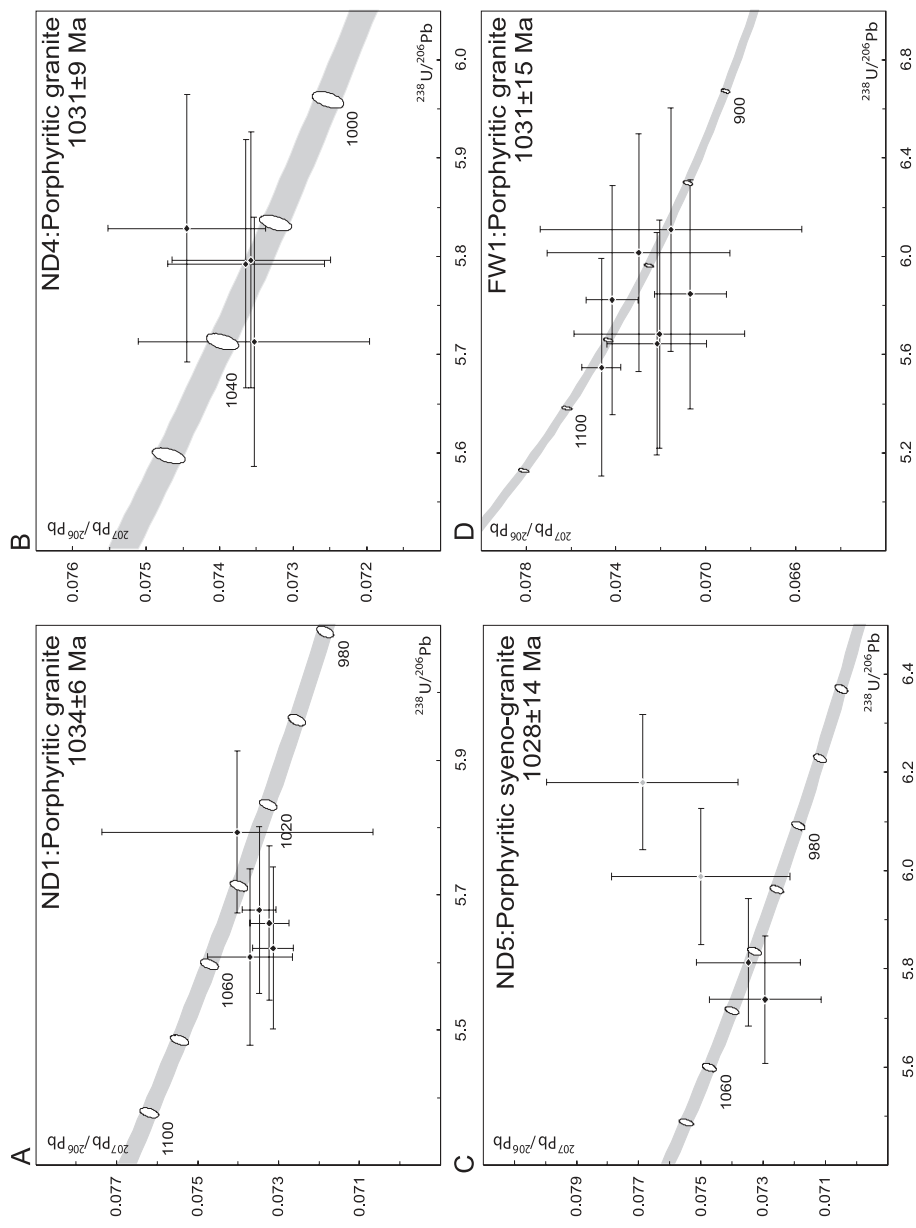

Fig. 9. U-Pb evolution diagram showing data for (A) ND1; (B) ND4; (C) ND5 and (D) FW1.

$\varepsilon_{Hf}(t)$ values between −13.1 and −10.8 and T_{DM} model ages between 2.09 and 1.93 Ga, indicating a substantial crustal component in the granite (table 3, fig. 4).

Sample ND5—Four zircons were analyzed, but two plot off Concordia due to overestimation of Pb_c (fig. 9C). The data show a narrow range of U and Th contents, as well as Th/U ratios. Two concordant points define a Concordia age of 1028 ± 14 Ma (MSWD = 0.25), which we can take as the best estimate for the age of the syenogranite.

Samples FW1 (granite) and FW2 (aplite dike)—Seven analyses were conducted on seven different zircon grains of the granite. The data indicate highly variable U content, between 203 and 2020 ppm, and variable Th/U ratios between 562 and 2442. The data yield a Concordia age of 1031 ± 15 Ma (fig. 9D; MSWD = 0.15) taken as a good approximation of the crystallization age of the porphyritic granite. Zircon grains from the aplite are subhedral, and comprise a wide variety of types based on morphology (see fig. 2D). U and Th values are also quite variable, with ranges of 77 to 1375 ppm U and 22 to 237 ppm Th, leading to Th/U ratios between 0.07 and 2.16. Thirteen analyses were completed on thirteen zircon grains (table 2), and additional analyses were abandoned due to high Pb_c. Nine zircon appear to define a single age group, for which a Concordia age of 2032 ± 12 Ma can be calculated (MSWD = 0.51, fig. 10A). We interpret this age to reflect underlying granitic basement and the zircon to be xenocrystic. Of the remaining five zircon analyses, two are concordant and define $^{207}Pb/^{206}Pb$ ages of 2773 ± 46 Ma and 1637 ± 93 Ma corresponding to additional basement sources sampled by the aplite.

Sample SASA2—A total of 10 zircon grains were analyzed of sample SASA2, including two core-rim pairs (figs. 2D, 10B; table 2). U and Th are very variable, as are the Th/U ratios. Analyses of the two core-rim pairs yielded identical results (within error) as analyses on single-growth zircon. A Concordia age can be calculated from the nine most concordant data points, yielding 1023 ± 13 Ma (MSWD = 0.13), which we take to be the most reliable estimate for the age of the Sasa Granite.

Sample SER53—Ten different zircon grains were analyzed (table 2), three of which show slightly elevated Pb_c and plot away from Concordia (fig. 10C). U and Th content are in the range 117 to 813 ppm and 123 to 761 ppm respectively, with Th/U between 0.50 and 1.74. A concordant cluster of seven data points corresponds to an age of 1036 ± 11 Ma (MSWD = 0.56, see fig. 10C), which we take as the best age estimate for crystallization of zircon in SER53.

Sample SER64—Ten analyses were conducted on ten zircon grains (fig. 10C, table 2). One analysis yielded a concordant $^{207}Pb/^{206}Pb$ age of 2000 ± 13 Ma and is interpreted as a xenocryst. Excluding one inversely discordant data point and two with high Pb_c a Concordia age of 1037 ± 11 Ma (MSWD = 1.12) can be calculated, which we consider the best estimate for the crystallization age of the porphyritic granite. It is worth noting that whole rock Sm-Nd analysis of a sample from the same locality, sample SR5 reported in De Waele and others (2006b), yielded an $\varepsilon_{Nd}(t)$ value of −15.2 and T_{DM} model age of 2.63 Ga, indicating this granite to be a crustal melt.

Sample SQG2—Eleven analyses were conducted on eleven zircon grains. U+Th contents are quite high, between 275 and 1048 ppm, with Th/U ratios between 0.38 and 1.04 (table 2). The data define a broad cluster close to Concordia with a weighted mean $^{207}Pb/^{206}Pb$ age of 1032 ± 16 Ma (MSWD = 3.4, fig. 11A). Using only a cluster of six coherent and concordant data points (7, 17, 20, 41, 48 and 60), a Concordia age of 1020 ± 8 Ma (MSWD = 2.8) can be calculated, which we propose to be the best estimate for the crystallization age of the granite. Twelve Lu-Hf isotopic analyses were conducted, recording a range of $\varepsilon_{Hf}(t)$ values between −13.3 and −5.5 and T_{DM} model ages between 2.03 and 1.79 Ga, indicating the crustally reworked nature of the granite (table 3, fig. 4).

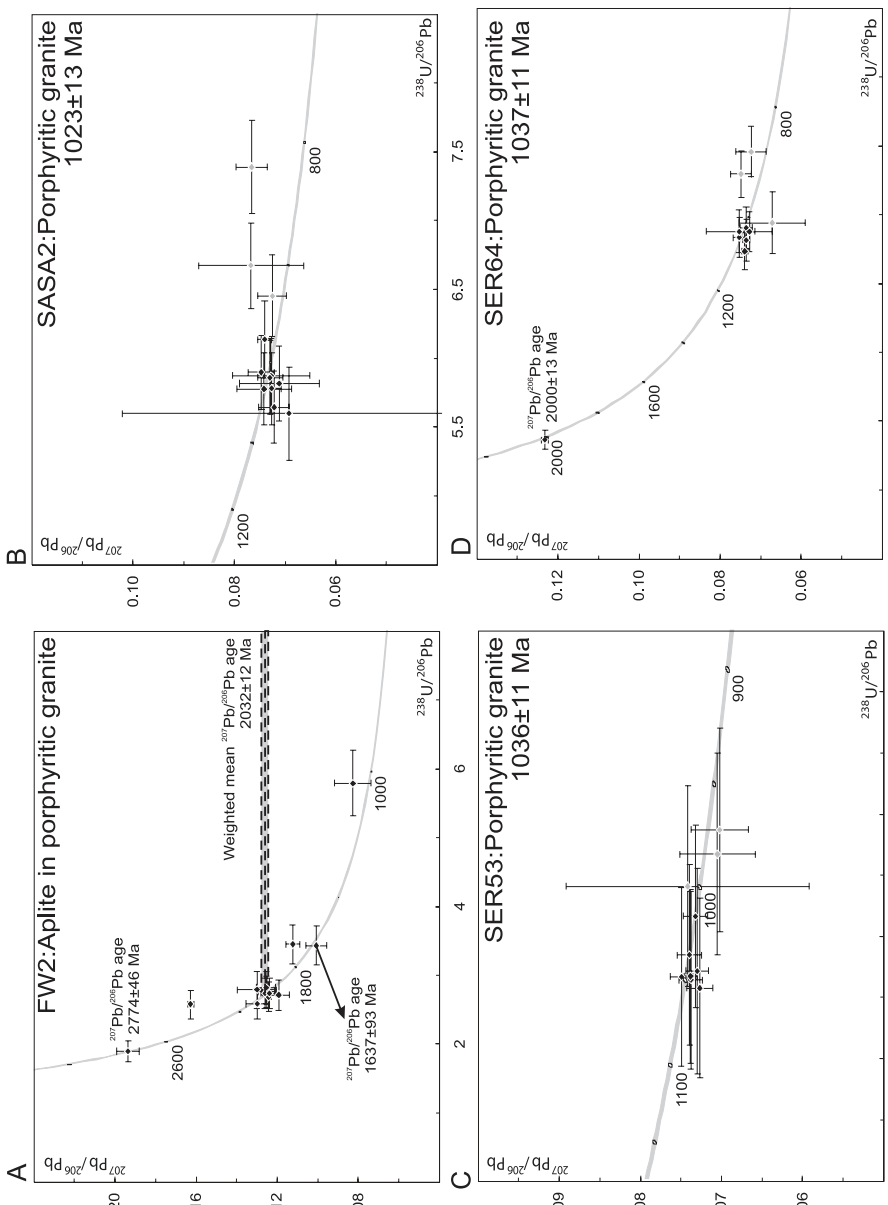

Fig. 10. U-Pb evolution diagram showing data for (A) FW2; (B) SASA2; (C) SER53 and (D) SER64.

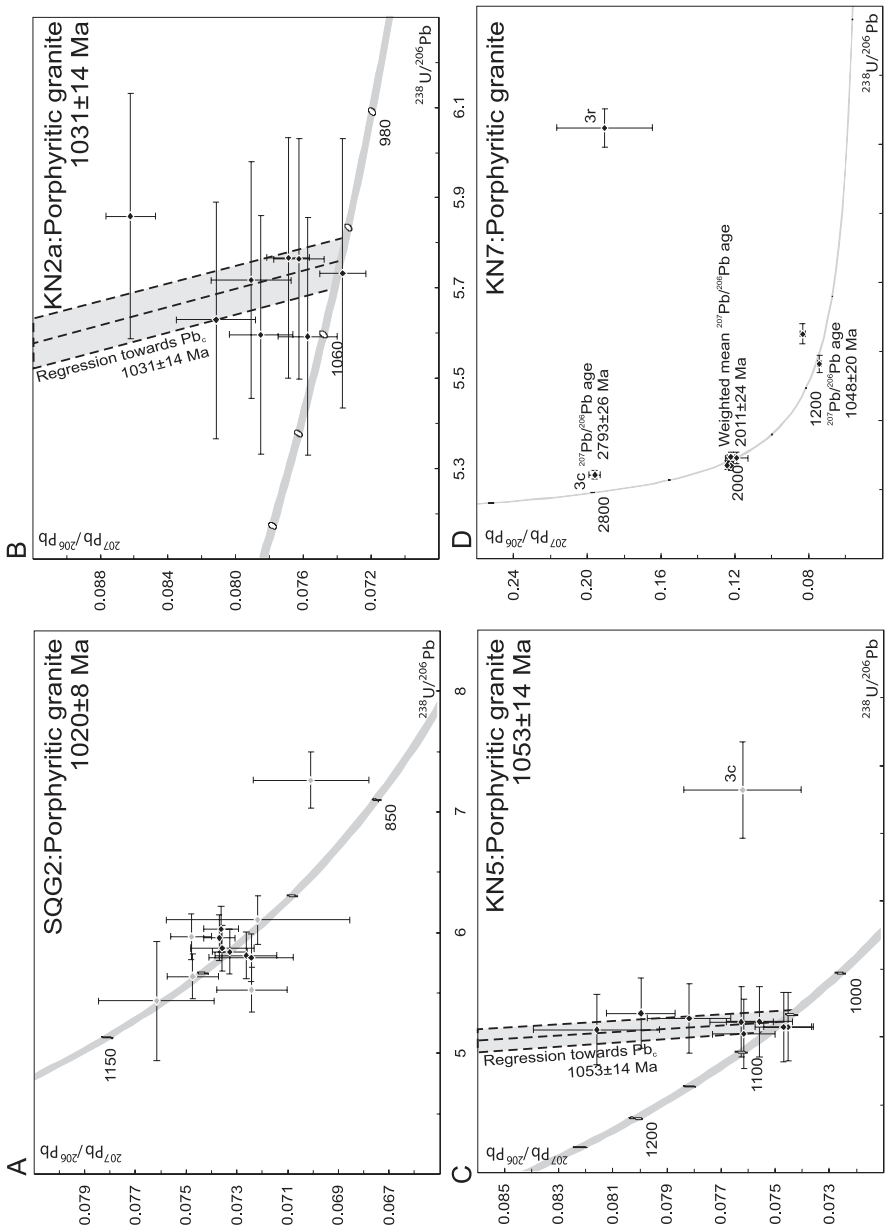

Fig. 11. U-Pb evolution diagram showing data for (A) SQG2; (B) KN2a; (C) KN5 and (D) KN7.

Sample KN2a—Eight analyses were conducted on eight different zircon grains, but an erratic drift normal to the Concordia curve is interpreted to reflect a problem with the common Pb correction (based on measured ^{204}Pb). The $^{206}Pb/^{238}U$ ratios are however closely clustered and give a weighted mean age of 1041 ± 15 Ma (MSWD = 0.51). The uncorrected data (as shown in fig. 11B) show a trend towards common Pb, and a regression towards a common Pb composition appropriate for the age of the sample (Stacey and Kramers, 1975) yields an intercept at 1031 ± 14 Ma (fig. 11B; MSWD = 0.81), which represents the best estimate for the crystallization age of the granite. Eight Lu-Hf isotopic analyses were conducted, recording a range of $\varepsilon_{Hf}(t)$ values between −14.7 and −13.3 and T_{DM} model ages between 2.09 and 2.04 Ga, indicating a significant crustal component in the granite (table 3, fig. 4).

Sample KN5—Nine analyses were conducted on eight zircon grains, including one core-rim pair (3c and 3r). The analyzed rim contains a high amount of U (2299 ppm) and is radiogenically damaged as evidenced by the significant Pb-loss and discordance (fig. 11C). The data range from discordant to concordant, and show the same drift, normal to the Concordia, as sample KN2a, indicative of incorrect Pb_c correction. The values, plotted uncorrected for common Pb (fig. 11C), can be regressed towards common Pb to yield an intercept at 1053 ± 14 Ma (MSWD = 0.24) providing the best estimate for the crystallization age of the granite.

Sample KN7—Eight analyses were conducted on seven zircon grains. One core and rim pair from the same grain yielded no significant difference in $^{207}Pb/^{206}Pb$ age (analyses 3c and 3r, table 2) but the rim analysis records anomalously high U and Th contents of 2878 and 39994 ppm respectively, and is extremely discordant (fig. 11D). The core, though discordant, defines a $^{207}Pb/^{206}Pb$ age of 2793 ± 26 Ma, taken to be the minimum age of this xenocryst. Four analyzed zircon define a broad age group, for which a weighted mean $^{207}Pb/^{206}Pb$ age of 2011 ± 24 Ma can be calculated (fig. 11D) interpreted to represent a second xenocrystic component. Analysis 7 yields a concordant $^{207}Pb/^{206}Pb$ age of 1048 ± 20 Ma and is interpreted to provide the only estimate for the crystallization age of the granite.

Sample KN8—Nine single and two core-rim pair analyses were conducted on complex zircon. Core analysis 1c yielded a concordant $^{207}Pb/^{206}Pb$ age of 2052 ± 26 Ma and confirms the presence of a ca. 2.05 Ga xenocrystic component (fig. 12A). Another core (4c) yielded discordant isotopic ratios and has a $^{207}Pb/^{206}Pb$ age of 2075 ± 70 Ma adding further weight to the interpretation of a Paleoproterozoic source at depth. Two strongly discordant data points 1r and 7 yielded $^{207}Pb/^{206}Pb$ ages of 1320 ± 31 Ma and 1626 ± 61 Ma, but because of their high discordance neither of these analyses lend themselves to simple interpretation. The remaining nine data points display an erratic drift normal to the Concordia curve, interpreted to reflect incorrect correction for common Pb. Uncorrected data, plotted on a Tera-Wasserburg Concordia diagram (fig. 12A), yield a regression towards common Pb, with an intercept at 1022 ± 16 Ma (MSWD = 1.40) which we consider the best estimate for the crystallization of the granite.

Sample CHT6—Nine analyses were conducted on nine zircon grains. The zircon are characterized by relatively low U and Th. Despite low counts on ^{204}Pb, values of f_{206} are therefore quite high, exceeding 1 percent in 4 analyses. The data give a Concordia age of 988 ± 23 Ma (MSWD = 1.5, fig. 12B), taken as the best estimate of the crystallization age of sample CHT6.

Sample ZM36—Ten zircon grains were analyzed, giving variable U, Th and Th/U values (table 2). A Concordia age of 1028 ± 12 Ma can be calculated on all data (MSWD = 0.01, fig. 12C) considered the best age estimate for the Mununga Granite. Twelve Lu-Hf isotopic analyses were conducted, recording a range of $\varepsilon_{Hf}(t)$ values between −16.4 and −11.5, as well as one very negative value of −23.1, and T_{DM} model

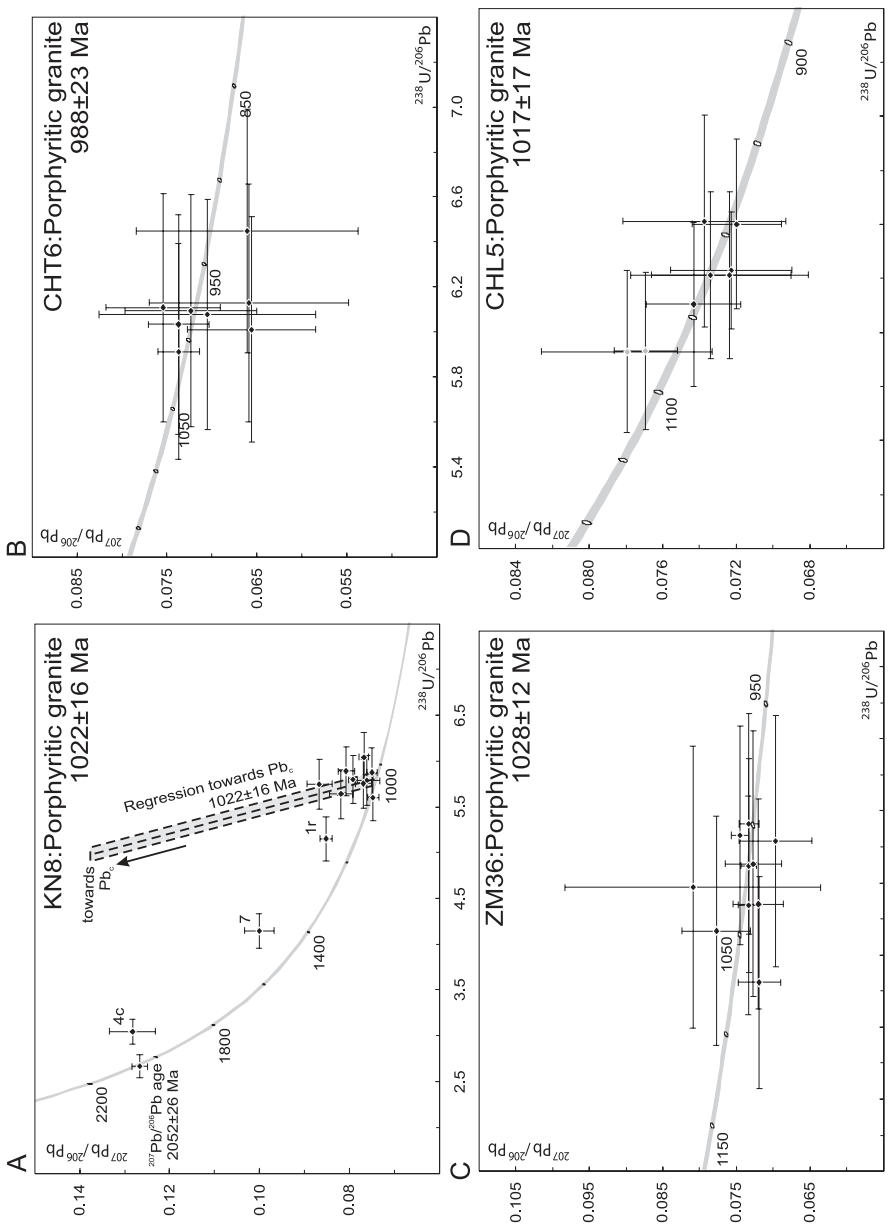

Fig. 12. U-Pb evolution diagram showing data for (A) KN8; (B) CHT6; (C) ZM36 and (D) CHL5.

ages between 2.14 and 1.95 Ga (2.42 Ga for the outlier), indicating crustally derived granite (table 3, fig. 4).

Sample CHL5—Eight analyses were conducted on eight different zircon and display variable U+Th content, ranging from 288 to 914 ppm. All data give a Concordia age of 1038 ± 15 Ma (MSWD = 2.8, fig. 12D). Two data point, however, plot well away from the cluster and correspond to zircon grains with anomalously high Th/U ratios (table 2). A Concordia age on the remaining six data points gives 1017 ± 17 Ma (MSWD = 0.05), which we interpret as the best estimate for the emplacement age of the granite.

Sample LW1—Only six analyses were conducted on six grains and yielded a wide range of U and Th contents as well as apparent ages (table 2). The youngest zircon yielded a concordant $^{207}Pb/^{206}Pb$ age of 1005 ± 43 Ma and represents the only estimate for the emplacement of the granite (fig. 13A). A group of three near-concordant analyses yield a Concordia age of 1526 ± 12 (MSWD = 0.07), and could represent xenocrysts from a granitic protolith of that age at depth.

Sample LW2—Eight analyses were conducted on eight different zircon (table 2), and yield a weighted mean $^{207}Pb/^{206}Pb$ age of 953 ± 19 Ma (MSWD = 0.62). A Concordia age can be calculated for three near concordant points (4, 5 and 6) which yields a more tightly constrained age of 942 ± 9 Ma (MSWD = 0.39, fig. 13B), which we take as the best estimate for the age of the syeno-granite in sample LW2.

Sample MTG4—Five core/rim pairs, one core and two rim analyses were completed on this sample. In two cases (9 and 10), both core and rim yielded the same result (within error), while three core/rim pairs (1c, 1r, 4c, 4r, 8c and 8r) yielded significant differences in age (table 2). Of the four older cores analyzed, three cores (1c, 4c and 7c) yielded $^{207}Pb/^{206}Pb$ ages of 2046 ± 21 Ma, 2017 ± 34 Ma and 2010 ± 15 Ma (fig. 13C). The first one of those corresponds to an inversely discordant point, while the two latter are concordant and correspond to a Concordia age of 2004 ± 14 Ma (MSWD = 6.2). All these cores are interpreted to represent xenocrystic components. The remaining core (8c) yielded a $^{207}Pb/^{206}Pb$ age of 1425 ± 94 Ma, and represents an additional xenocrystic component. The remaining data plot in a tight cluster on the U-Pb evolution diagram (fig. 13C) and define a single age population with weighted mean $^{207}Pb/^{206}Pb$ age of 1019 ± 13 Ma. Excluding data point 5c, on the basis of its high f_{206} value of 4.33 percent (table 2), a Concordia age of 1006 ± 8 Ma can be calculated (MSWD = 0.33). These ages are calculated from both core and rim analyses indicating that growth of low $^{232}Th/^{238}U$ rims happened very soon after crystallization of magmatic zircon. In conclusion, the Chilubanama Granite of sample MTG4 appears to have sampled sources of an estimated age ~2050 to 2000 and 1425 Ma, and was emplaced at around 1006 ± 8 Ma coeval with regional metamorphism.

Sample ZM32—A total of six analyses were conducted on six zircon (table 2) and record a wide variety of apparent ages. $^{207}Pb/^{206}Pb$ ages of 2036 ± 61, 1859 ± 39 Ma and 1649 ± 45 Ma are recorded on zoned cores and interpreted to represent various xenocrystic components (fig. 13D). The remaining two zircons record poorly constrained $^{207}Pb/^{206}Pb$ ages of 946 ± 50 Ma and 853 ± 85 Ma and have relatively high f_{206} (1.02 and 0.75% respectively) and are therefore difficult to interpret.

DISCUSSION

Pre-Irumide Magmatism

The data presented here has shown that the Irumide Belt includes a poly-modal granitic basement comprising an Archean component dated at 2726 ± 36 Ma and Paleoproterozoic units dated between 2050 and 1930 Ma. This basement is unconformable, and in places structurally overlain by the ca. 1.8 Ga Muva Supergroup (De Waele and Fitzsimons, 2007). Within the Irumide Belt, the basement and supracrustal units

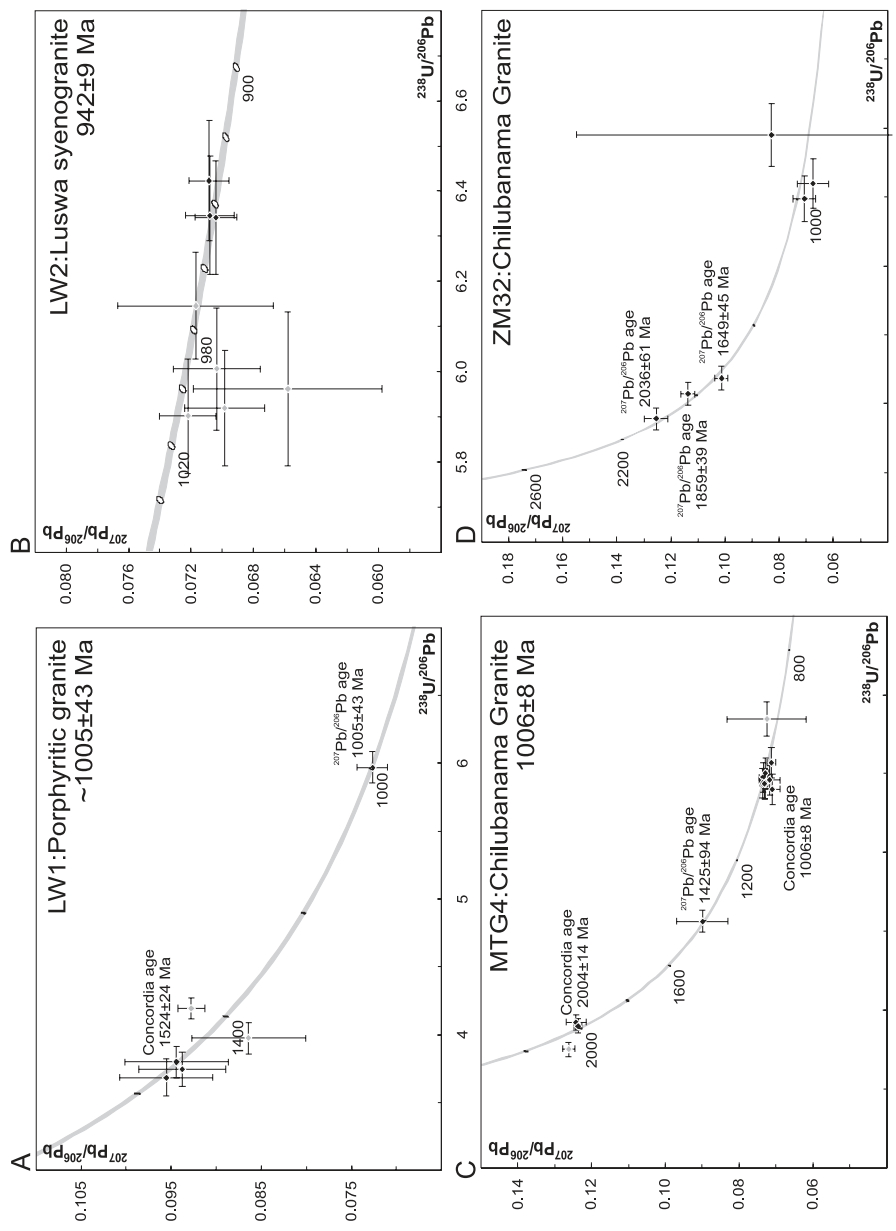

Fig. 13. U-Pb evolution diagram showing data for (A) LW1; (B) LW2; (C) MTG4 and (D) ZM32.

were intruded by Labradorian-aged granitoids dated between 1665 and 1630 Ma in the southwest and between 1590 and 1530 Ma in the northeast. These 1.65 to 1.53 Ga granitoid rocks provide among the first evidence of Labradorian-aged magmatic activity in Africa, and provide an interesting marker against which to investigate possible similarities between the tectono-thermal history of the Congo Craton and other regions of the world. Broadly similar-aged plutons are recorded in the Epupa Complex across the Angola-Nambian border (Seth and others, 1998, 2003, 2005; Kröner and others, 2004), but none of the ages reported overlap with the 1.65 to 1.53 Ga age window recognized in the Irumide Belt.

Labradorian-aged magmatism is widely recognized in the type area of the Grenville Belt of Laurentia (Rivers, 1997; Rivers and Corrigan, 2000; Gower and Krogh, 2002) and the southward extension of the province into Mexico (Mazatzal Province, see Karlstrom and others, 2001; Rämo and others, 2003). However, both provinces are characterized by a number of magmatic episodes directly following the 1.6 Ga magmatic event, in contrast to the distinct gap of magmatic activity in the Irumide Belt.

Another region with well-documented 1.6 Ga magmatism is the Baltic Shield. There, a series of accretionary events make up the Gothian Orogen, spanning the period between 1.65 and 1.42 Ga, and followed by a series of extensional events between 1.34 and 1.21 Ga (Gorbatschev and Bogdanova, 1993; Andersson and others, 1999; Åhäll and others, 2000; Andersson, ms, 2000). Palaeomagnetic data for Baltica and Laurentia at 1265 Ma reported in Pesonen and others (2003), argue for the alignment of the Gothian-Mazatzal-Labradorian Belts along a large accretionary margin, a configuration which would explain the broadly coeval thermo-tectonic evolution of these belts prior to 1.5 Ga, as well as the active continental margin setting for both the Grenville and Sveconorwegian margins at 1.26 Ga (Bingen and others, 2002). As was the case for Laurentia, the margin of the Baltic Shield is characterized by a much more protracted and punctuated Mesoproterozoic geological evolution than that of the margin of the Congo Craton, making a potential link between the two between 1.6 and 1.2 Ga unlikely. The southwestern parts of the Amazonian Craton also record various episodes of granitic magmatism, which have prompted many authors to consider a connection between Amazonia, Baltica and Laurentia in a contiguous landmass (see Pesonen and others, 2003). Again, the magmatic record along the margin of Amazonia is far more extensive than that recognized along the Congo margin, making a direct link between the two in the period 1.6 to 1.1 Ga unlikely.

In summary, a comparison of the southern margin of the Congo Craton with cratonic margins that record magmatism at about 1.6 Ga elsewhere indicates a marked absence of magmatic, thermal or tectonic events within the Irumide Belt between 1.55 Ga and the onset of Irumide tectonism at 1.02 Ga, in stark contrast with those from other regions. Given the fact that the ages reported in this and in previous studies cover the entire strike length of the Irumide Belt, this hiatus in geological activity is likely to be a true characteristic of this orogen. With the absence of clear rift deposits post-dating the Labradorian-aged (1.6 Ga) events in the Irumide Belt, this makes any link between the Congo Craton and other regions with known 1.6 Ga magmatism prior to the assembly of Rodinia unlikely.

Timing and Extent of Irumide Magmatism

On the basis of this study, it can be stated that the Irumide Orogeny was characterized by voluminous granitic (s.l.) magmatism, which makes up about 70 percent of the magmatic rocks recognized in the belt. This magmatism took place between 1053 ± 14 and 942 ± 9 Ma, and defined a major magmatic pulse with a calculated weighted mean age of 1015 ± 18 Ma, corresponding closely to the reported timing of peak metamorphism at 1020 Ma (De Waele, ms, 2005). It is worth noting that the youngest ages seem to be recorded in the northeastern Irumide Belt. A weighted

mean age of 993 ± 30 Ma can be obtained for sample CHT6 and those northeast of that, while a weighted mean age on all samples southwest of CHT6 yields 1032 ± 4 Ma. This may record some diachronicity along the strike-length of the Irumide Belt. Of the twenty six different granitoid bodies dated in the Irumide Belt, eighteen (70%) fall within fifteen million years of peak metamorphism at 1.02 Ga. The ca. 1.02 Ga granitoid bodies range from undeformed to strongly deformed, indicating heterogeneous distribution of strain during contractional tectonics. The widespread coverage of the sample set presented here, together with previously published and unpublished data (De Waele, ms, 2005; Johnson and others, 2005a, 2005b; De Waele and others, 2006a, 2006b, 2008; De Waele and Fitzsimons, 2007) suggest it is unlikely that additional magmatic pulses will be identified within the Irumide Orogen. As a result, the age histogram in figure 14A is considered to represent a reliable fingerprint for the Irumide Orogen, against which other orogenic belts can be compared.

Implications of Xenocrystic Zircon and Lu-Hf data

Thirty of the analyses carried out in the course of this study are interpreted to represent xenocrystic zircon. These include analyses on core of complex grains, as well as single magmatic grains that yield ages older than the inferred crystallization age. The analytical data for xenocrystic zircon are tabulated in table 4 and a histogram of those with concordant (±5%) $^{207}Pb/^{206}Pb$ ages is shown in figure 14B. Since the Irumide granitoids intrude both basement and supracrustal units, either of those could represent sources for the xenocrysts. However, detrital analyses conducted on the supracrustal successions (Rainaud and others, 2003; De Waele, ms, 2005; De Waele and Fitzsimons, 2007) show that the successions in the Irumide Belt have no zircon younger than 1.8 Ga.

The zircon xenocrysts document a main population between 2.05 and 1.95 Ga, corresponding to both the main detrital zircon population reported for the Muva Supergroup and the reported age of known basement units in the Irumide Belt (De Waele, ms, 2005; Rainaud and others, 2005; De Waele and Fitzsimons, 2007). Additional small populations of xenocrystic zircon with ages of 2.7 Ga, 1.86 to 1.84 Ga and 1.65 to 1.64 Ga correspond respectively to the oldest known part of the basement in the Irumide Belt (Kapiri Mposhi Granite Gneiss, 2.73 Ga, De Waele, ms, 2005), the volcanic units within the Muva Supergroup (1.88−1.85 Ga, De Waele, ms, 2005; De Waele and others, 2006b) and late-Paleo- to early Mesoproterozoic granitoid rocks in the Irumide Belt (Lukamfwa Granite, 1.65−1.64 Ga, De Waele, ms, 2005; De Waele and others, 2003, 2006b). In the northeastern Irumide Belt, several xenocrystic zircon record ages between 1.54 and 1.35 Ga, for which no magmatic source is known. These may either represent evidence for an as yet unidentified cryptic magmatic terrane below the northeastern Irumide Belt, or, more likely, represent preserved detrital zircon from the Kasama Formation further north where a single concordant zircon was dated at 1.43 Ga (De Waele and Fitzsimons, 2007). In summary, the xenocrystic zircon record confirms the presence of pre-Irumide basement units throughout the entire strike-length of the belt, supporting the notion that the Irumide Belt represents a thrust system developed along the southern margin of an Archean to Paleoproterozoic crustal block. The Lu-Hf data presented in this paper support the presence of Archean crust within and below the Irumide Belt. Median $\varepsilon_{Hf}(t)$ values are generally strongly negative for the Irumide granitoid rocks (~1.0 Ga), in the range −14.6 to −11.3 (table 3), indicating that they represent crustal melts with little or no juvenile input. The median Hf model ages for these units are within a very narrow range, 1.96 to 2.08 Ga (table 3), consistent with their derivation through total remelting of the Mkushi Gneiss and its age equivalents in the Irumide Belt. The ~1.6 Ga granitoid rocks have much more variable $\varepsilon_{Hf}(t)$ values and range from juvenile, with positive $\varepsilon_{Hf}(t)$, to slightly reworked with slightly negative $\varepsilon_{Hf}(t)$ (table 3). Hf model ages for the ~1.6 Ga

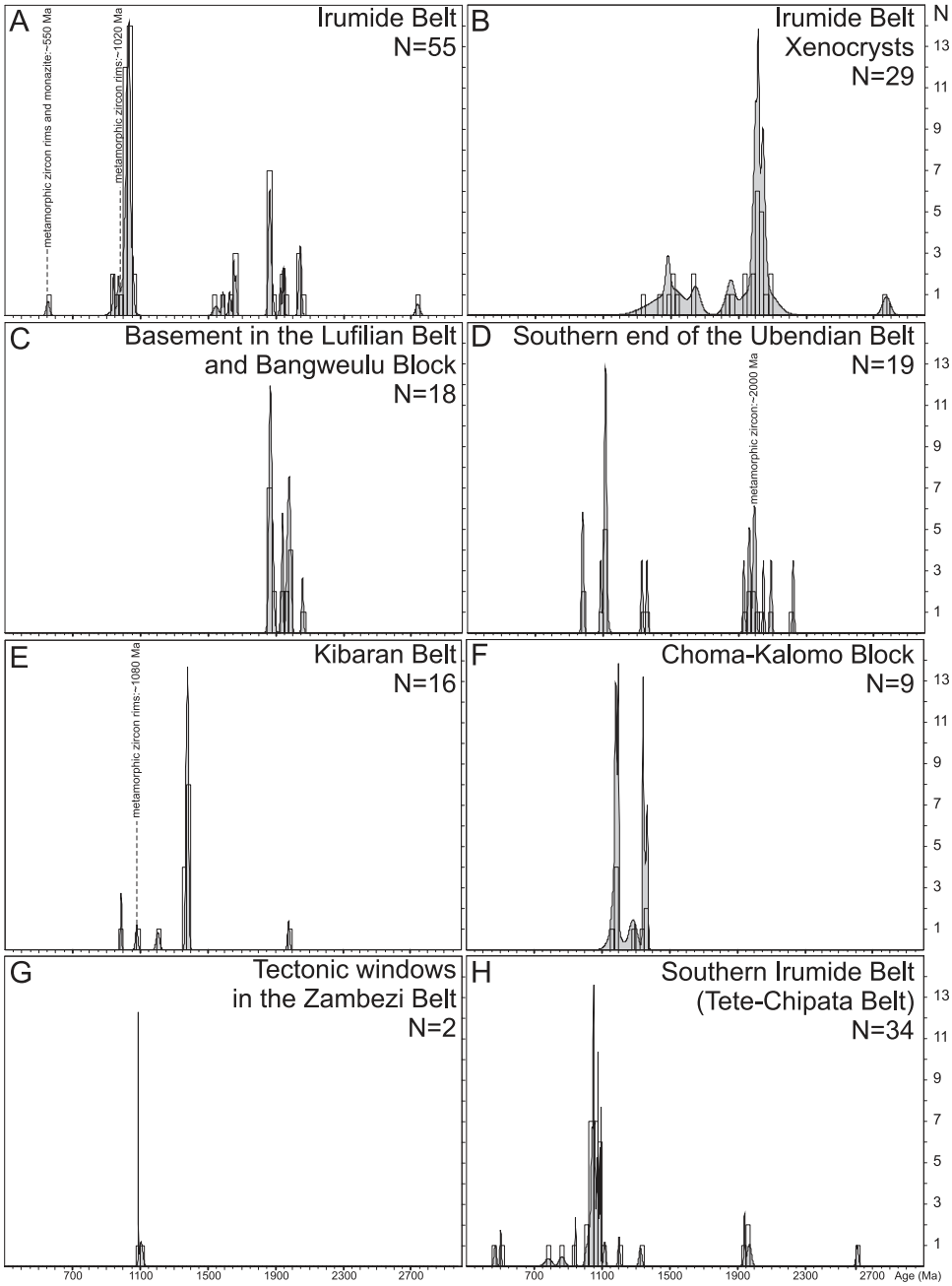

Fig. 14. Combined histograms and probability density diagrams of (A) emplacement ages of granitoid rocks in the Irumide Belt; (B) zircon $^{207}Pb/^{206}Pb$ crystallization ages of xenocrysts in granitoid rocks in the Irumide Belt (age data is tabulated in table 4); (C) emplacement ages of basement in the Lufilian Belt and Bangweulu Block; (D) emplacement ages of granitoid rocks in the southern end of the Ubendian Belt; (E) emplacement ages of granitoid rocks in the Kibaran Belt; (F) emplacement ages of granitoid rocks in the Choma-Kalomo Block; (G) emplacement ages of granitoid rocks exposed in basement windows in the Zambezi Belt; (H) emplacement and metamorphic ages of granitoid rocks in the Southern Irumide Belt. Refer to tables 2 and 5 for age data and sources. The bin size for all histograms is 25 Million years.

Table 4

Zircon U-Pb ages of xenocrysts from magmatic rocks of the Irumide Belt

Sample	Name	$^{207}Pb/^{206}Pb$ age (Ma)	Concordance (%)	Age (Ma)
LW1	Porphyritic granite	1348 ± 66	107.6	1005 ± 21
MTG4	Chilubanama Granite	1425 ± 47	98.4	1010 ± 22
LW1	Porphyritic granite	1483 ± 12	93.2	1005 ± 21
LW1	Porphyritic granite	1503 ± 46	101.7	1005 ± 21
LW1	Chilubanama Granite	1516 ± 56	99.6	1005 ± 21
LW1	Porphyritic granite	1539 ± 48	100.8	1005 ± 21
FW2	Aplite in porphyritic granite	1637 ± 46	102.2	1038 ± 17
ZM32	Chilubanama Granite	1649 ± 23	101.5	~1000
FW2	Aplite in porphyritic granite	1837 ± 28	90.7	1038 ± 17
ZM32	Chilubanama Granite	1859 ± 20	95.8	~1000
KN7	Porphyritic granite	1944 ± 46	97.9	1048 ± 10
FW2	Aplite in porphyritic granite	1945 ± 39	105.4	1038 ± 17
KN7	Porphyritic granite	1987 ± 16	94.9	1048 ± 10
KN7	Porphyritic granite	1988 ± 9	102.4	1048 ± 10
SER6-4	Porphyritic granite	2000 ± 6	102.7	1036 ± 13
FW2	Aplite in porphyritic granite	2010 ± 21	101.3	1038 ± 17
MTG4	Chilubanama Granite	2010 ± 8	98.3	1010 ± 22
FW2	Aplite in porphyritic granite	2017 ± 10	102.6	1038 ± 17
MTG4	Chilubanama Granite	2017 ± 17	96.6	1010 ± 22
KN7	Porphyritic granite	2017 ± 4	100.5	1048 ± 10
FW2	Aplite in porphyritic granite	2032 ± 28	99.4	1038 ± 17
FW2	Aplite in porphyritic granite	2034 ± 31	97.7	1038 ± 17
ZM32	Chilubanama Granite	2036 ± 23	97.2	~1000
FW2	Aplite in porphyritic granite	2044 ± 8	99.5	1038 ± 17
MTG4	Chilubanama Granite	2046 ± 11	106.1	1010 ± 22
KN8	Porphyritic granite	2052 ± 13	99.7	1022 ± 16
FW2	Aplite in porphyritic granite	2096 ± 38	102.1	1038 ± 17
FW2	Aplite in porphyritic granite	2098 ± 65	95.5	1038 ± 17
FW2	Aplite in porphyritic granite	2774 ± 23	99.8	1038 ± 17

granitoid units are in the range 1.94 to 2.22 Ga, indicating crustal residence times of at least 400 Million years. The oldest granitoids (2.0 Ga) record $\varepsilon_{Hf}(t)$ values of -0.1 and +2.0, and Hf-model ages of 2.24 and 2.40 Ga, indicating a dominant juvenile character. Although the data confirm earlier suggestions of older crust below the Irumide Belt (De Waele and others, 2006b), the zircon Lu-Hf data seem to suggest that this crust on average has a mid-Paleoproterozoic age. Hf-model ages overall are in the range 1.94 to 2.40 Ga, with a median model age at 2040 Ma. We interpret this to reflect the pervasive presence of a 2.0 Ga-old juvenile crust in the Irumide Belt, with minor older Archean components, that was remelted several times to yield the 1.6 Ga and 1.0 Ga suites. Juvenile additions to the crust within the Irumide Belt are low, in keeping with the interpretation it represents the reworked margin of an Archean-Paleoproterozoic craton (the Bangweulu Craton, which forms part of the greater Congo Craton).

Regional Correlations

The Extent of the Irumide Belt.—A possible continuation of the Irumide Belt to the northwest is masked by Neoproterozoic Katangan strata and Recent sedimentary cover. Available age data for the Bangweulu Block foreland northwest of these successions, and age data for basement units within the Lufilian Belt, indicate magmatic activity

between 2.05 and 1.85 Ga (data summarized in table 5, and histogram shown in fig. 14C), with a notable absence of any Mesoproterozoic magmatism. This suggests that the magmatic front of the Irumide Orogen does not extend much to the northwest of the present outcrop of the belt. The northeastern limit of the Irumide Belt is defined by a large megashear [Mugesse Shear Zone (MSZ), see fig. 1B] within the southern part of the Paleoproterozoic Ubendian Belt (Daly and others, 1985a, 1985b; Daly, ms, 1986). To the northeast of that, no age data are available to unequivocally demonstrate the termination of the Irumide Belt along this megashear. Age data for the southern part of the Ubendian Belt (Dodson and others, 1975; Ring and others, 1997, 1999; Vrána and others, 2004) demonstrate the widespread occurrence of Paleoproterozoic basement units aged between 2.22 and 1.93 Ga (fig. 14D) and metamorphism at ca. 2.0 Ga (Ring and others, 1997). These Paleoproterozoic units were locally intruded by syenite and tonalite (1.36 and 1.33 Ga respectively, Vrána and others, 2004), and by several shear-bounded A-type granitoids between 1.12 and 1.09 Ga (Ring and others, 1999). A comparison of emplacement ages for the Southern Ubendian Belt (fig. 14D) and the Irumide Belt (fig. 14A), shows some similarities in the age of basement units, but no overlap in later magmatic activity, strongly suggesting that the Irumide Orogen does in fact terminate at the Mugesse Shear Zone.

A noteworthy feature of the regional geology is the apparent continuation of the northeast oriented Irumide Belt to the southwest, across the Neoproterozoic Zambezi Belt, and into the northeast-trending Choma-Kalomo Block. Apart from the similar structural trends of these terranes, previous age data, based on Rb-Sr whole-rock and bulk zircon U-Pb TIMS work (Hanson and others, 1988b), had supported the notion of a single Mesoproterozoic orogen, implying limited relative displacement during the Neoproterozoic and the formation of the Zambezi Orogen. Modern single zircon U-Pb SHRIMP dating on the Irumide Belt (De Waele and others, 2003, 2006a, 2006b; De Waele, ms, 2005) and Choma-Kalomo Block (Bulambo and others, 2004), however, disprove the previously proposed correlations and strongly suggest that the two orogenic segments were not contiguous between 1.4 and 1.0 Ga, and only became juxtaposed during the Neoproterozoic Zambezi orogeny. The evidence for this statement is shown in figures 14A and F, which show histograms of zircon U-Pb ages reported for the Irumide Belt and Choma-Kalomo Block respectively (refer to table 5 for data). The data clearly show the mismatch of Mesoproterozoic magmatic events in the Choma-Kalomo Block and the Irumide Belt. Magmatism at ca. 1.37 to 1.34, 1.28 and 1.19 to 1.10 Ga in the Choma-Kalomo Block (Hanson and others, 1988b; Bulambo and others, 2004) has not been recognized in the Irumide Belt, and conversely, peak magmatism at 1020 $\pm$ 20 Ma in the Irumide Belt has no expression in the Choma-Kalomo Block. Isolated basement domes do occur between the two Mesoproterozoic provinces in tectonic windows of the Zambezi Belt (fig. 14G), but the crystallization ages of magmatic rocks in them of ca. 1.10 Ga (Hanson and others, 1988a; Katongo and others, 2004) favor a possible link with the Choma-Kalomo Block (fig. 14F) or Southern Irumide Belt (fig. 14H, see below) rather than a genetic link with the Irumide Orogen (fig. 14A). This implies that the southern limit of the Irumide Orogen lies to the north of the Mpande Gneiss, perhaps coinciding with the Neoproterozoic Mwembeshi Shear Zone (fig. 1B).

The Irumide Belt is truncated to the southeast by sedimentary grabens of Karoo age (see fig. 1B). These younger structures, which are parallel to the structural trends of the Irumide Belt, make any correlation between the Irumide Belt and pre-Karoo rocks exposed to the southeast difficult. Regional studies (Johns and others, 1989; Oliver and others, 1998; Mapani and others, 2001, 2004; Johnson and Oliver, 2004; Johnson and others, 2005b, 2006, 2007; Macey and others, 2007; Westerhof and others, 2008) have shown that the area to the south of the Karoo graben comprises a variety of

TABLE 5

Zircon U-Pb ages of magmatic rocks in and around the Irumide Belt and previously reported ages from the Irumide Belt

Sample	Age (Ma)	Method used	Data source
Irumide Belt			
Kaunga Granite	970 ± 5	U-Pb TIMS	Daly, 1986
SER6-6; Lukusashi Migmatite	*1018 ± 5*	U-Pb SHRIMP	De Waele, 2005
SER6-7; Fukwe Migmatite	*1021 ± 16*	U-Pb SHRIMP	De Waele, 2005
MTGG-2; Mutangoshi Gneissic Granite	1055 ± 13	U-Pb SHRIMP	De Waele, 2005
IS20; Kachinga Tuff	1856 ± 4	U-Pb SHRIMP	De Waele and Fitzsimons, 2007
KB5; Katibunga Basalt	1871 ± 24	U-Pb SHRIMP	De Waele and Fitzsimons, 2007
ZM31; Luswa River Tuff	1879 ± 13	U-Pb SHRIMP	De Waele and Fitzsimons, 2007
Mkushi Gneiss	2049 ± 6	U-Pb SHRIMP	Rainaud and others, 2002
Southern Irumide Belt			
Luangwa Gneiss	*1043 ± 19*	LA-ICP-MS	Cox and others, 2002
Luangwa Gneiss	2608 ± 14	LA-ICP-MS	Cox and others, 2002
Luangwa Gneiss	~2033	LA-ICP-MS	Cox and others, 2002
Madzimoyo xenolith	1974 ± 19	U-Pb SHRIMP	Johnson and others, 2006
Madzimoyo Granulite	1076 ± 6	U-Pb SHRIMP	Johnson and others, 2006
Madzimoyo Granulite	1047 ± 20	U-Pb SHRIMP	Johnson and others, 2006
Porphyritic granite	1060 ± 7	U-Pb SHRIMP	Johnson and others, 2006
Migmatite	1942 ± 5	U-Pb SHRIMP	Johnson and others, 2006
Nyamadzi Gneiss	1961 ± 31	U-Pb SHRIMP	Johnson and others, 2006
Nyamadzi Gneiss	*1065 ± 13*	U-Pb SHRIMP	Johnson and others, 2006
Mtanzi Gneiss	1008 ± 17	U-Pb SHRIMP	Johnson and others, 2006
Ultramylonitised granite	1023 ± 12	U-Pb SHRIMP	Johnson and others, 2006
Katanga Resources Granite	1043 ± 14	U-Pb SHRIMP	Johnson and others, 2006
Great East Road Migmatite	1057 ± 5	U-Pb SHRIMP	Johnson and others, 2006
Metadacite	944 ± 5	U-Pb SHRIMP	Johnson and others, 2006
Metadacite	1083 ± 18	U-Pb SHRIMP	Johnson and others, 2006
Mafic banded gneiss	1051 ± 12	U-Pb SHRIMP	Johnson and others, 2006
Leucogneiss	1038 ± 14	U-Pb SHRIMP	Johnson and others, 2006
K-feldspar augen gneiss	1094 ± 2	U-Pb SHRIMP	Johnson and others, 2006
K-feldspar augen gneiss	1088 ± 4	U-Pb SHRIMP	Johnson and others, 2006
Leucogneiss	1070 ± 3	U-Pb SHRIMP	Johnson and others, 2006
moz-12	502 ± 8	U-Pb SHRIMP	Mänttäri and others, 2008
moz-15	1117 ± 12	U-Pb SHRIMP	Mänttäri and others, 2008
moz-9	1077 ± 2	U-Pb TIMS	Mänttäri and others, 2008
moz-8	470 ± 14	U-Pb SHRIMP	Mänttäri and others, 2008
moz-10	1050 ± 8	U-Pb TIMS	Mänttäri and others, 2008
moz-34	1327 ± 16	U-Pb SHRIMP	Mänttäri and others, 2008
moz-18	1086 ± 7	U-Pb TIMS	Mänttäri and others, 2008
moz-17	1047 ± 29	Sm-Nd mineral	Mänttäri and others, 2008
moz-1	1201 ± 10	U-Pb SHRIMP	Mänttäri and others, 2008
moz-13	1050 ± 2	U-Pb TIMS	Mänttäri and others, 2008
moz-11	1041 ± 4	U-Pb TIMS	Mänttäri and others, 2008
moz-16	784 ± 36	U-Pb SHRIMP	Mänttäri and others, 2008
moz-14	864 ± 30	Sm-Nd mineral	Mänttäri and others, 2008
moz-5	1046 ± 20	U-Pb SHRIMP	Mänttäri and others, 2008
Bangweulu Block			
MA1; Mansa Granite	1860 ± 13	U-Pb SHRIMP	De Waele and Fitzsimons, 2007
MA5; Mansa Volcanic	1862 ± 19	U-Pb SHRIMP	De Waele and Fitzsimons, 2007
MA2; Mansa Granite	1862 ± 8	U-Pb SHRIMP	De Waele and Fitzsimons, 2007
MA9; Musonda Falls Granite	1866 ± 9	U-Pb SHRIMP	De Waele and Fitzsimons, 2007
MA3; Mansa Volcanic	1868 ± 7	U-Pb SHRIMP	De Waele and Fitzsimons, 2007
Tectonic windows in the Zambezi Belt			
Munali Granite	1090 ± 1	U-Pb TIMS	Katongo and others, 2004
Mpande Gneiss	1106 ± 19	U-Pb TIMS	Hanson and others, 1988a

Table 5
(continued)

Sample	Age (Ma)	Method used	Data source
Choma-Kalomo Block			
Granite (Choma-Kalomo Block)	1174 ± 27	U-Pb SHRIMP	Bulambo and others, 2004
Granite	1177 ± 70	U-Pb SHRIMP	Bulambo and others, 2004
Granite	1181 ± 9	U-Pb SHRIMP	Bulambo and others, 2004
Granite	1188 ± 11	U-Pb SHRIMP	Bulambo and others, 2004
Semahwa Gneiss	1198 ± 6	U-Pb TIMS	Hanson and others, 1988b
Chilala Gneiss	1285 ± 64	U-Pb TIMS	Hanson and others, 1988b
Zongwe Gneiss	1343 ± 6	U-Pb TIMS	Hanson and others, 1988b
Siasikabole Granite	1352 ± 14	U-Pb TIMS	Hanson and others, 1988b
Granite	1368 ± 10	U-Pb SHRIMP	Bulambo and others, 2004
Lufilian Belt			
Kinsenda Lufubu Schist	1873 ± 8	U-Pb SHRIMP	Rainaud and others, 2002
Solwezi Granite	1874 ± 9	U-Pb TIMS	John, 2001
Kinsenda Granite (Luina dome)	1882 ± 23	U-Pb TIMS	Ngoyi and others, 1991
Kabompo Granite	1884 ± 10	U-Pb TIMS	John, 2001
Kabompo Dome Granite	1934 ± 6	U-Pb TIMS	Key and others, 2001
Kabompo Dome Granite	1940 ± 3	U-Pb TIMS	Key and others, 2001
Samba Porphyry	1964 ± 12	U-Pb SHRIMP	Rainaud and others, 2002
Lufubu Schist	1970 ± 10	U-Pb SHRIMP	Rainaud and others, 2002
Chambishi Granite	1980 ± 7	U-Pb SHRIMP	Rainaud and others, 2002
Chambishi Granite	1983 ± 5	U-Pb SHRIMP	Rainaud and others, 2002
Mufulira Granite	1991 ± 3	U-Pb SHRIMP	Rainaud and others, 2002
Mulungushi Gneiss	1976 ± 5	U-Pb SHRIMP	Rainaud and others, 2005
Mwinilunga Granite	2058 ± 7	U-Pb SHRIMP	Key and others, 2001
Kibaran Belt			
Rumeza Granite	1383 ± 17	U-Pb SHRIMP	Tack and others, pers.comm.
Mugere Granite	1379 ± 10	U-Pb SHRIMP	Tack and others, pers.comm.
Mugere Migmatite	1380 ± 8	U-Pb SHRIMP	Tack and others, pers.comm.
Kiganda Granite	1371 ± 7	U-Pb SHRIMP	Tack and others, pers.comm.
Muramba Granite	1380 ± 6	U-Pb SHRIMP	Tack and others, pers.comm.
Kilimbi-Muzumu Granite	1373 ± 6	U-Pb SHRIMP	Tack and others, pers.comm.
Butare Gneiss	1979 ± 12	U-Pb SHRIMP	Tack and others, pers.comm.
Musongati Massif Norite	1374 ± 14	U-Pb SHRIMP	Tack and others, pers.comm.
Bukirasazi Granite	1205 ± 19	U-Pb SHRIMP	Tack and others, pers.comm.
Kasika Sn Granite	987 ± 6	U-Pb SHRIMP	Tack and others, pers.comm.
Kisele Monzogranite Gneiss	1386 ± 8	U-Pb SHRIMP	Kokonyangi and others, 2004
Kabonvia Gneiss	1386 ± 7	U-Pb SHRIMP	Kokonyangi and others, 2004
Nyangwa Monzogranite	1383 ± 5	U-Pb SHRIMP	Kokonyangi and others, 2004
Kungwe-Kalumengongo Monzogranite	1377 ± 10	U-Pb SHRIMP	Kokonyangi and others, 2004
Fwifwi Leucomonzogranite	1372 ± 10	U-Pb SHRIMP	Kokonyangi and others, 2004
Kisele Monzogranite Gneiss	*1079 ± 14*	U-Pb SHRIMP	Kokonyangi and others, 2004
Southern Ubendian Belt			
Aplite (Luromo Granite)	977 ± 1	Pb evaporation	Ring and others, 1999
Aplite (Wililo Granite)	983 ± 1	Pb evaporation	Ring and others, 1999
Lwakwa Granite	1087 ± 11	U-Pb TIMS	Ring and others, 1999
Luromo Granite	1108 ± 1	Pb evaporation	Ring and others, 1999
Wililo Granite	1115 ± 1	Pb evaporation	Ring and others, 1999
Wililo Granite	1116 ± 1	Pb evaporation	Ring and others, 1999
Wililo Granite	1118 ± 1	Pb evaporation	Ring and others, 1999
Mwenga Granite	1119 ± 20	U-Pb TIMS	Ring and others, 1999
Ntendele Metatonalite	1329 ± 1	Pb evaporation	Vrána and others, 2004
Mivula Syenite	1360 ± 1	Pb evaporation	Vrána and others, 2004
Nyika Granite	1932 ± 9	U-Pb TIMS	Dodson and others, 1975
Biotite Metatonalite	1961 ± 1	Pb evaporation	Vrána and others, 2004
Nyika Granite	1969 ± 1	Pb evaporation	Ring and others, 1997
Rumphi Granite	1988 ± 1	Pb evaporation	Ring and others, 1997
Chelinda Granite	1995 ± 1	Pb evaporation	Ring and others, 1997
Luromo Granite	*2002 ± 1*	Pb evaporation	Ring and others, 1997
Rumphi Granite	2048 ± 1	Pb evaporation	Ring and others, 1997
Luromo Granite	2093 ± 1	Pb evaporation	Ring and others, 1997
Luromo Granite	2224 ± 1	Pb evaporation	Ring and others, 1997

lithotectonic terrains. Johnson and others (2006) introduced the term Southern Irumide Belt to denote the area to the south of the Karoo grabens, but Westerhof and others prefer to use the name Tete-Chipata Belt (Westerhof and others, 2008). In this paper we will use the earlier nomenclature. Published and unpublished age data, reported in table 5 and shown in figure 14H, show the presence of a Paleoproterozoic basement at about 2.0 Ga, similar to that occurring within the Irumide Belt, but indicate magmatic events spanning between 1.10 and 0.95 Ga and accompanying peak metamorphic conditions between 1.06 and 1.05 Ga. These data clearly demonstrate that Mesoproterozoic magmatism and associated metamorphic conditions in the Southern Irumide Belt predate those in the Irumide Belt, as previously stated by Johnson and others (2006). Because of the fact that these age differences occur across strike, with no apparent gradual transition between the two terranes, it is considered unlikely that the differences can be ascribed to diachronous development of a single Irumide Orogen. Moreover, geochemical and isotopic data for magmatic rocks of the Irumide Belt (De Waele, ms, 2005; De Waele and others, 2006b) and the Southern Irumide Belt (Johnson and others, 2007; Macey and others, 2007; Mäkitie and others, 2008; Westerhof and others, 2008) clearly demonstrate significant petrological differences between the two terrains, suggesting that the Irumide Belt and Southern Irumide Belt developed separately and were juxtaposed along a suture now obscured by the Karoo graben.

The Irumide and Kibaran belts.—In the past, the Irumide Belt has often been correlated with the subparallel Kibaran Belt to the northwest, based on Rb-Sr and K-Ar data that indicate that both belts are Mesoproterozoic, and on their similar northeast-oriented structural trend. The geochronological framework of the Kibaran Belt has recently been refined using SHRIMP U-Pb geochronology into two main contractional deformation events, followed by the intrusion of the tin-bearing granitoids. Kokonyangi and others (2004) reported ages of 1386 ± 8 Ma, 1385 ± 7 Ma, 1383 ± 5 Ma, 1372 ± 10 Ma and 1377 ± 10 Ma for various phases of the Mitwaba granites in Congo D.R., while Tack and others (2002) reported ages of 1383 ± 17 Ma, 1379 ± 10 Ma, 1371 ± 7 Ma and 1374 ± 14 Ma for granitoid rocks in the northeastern part of the Kibaran Belt. These ages tightly constrain the main Kibaran magmatic pulse between 1386 ± 8 Ma and 1371 ± 7 Ma (fig. 14E). One granite in the northeastern part of the Kibaran Belt yielded an age of 1205 ± 19 Ma and indicates the presence of a localized second magmatic pulse at that time (Tack and others, 2002). In the central Kibaran Belt, Kokonyangi and others (2004) reported a metamorphic zircon U-Pb SHRIMP age of 1079 ± 14 Ma, suggesting at least a local metamorphic event around that time. These new data render a correlation between the Irumide Belt and the Kibaran Belt untenable (see histograms in figs. 14A and 14E), but bring out striking similarities between Choma-Kalomo Block (fig. 14F) and the Kibaran Belt, raising the possibility of their original continuity. Unrug (1992) pointed out that a sinistral movement of 150 to 200 km along the Mwembeshi Shear Zone would place the Choma-Kalomo Block in direct continuation with the Kibaran Belt, but evaluation of this prediction awaits additional work.

ACKNOWLEDGMENTS

Fieldwork and research by BDW was funded by the Australian Research Councils' Tectonics Special Research Centre and by an International Postgraduate Research Scholarship to BDW at Curtin University of Technology in Perth, Australia. BDW wishes to thank the staff at the Perth Consortium SHRIMP facilities, the Geological Society of Zambia and the Geology Department at the University of Zambia for support throughout the work. The authors wish to thank the reviewers, Drs. Toby Rivers, Simon P. Johnson and Luc Tack for constructive comments that have greatly enhanced the manuscript. This publication is a contribution to IGCP projects 418 and 440.

References

Ackermann, E. H., 1950, Ein neuer faltengurtel in Nordrhodesien und seine tectonische Stellung im Afrikanishen grundgebirge: Geologische Rundschau, v. 38, p. 24–39, doi:10.1007/BF01766570.

——— 1960, Strukturen im untergrund eines intrakratonischen Doppel-Orogens (Irumiden Nordrhodesien): Geologische Rundschau, v. 50, p. 538–553, doi:10.1007/BF01786869.

Åhäll, K.-I., Connelly, J. N., and Brewer, T. S., 2000, Episodic rapakivi magmatism due to distal orogenesis?: Correlation of 1.69-1.50 Ga orogenic and inboard, "anorogenic" events in the Baltic Shield.: Geology, v. 28, p. 823–826, doi:10.1130/0091-7613(2000)28⟨823:ERMDTD⟩2.0.CO;2.

Andersson, J., ms, 2000, Sveconorwegian orogenesis in the southwestern Baltic Shield: Zircon geochronology and tectonothermal setting of orthogneisses in SW Sweden: Lund, Sweden, Lund University, Ph. D. thesis, 155 p.

Andersson, J., Süderlund, U., Cornell, D., Johannson, L., and Moller, C., 1999, Sveconorwegian (-Grenvillian) deformation, metamorphism and leucosome formation in SW Sweden, SW Baltic Shield: constraints from a Mesoproterozoic granite intrusion: Precambrian Research, v. 98, p. 151–171, doi:10.1016/S0301-9268(99)00048-0.

Bingen, B., Mansfeld, J., Sigmond, E. M. O., and Stein, H., 2002, Baltica-Laurentia link during the Mesoproterozoic: 1.27 Ga development of continental basins in the Sveconorwegian Orogen, southern Norway: Canadian Journal of Earth Sciences, v. 39, p. 1425–1440. doi:10.1139/e02-054.

Blichert-Toft, J., Chauvel, C., and Albarede, F., 1997, The Lu-Hf geochemistry of chondrites and the evolution of the mantle-crust system: Earth and Planetary Science Letters, v. 148, p. 243–258, doi:10.1016/S0012-821X(97)00040-X.

Brewer, M. S., Haslam, H. W., Darbyshire, P. F. P., and Davis, A. E., 1979, Rb-Sr age determinations in the Bangweulu block, Luapula Province, Zambia: London, Institute of Geological Sciences, Report 79/5, p. 1–11.

Bulambo, M., De Waele, B., Kampunzu, A. B., and Tembo, F., 2004, SHRIMP U-Pb geochronology of the Choma-Kalomo block (Zambia) and geological implications: Orleans, France, 20th Colloquium of African Geology, 2–7 June 2004, p. 96.

Bulambo, J.-P., De Waele, B., Kampunzu, A. B., and Tembo, F., 2006, SHRIMP U-Pb geochronology of the Choma -Kalomo block (Zambia) and geological implications: Maputo, 21st Colloquium on African Geology, 03–05 July 2006, 3 p.

Cox, R. A., Rivers, T., Mapani, B., Tembo, F., and De Waele, B., 2002, New U-Pb data for the Irumide belt: LAM-ICP-MS results for Luangwa Terrane: Windhoek, Namibia, Geological Survey of Nambia, 11th IAGOD Quadrennial Symposium and Geocongress, technical meeting IGCP 440, Assembly and Breakup of Rodinia, p. 10.

Cvetcovic, D., 1973, The geology of the Mita hills area; explanation of degree sheet 1429, NW quarter: Lusaka, Geological Survey Department of Zambia, p. 12.

Daly, M. C., ms, 1986, The tectonic and thermal evolution of the Irumide belt, Zambia, Institute of African Geology: Leeds, University of Leeds, Ph. D. thesis, 326 p.

——— 1995a, The geology of Chinsali and Mutangoshi Hills area; explanation of degree sheet 1032, SE and SW quarter: Lusaka, Geological Survey Department of Zambia.

——— 1995b, The geology of Mulilansolo Mission and Isoka areas; explanation of degree sheet 1032, NE and NW quarter: Lusaka, Geological Survey Department of Zambia.

Daly, M. C., and Unrug, R., 1982, The Muva Supergroup, northern Zambia: Transactions of the Geological Society of South Africa, v. 85, p. 155–165.

Daly, M. C., Klerkx, J., and Nanyaro, J. T., 1985a, Early Proterozoic exotic terranes and strike-slip accretion in the Ubendian belt of southwest Tanzania: Terra Cognita, v. 5, p. 257.

——— 1985b, Early Proterozoic strike-slip accretion in the Ubendian belt of southwest Tanzania, *in* Bowden, P., Kinnaird, J. A., and Van, H. F. D., editors, 13th Colloquium of African geology: Centre International pour la Formation et les Echanges Géologiques (CIFEG).

De Waele, B., ms, 2005, The Proterozoic geological history of the Irumide belt, Zambia, Department of Applied Geology: Perth, Curtin University of Technology, Ph. D. thesis, 468 p.

De Waele, B., and Fitzsimons, I. C. W., 2007, The nature and timing of Palaeoproterozoic sedimentation at the southeastern margin of the Congo Craton; zircon U–Pb geochronology of plutonic, volcanic and clastic units in northern Zambia: Precambrian Research, v. 159, p. 95–116, doi:10.1016/j.precamres.2007.06.004.

De Waele, B., and Mapani, B., 2002, Geology and correlation of the central Irumide belt: Journal of African Earth Sciences, v. 35, p. 385–397, doi:10.1016/S0899-5362(02)00149-5.

De Waele, B., Wingate, M. T. D., Mapani, B., and Fitzsimons, I. C. W., 2003, Untying the Kibaran knot: A reassessment of Mesoproterozoic correlations in southern Africa based on SHRIMP U-Pb data from the Irumide belt: Geology, v. 31, p. 509–512, doi:10.1130/0091-7613(2003)031<0509:UTKKAR>2.0.CO;2.

De Waele, B., Kampunzu, A. B., Mapani, B. S. E., and Tembo, F., 2006a, The Mesoproterozoic Irumide belt of Zambia: Journal of African Earth Sciences, v. 46, p. 36–70, doi:10.1016/j.jafrearsci.2006.01.018.

De Waele, B., Liégeois, J. P., Nemchin, A. A., and Tembo, F., 2006b, Isotopic and geochemical evidence of Proterozoic episodic crustal reworking within the Irumide Belt of south-central Africa, the southern metacratonic boundary of an Archaean Bangweulu Craton: Precambrian Research, v. 148, p. 225–256, doi:10.1016/j.precamres.2006.05.006.

De Waele, B., Johnson, S. P., and Pisarevsky, S. A., 2008, Palaeoproterozoic to Neoproterozoic growth and evolution of the eastern Congo Craton: Its role in the Rodinia puzzle: Precambrian Research, v. 160, p. 127–141, doi:10.1016/j.precamres.2007.04.020.

Dodson, M. H., Cavanagh, B. J., Thatcher, E. C., and Aftalion, M., 1975, Age limits for the Ubendian metamorphic episode in northern Malawi: Geological Magazine, v. 112, p. 403–410.

Gorbatschev, R., and Bogdanova, S., 1993, Frontiers in the Baltic Shield: Precambrian Research, v. 64, p. 3–21, doi:10.1016/0301-9268(93)90066-B.

Goscombe, B., Armstrong, R. A., and Barton, J. M., 2000, Geology of the Chewore Inliers, Zimbabwe: Constraining the Mesoproterozoic to Palaeozoic evolution of the Zambezi belt: Journal of African Earth Sciences, v. 30, p. 589–627, doi:10.1016/S0899-5362(00)00041-5

Gower, C. F., and Krogh, T. E., 2002, A U-Pb geochronological review of the Proterozoic history of the eastern Grenville Province: Canadian Journal of Earth Sciences, v. 39, p. 795–829, doi:10.1139/e01-090.

Griffin, W. L., Pearson, N. J., Belousova, E., Jackson, S. E., van Achterbergh, E., O'Reilly, S. Y., and Shee, S. R., 2000, The Hf isotope composition of cratonic mantle: LAM-MC-ICPMS analysis of zircon megacrysts in kimberlites: Geochimica et Cosmochimica Acta, v. 64, p. 133–147, doi:10.1016/S0016-7037(99)00343-9.

Griffin, W. L., Belousova, E. A., Shee, S. R., Pearson, N. J., and O'Reilly, S. Y., 2004, Archean crustal evolution in the northern Yilgarn Craton: U-Pb and Hf-isotope evidence from detrital zircons: Precambrian Research, v. 131, p. 231–282, doi:10.1016/j.precamres.2003.12.011.

Hanson, R. E., 2003, Proterozoic geochronology and tectonic evolution of southern Africa, *in* Yoshida, M., Windley, B. F., and Dasgupta, S., editors, Proterozoic East Gondwana: Supercontinent Assembly and Breakup: Geological Society, London, Special Publication, v. 206, p. 427–463.

Hanson, R. E., Wilson, T. J., and Wardlaw, M. S., 1988a, Deformed batholiths in the Pan African Zambezi belt, Zambia: Age and implications for regional Proterozoic tectonics: Geology, v. 16, p. 1134–1137, doi:10.1130/0091-7613(1988)016(1134:DBITPA)2.3.CO;2.

Hanson, R. E., Wilson, T. J., Brueckner, H. K., Onstott, T. C., Wardlaw, M. S., Johns, C. C., and Hardcastle, K. C., 1988b, Reconnaissance geochronology, tectonothermal evolution, and regional significance of the Middle Proterozoic Choma-Kalomo block, southern Zambia: Precambrian Research, v. 42, p. 39–61, doi:10.1016/0301-9268(88)90009-5.

Hoskin, P. W. O., and Black, L. P., 2000, Metamorphic zircon formation by solid-state recrystallization of protolith igneous zircon: Journal of Metamorphic Geology, v. 18, p. 423–439, doi:10.1046/j.1525-1314.2000.00266.x.

John, T., ms, 2001, Subduction and continental collision in the Lufilian Arc -Zambezi belt orogen: A petrological, geochemical, and geochronological study of eclogites and whiteschists (Zambia), Mathematisch-Naturwissenschaftlichen Fakultat: Kiel, University of Kiel, Ph. D. thesis, 78 p.

John, T., Schenk, V., and Tembo, F., 1999, The metamorphic evolution and U/Pb dating of monazites of the southern Irumide belt, SE-Zambia, *in* De Waele, B., Tembo, F., and Key, R. M., editors, Abstracts Volume IGCP 419/419: Lusaka, Geological Society of Zambia, p. 7.

Johns, C. C., Liyungu, K., Mabuku, S., Mwale, G., Sakungo, F., Tembo, D., Vallance, G., and Barr, M. W. C., 1989, The stratigraphic and structural framework of eastern Zambia: Results of a geotraverse: Journal of African Earth Sciences, v. 9, p. 123–136, doi:10.1016/0899-5362(89)90015-8.

Johnson, S. P., and Oliver, G. J. H., 2004, Tectonothermal history of the Kaourera Arc, northern Zimbabwe: implications for the tectonic evolution of the Irumide and Zambezi Belts of south central Africa: Precambrian Research, v. 130, p. 71–97, doi:10.1016/j.precamres.2003.10.016.

Johnson, S. P., De Waele, B., Tani, K., and Tembo, F., 2005a, Mesoproterozoic supra-subduction magmatism in the southern Irumide Belt, central southern Africa: implications for the Congo Craton *in* Rodinia reconstructions, Supercontinents and Earth Evolution Symposium: Fremantle, Western Australia, 26-30 September, 2005, p. 83–84.

Johnson, S. P., Rivers, T., and De Waele, B., 2005b, A Review of the Mesoproterozoic to early Palaeozoic magmatic and tectonothermal history of south-central Africa: implications for Rodinia and Gondwana: London, Journal of the Geological Society, v. 162, p. 433–450, doi:10.1144/0016-764904-028.

Johnson, S. P., De Waele, B., and Liyungu, A. K., 2006, U-Pb sensitive high-resolution ion microprobe (SHRIMP) zircon geochronology of granitoid rocks in eastern Zambia: Terrane subdivision of the Mesoproterozoic Southern Irumide Belt: Tectonics, v. 25, p. TC6004, doi:10.1029/2006TC001977.

Johnson, S. P., De Waele, B., Tembo, F., Katongo, C., Tani, K., Chang, Q., Iizuka, T., and Dunkley, D., 2007, Geochemistry, geochronology and isotopic evolution of the Chewore-Rufunsa terrane, Southern Irumide Belt. A Mesoproterozoic continental margin arc: Journal of Petrology, v. 48, p. 1411–1441, doi:10.1093/petrology/egm025.

Karlstrom, K. E., Åhäll, K.-I., Harlan, S. S., Williams, M. L., McLelland, J., and Geissman, J. W., 2001, Long-lived (1.8–1.0 Ga) convergent orogen in southern Laurentia, its extensions to Australia and Baltica, and implications for refining Rodinia: Precambrian Research, v. 111, p. 5–30, doi:10.1016/S0301-9268(01)00154-1.

Katongo, C., Köller, F., Klötzli, U., Koeberl, C., Tembo, F., and De Waele, B., 2004, Petrography, geochemistry and geochronology of granitoid rocks in the Neoproterozoic-Paleozoic Lufilian–Zambezi belt, Zambia: Implications for tectonic setting and regional correlation: Journal of African Earth Sciences, v. 40, p. 219–244, doi:10.1016/j.jafrearsci.2004.12.007.

Key, R. M., Liyungu, A. K., Njamu, F. M., Somwe, V., Banda, J., Mosley, P. N., and Armstrong, R. A., 2001, The western arm of the Lufilian Arc in NW Zambia and its potential for copper mineralization: Journal of African Earth Sciences, v. 33, p. 503–528, doi:10.1016/S0899-5362(01)00098-7.

Kokonyangi, J., Armstrong, R. A., Kampunzu, A. B., Yoshida, M., and Okudaira, T., 2004, U–Pb zircon geochronology and petrology of granitoids from Mitwaba (Katanga, Congo): implications for the evolution of the Mesoproterozoic Kibaran belt: Precambrian Research, v. 132, p. 79–106, doi:10.1016/j.precamres.2004.02.007.

Kröner, S., Konopásek, J., Kröner, A., Passchier, C. W., Poller, U., Wingate, M. T. D., and Hoffman, K. H., 2004, U-Pb and Pb-Pb zircon ages for metamorphic rocks in the Kaoko Belt of Northwestern Namibia: A Palaeo- to Mesoproterozoic basement reworked during the Pan-African orogeny: South African Journal of Geology, v. 107, p. 455–476, doi:10.2113/107.3.455.

Ludwig, K. R., 2001a, Isoplot/Ex rev. 2.49: Berkeley, California, Berkeley Geochronology Center, p. 54.
——— 2001b, Squid 1.02: A User's Manual: Berkeley, Berkeley Geochronology Center, p. 19.
Macey, P. H., Ingram, B. A., Cronwright, M. S., Botha, G. A., Roberts, M. R., Grantham, G. H., Maree, L. P., Botha, P. M. W., Kota, M., Opperman, R., Haddon, I. G., Nolte, J. C., and Rower, M., 2007, Map Explanation of Sheets Alto Molócuè (1537), Murrupula (1538), Nampula (1639), Mogincual (1540), Errego (1637), Gilé (1638) and Angoche (1639-40): Maputo, National Directorate of Geology, Mozambique, p. 402.
Mäkitie, H., Lehtonen, M., I., Manninen, T., Marques, J. M., Cune, G., and Mavíe, H., 2008, Petrography and Geochemistry of Granitoid Rocks in the Northern Part of Tete Province, Mozambique, *in* Pekkala, Y., Lehto, T., and Mäkitie, H., editors, GTK Consortium Geological Surveys in Mozambique 2002-2007: Geological Survey of Finland, Special Paper 48, p. 167–189.
Mapani, B., 1999, Tectonic and metamorphic evolution of the Serenje and adjoining areas, *in* De Waele, B., Tembo, F., and Key, R. M., editors, Abstracts Volume IGCP 418/419: Lusaka, Geological Society of Zambia, p. 16.
Mapani, B. S. E., Rivers, T., Tembo, F., and Katongo, C., 2001, Terrane Mapping in the eastern Irumide and Mozambique belts: Implications for the assembly and dispersal of Rodinia, *in* McCourt, S., editor, IGCP 418 4th fieldmeeting: Durban, South Africa, University of Durban-Westville, p. 10–11.
Mapani, B., Rivers, T., Tembo, F., De Waele, B., and Katongo, C., 2004, Growth of the Irumide terranes and slices of Archaean age in eastern Zambia: Johannesburg, South Africa, Geoscience Africa 2004, p. 414–415.
Mosley, P. N., and Marten, B. S., 1979, The Geology of the Katibunga mission area, explanation of degree sheet 1131, SE quarter: Lusaka, Geological Survey Department of Zambia.
Ngoyi, K., Liégeois, J.-P., Demaiffe, D., and Dumont, P., 1991, Age tardi-ubendien (Protérozoïque inférieur) des dômes granitiques de l'arc cuprifére zaïro-zambien: Comptes Rendu de l'Academie de Sciences, v. 313, p. 83–89.
Oliver, G. J. H., Johnson, S. P., Williams, I. S., and Herd, D. A., 1998, Relict 1.4 Ga oceanic crust in the Zambezi Valley, northern Zimbabwe: Evidence for Mesoproterozoic supercontinental fragmentation: Geology, v. 26, p. 571–573, doi:10.1130/0091-7613(1998)026<0571:RGOCIT>2.3.CO;2.
Pesonen, L. J., Elming, S.-A., Mertanen, S., Pisarevsky, S., D'Agrella-Filho, M. S., Meert, J. G., Schmidt, P. W., Abrahamsen, N., and Bylund, G., 2003, Palaeomagnetic configuration of continents during the Proterozoic: Tectonophysics, v. 375, p. 289–324, doi:10.1016/S0040-1951(03)00343-3.
Pidgeon, R. T., Furfaro, D., Kennedy, A. K., Nemchin, A. A., and Van Bronswijk, W., 1994, Calibration of zircon standards for the Curtin SHRIMP II: United States Geological Survey circular, v. 1107, p. 251.
Rainaud, C., Master, S., Armstrong, R. A., and Robb, L. J., 2003, A cryptic Mesoarchean terrane in the basement to the central African Copperbelt: London, Journal of the Geological Society, v. 160, p. 11–14, doi:10.1144/0016-764902-087.
——— 2005, Geochronology and nature of the Palaeoproterozoic basement in the Central African Copperbelt (Zambia and the Democratic Republic of Congo), with regional implications: Journal of African Earth Sciences, v. 42, p. 1–31.
Rainaud, C. L., Armstrong, R. A., Master, S., Robb, L. J., and Mumba, P. A. C. C., 2002, Contributions to the geology and mineralisation of the central African Copperbelt: I. Nature and geochronology of the pre-Katangan basement: Windhoek, Namibia, Geological Survey of Namibia, 11th IAGOD Quadrennial Symposium and Geocongress, p. 5.
Rämö, O. T., McLemore, V. T., Hamilton, M. A., Kosunen, P. J., Heizler, M., and Haapala, I., 2003, Intermittent 1630-1220 Ma magmatism in central Mazatzal Province: new geochronologic piercing points and some tectonic implications: Geology, v. 31, p. 335–338, doi:10.1130/0091-7613(2003)031<0335:IMMICM>2.0.CO;2.
Ring, U., Kröner, A., and Toulkeredis, T., 1997, Palaeoproterozoic granulite-facies metamorphism and granitoid intrusions in the Ubendian-Usagaran Orogen of northern Malawi, east-central Africa: Precambrian Research, v. 85, p. 27–51, doi:10.1016/S0301-9268(97)00028-4.
Ring, U., Kröner, A., Layer, P., Buchwaldt, R., and Toulkeredis, T., 1999, Deformed A-type granites in northern Malawi, east-central Africa: pre- or syntectonic: London, Journal of the Geological Society, v. 156, p. 695–714, doi:10.1144/gsjgs.156.4.0695.
Rivers, T., 1997, Lithotectonic elements of the Grenville Province: review and tectonic implications: Precambrian Research, v. 86, p. 117–154, doi:10.1016/S0301-9268(97)00038-7.
Rivers, T., and Corrigan, D., 2000, Convergent margin on southeastern Laurentia during the Mesoproterozoic: tectonic implications: Canadian Journal of Earth Sciences, v. 37, p. 359–383, doi:10.1139/cjes-37-2-3-359.
Romer, R. L., 1996, Contiguous Laurentia and Baltica before the Grenvillian-Sveconorwegian orogeny?: Terra Nova, v. 8, p. 173–181, doi:10.1111/j.1365-3121.1996.tb00741.x
Schenk, V., and Appel, P., 2001, Anti-clockwise P-T path during ultrahigh-temperature (UHT) metamorphism at ca. 1050 Ma in the Irumide Belt of Eastern Zambia: Berichte der Deutschen Mineralogischen Gesellschaft, Beihefte zum European Journal of Mineralogy, v. 13, p. 161.
Seth, B., Kröner, A., Mezger, K., Nemchin, A. A., Pidgeon, R. T., and Okrusch, M., 1998, Archaean to Neoproterozoic magmatic events in the Kaoko belt of NW Namibia and their geodynamic significance: Precambrian Research, v. 92, p. 341–363, doi:10.1016/S0301-9268(98)00086-2.
Seth, B., Armstrong, R. A., Brandt, S., Villa, I. M., and Kramers, J. D., 2003, Mesoproterozoic U–Pb and Pb–Pb ages of granulites in NW Namibia: reconstructing a complete orogenic cycle: Precambrian Research, v. 126, p. 147–168, doi:10.1016/S0301-9268(03)00193-1.
Seth, B., Armstrong, R. A., Büttner, A., and Villab, I. M., 2005, Time constraints for Mesoproterozoic upper amphibolite facies metamorphism in NW Namibia: a multi-isotopic approach: Earth and Planetary Science Letters, v. 230, p. 355–378, doi:10.1016/j.epsl.2004.11.022.

Smith, A. G., 1966, The geology of the Kapiri Mposhi area; explanation of degree sheet 1328, SE quarter: Lusaka, Geological Survey Department of Zambia, p. 32.
Stacey, J. S., and Kramers, J. D., 1975, Approximation of terrestrial lead isotopic evolution by a two-stage model: Earth and Planetary Science Letters, v. 26, p. 207–221, doi:10.1016/0012-821X(75)90088-6.
Stillman, C. J., 1965, The geology of the Musofu River and Mkushi areas; explanation of degree sheet 1329, part of NW quarter and SW quarter: Lusaka, Geological Survey Department of Zambia, p. 52.
Sykes, J. M. D., 1995, The geology of the Luswa River area, degree sheet 1132, NW quarter: Lusaka, Geological Survey Department, p. 20.
Tack, L., Fernandez-Alonso, M., Tahon, M., Wingate, M. T. D., and Barritt, S., 2002, The "northeastern Kibaran belt" (NKB) and its mineralisations reconsidered: new constraints from a revised lithostratigraphy, a GIS-compilation of existing geological maps and a review of recently published as well as unpublished igneous emplacement ages in Burundi, *in* Geological Survey of Namibia, editor, 11th IAGOD Quadrennial Symposium and Geocongress: Windhoek, Namibia, Geological Survey of Namibia, p. 6.
Unrug, R., 1992, Kibaran terranes with cassiterite mineralisation in the Zambezi belt, Zambia and Zimbabwe: IGCP Bulletin, v. 4, p. 121–124.
Van Tuijl, M. M., and Verhoog, B. J., 1995, The geology of the Kalungu and Mututa Hills area; explanation of degree sheet 0932, SE and SW quarter: Lusaka, Geological Survey Department of Zambia.
Verhoog, B. J., and Van Tuijl, M. M., 1995a, The geology of the Chozi area; explanation of degree sheet 0932, NW quarter: Lusaka, Geological Survey Department of Zambia.
——— 1995b, The geology of the Nakonde area; explanation of degree sheet 0932 NE quarter: Lusaka, Geological Survey Department of Zambia.
Vrána, S., Kachlík, V., Kröner, A., Marheine, D., Seifert, A. V., Zácek, V., and Baburek, J., 2004, Ubendian basement and its late Mesoproterozoic and early Neoproterozoic structural and metamorphic overprint in northeastern Zambia: Journal of African Earth Sciences, v. 38, p. 1–21, doi:10.1016/j.jafrearsci.2003.09.001.
Westerhof, A. B. P., Lehtonen, M. I., Mäkitie, H., Manninen, T., Pekkala, Y., Gustafsson, B., and Tahon, A., 2008, The Tete-Chipata Belt: A New Multiple Terrane Element from Western Mozambique and Southern Zambia, *in* Pekkala, Y., Lehto, T., and Mäkitie, H., editors, GTK Consortium Geological Surveys in Mozambique 2002–2007: Geological Survey of Finland, Special Paper 48, p. 145–166.